INFORMATION TO USERS

This manuscript has been reproduced from the microfilm master. UMI films the text directly from the original or copy submitted. Thus, some thesis and dissertation copies are in typewriter face, while others may be from any type of computer printer.

The quality of this reproduction is dependent upon the quality of the copy submitted. Broken or indistinct print, colored or poor quality illustrations and photographs, print bleedthrough, substandard margins, and improper alignment can adversely affect reproduction.

In the unlikely event that the author did not send UMI a complete manuscript and there are missing pages, these will be noted. Also, if unauthorized copyright material had to be removed, a note will indicate the deletion.

Oversize materials (e.g., maps, drawings, charts) are reproduced by sectioning the original, beginning at the upper left-hand corner and continuing from left to right in equal sections with small overlaps.

Photographs included in the original manuscript have been reproduced xerographically in this copy. Higher quality 6" x 9" black and white photographic prints are available for any photographs or illustrations appearing in this copy for an additional charge. Contact UMI directly to order.

Bell & Howell Information and Learning
300 North Zeeb Road, Ann Arbor, MI 48106-1346 USA
800-521-0600

REACTIVITY OF MANGANESE OXIDE MINERALS WITH SOIL ORGANIC MATTER AND LEAD

by

Christopher J. Matocha

A dissertation submitted to the Faculty of the University of Delaware in partial fulfillment of the requirements for the degree of Doctor of Philosophy in Plant and Soil Sciences

Spring 2000

REACTIVITY OF MANGANESE OXIDE MINERALS

WITH SOIL ORGANIC MATTER AND LEAD

by

Christopher J. Matocha

Approved: Donald L. Sparks

Donald L. Sparks, Ph.D.
Chair of the Department of Plant and Soil Sciences

Approved: John C Nye

John C. Nye, Ph.D.
Dean of the College of Agriculture and Natural Resources

Approved:

Conrado M. Gempesaw II, Ph.D.
Vice Provost for Academic Programs and Planning

I certify that I have read this dissertation and that in my opinion it meets the academic and professional standard required by the University as a dissertation for the degree of Doctor of Philosophy.

Signed: 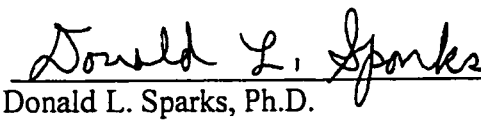

Donald L. Sparks, Ph.D.
Professor in charge of dissertation

I certify that I have read this dissertation and that in my opinion it meets the academic and professional standard required by the University as a dissertation for the degree of Doctor of Philosophy.

Signed: 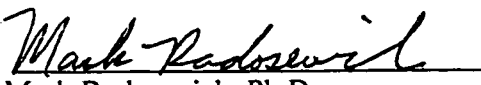

Mark Radosevich, Ph.D.
Member of dissertation committee

I certify that I have read this dissertation and that in my opinion it meets the academic and professional standard required by the University as a dissertation for the degree of Doctor of Philosophy.

Signed: 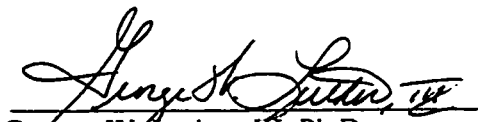

George W. Luther, III, Ph.D.
Member of dissertation committee

I certify that I have read this dissertation and that in my opinion it meets the academic and professional standard required by the University as a dissertation for the degree of Doctor of Philosophy.

Signed: 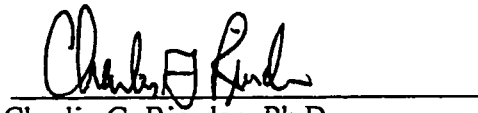

Charlie G. Riordan, Ph.D.
Member of dissertation committee

ACKNOWLEDGMENTS

Dr. D.L. Sparks, Ph.D., for his guidance, constant support, and encouragement during my stay at the University of Delaware. I appreciate the support of a DuPont Graduate Research Fellowship. Drs. C.G. Riordan, G.W. Luther III, and Mark Radosevich, Ph.D.s, who challenged me to think mechanistically and were always available for questions. Jerry Hendricks and the entire Soil Chemistry research group for assistance and constructive interactions in all aspects of this research. Drs. Jim Amonette and Ravi Kukkadapu at the William R. Wiley Environmental Molecular Science Laboratory in Richland, WA for their thoughtful assistance and hospitality during the electron paramagnetic resonance studies. Drs. Brian McCandless and Raul Lobo for unlimited use of the diffuse reflectance spectrometer and x-ray diffractometer. I thank the InterVarsity Christian Fellowship group for their love and prayers. I sincerely thank my Proverbs 31 wife, Jennifer, for her unending love, encouragement, and understanding throughout the pursuit of this degree and for choosing a more honorable career than Soil Chemistry by staying at home with our two brave soldiers, Joshua and Caleb.

This dissertation is dedicated to:

Jesus Christ, who stated in John 19:30, "It is finished." Manganese chemistry is not finished, in contrast to what Jesus did as He paid the price entirely for our sins on the cross by the grace of God.

TABLE OF CONTENTS

LIST OF TABLES

LIST OF FIGURES

Chapter 1

INTRODUCTION

1.1 Scope of Research

Manganese (III,IV) (hydr) oxides have long been recognized as effective oxidants of organic and inorganic reductants. Aromatic and nonaromatic ligands resembling soil organic matter have been reported to reductively dissolve Mn(III,IV) (hydr) oxides (Stone and Morgan, 1984a,b). The reactivity of Mn(III,IV) (hydr) oxides in soils makes them important regulators of plant available Mn in soil solution (McBride, 1989b; McKenzie, 1989). Sorbed metal contaminants such as Pb(II) can be released into solution following reductive dissolution of solid Mn(III,IV) (hydr) oxides by oxidizable organic ligands and reactive compounds may be sorbed or coprecipitated as a consequence of Mn(II) hydrolysis (Xyla et al., 1992; Godtfredsen and Stone, 1994). The redox cycling of Mn is coupled to: 1) the geochemical cycling of metals (Hem, 1978); 2) carbon turnover in soils (Wang and Huang, 1992; Naidja et al., 1998); and 3) nitrogen transformation in soils (Bartlett, 1981; Wang and Huang, 1987; Laha and Luthy, 1990) and marine sediments (Luther et al., 1997). The Mn dissolution reaction itself is abiotic, although oxidizable organic ligand reductants in soils may be exuded from roots or microorganisms (Jauregui and Reisenauer, 1982; McBride,

1989b). There is a need to elucidate the fundamental mechanisms controlling these reactions in natural settings.

1.2 Literature Review

1.2.1 Manganese Chemistry

Manganese occurs in three oxidation states in minerals and natural waters: II, III, and IV. Assuming octahedral coordination, possible electronic configurations and ionic radii of the Mn cations taken from Burns (1976) are shown below:

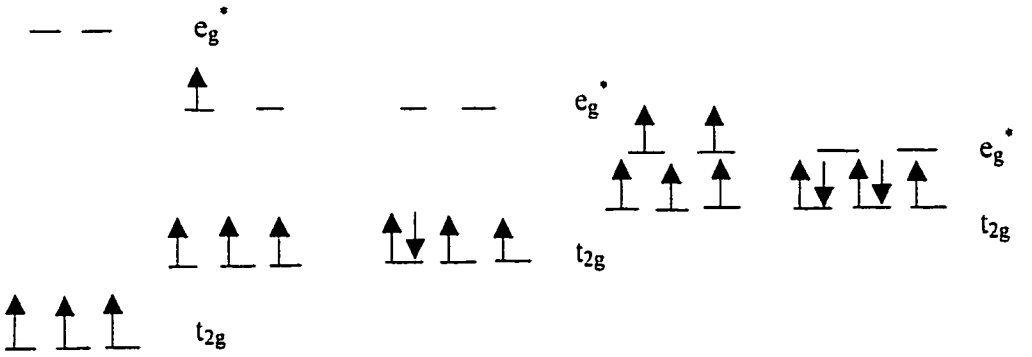

Mn(IV)	Mn(III)	Mn(III)	Mn(II)	Mn(II)
	High-spin	Low-spin	High-spin	Low-spin
0.54 Å	0.65 Å	0.58 Å	0.82 Å	0.67 Å

where the gap between the t_{2g} and e_g^* orbitals is the relative energy difference due to crystal field splitting(Δ_0). Crystal field stabilization energy (CFSE) decreases in the order Mn(IV) > Mn(III) >Mn(II) because 2 Δo/5 is added for each electron in a t_{2g} orbital, and 3 Δo/5 is subtracted for each electron in an e_g^* orbital (McKenzie, 1970). Thus, electrons in t_{2g} orbitals increase the stability of an ion in octahedral coordination

and electrons in e_g^* orbitals decrease the stability (McKenzie, 1970). Only the high-spin species of Mn(II) and Mn(III) occur in minerals (Burns, 1976).

Manganese(II) and Mn(IV) have received the most attention in aquatic chemistry (Morgan, 1967) because Mn(III) has an extensive coordination chemistry (Yamaguchi and Sawyer, 1985) and in the absence of complexing ligands, is unstable and disproportionates to Mn (II) and MnO_2 in aqueous solution (Davies, 1969; Burns, 1993).

$$2Mn^{III} + 2H_2O \leftrightarrow Mn(II) + MnO_2 + 4H^+ \qquad (1)$$

$$\Delta G^o_{298} = -109 \text{ kJ mole}^{-1}$$

Low pH, high Mn(II) concentration, and low Mn(III) concentration will slow the rate of disproportionation based on Le Chatelier's principle (Davies, 1969). Solution complexes of Mn(III) with unsaturated complexing ligands such as carboxylic acid and aromatic functional groups undergo internal metal-ligand redox reactions rather than disproportionation (Magers et al., 1978; Luther et al., 1998). In contrast, ligands such as bis-tris and pyrophosphate can chelate Mn(III) without subsequent electron transfer (Luther et al., 1998; Klewicki and Morgan, 1998). Half lives of Mn(III)-pyrophosphate complex decomposition ranged from 25 to 530 days depending on pH due to hydrolysis of pyrophosphate followed by disproportionation (Klewicki and Morgan, 1998). The importance of the dissolved Mn (III)-pyrophosphate complex as an environmental oxidant has been reported recently and coupled to Fe, S, and C cycling (Kostka et al., 1995).

Manganese (II) complexes are labile to ligand substitution reactions and complexation of Mn (II) is necessary to remove octahedral symmetry and rearrange the energies of the d orbitals to effect electron transfer (Luther, 1990). Oxidation of Mn(II) by O_2 is slow (Diem and Stumm, 1984) unless catalyzed by a surface (Coughlin and Matsui, 1976; Davies and Morgan, 1989; Junta and Hochella, 1994) with O donor ligating atoms (hard ligands of low polarizability) such as O^{2-} and OH^- which facilitate electron transfer (Luther,1990). Manganese (II) oxidation must occur by way of an inner-sphere mechanism based on its d^5 $[t_{2g}^3 e_g^2]$ electronic configuration because the σ to π electron transfer from the HOMO of Mn (II) to the LUMO of O_2 is not symmetry allowed. In addition, π to π electron transfers are favored for outer-sphere mechanisms (Luther, 1990).

1.2.2 Occurrence of Mn(III,IV) (Hydr) Oxides

Manganese (III,IV) (hydr) oxide minerals are often concentrated in nodules intimately associated with Fe oxide minerals and often contain inclusions of the soil matrix (White and Dixon, 1996). Most of the work conducted on secondary Mn minerals in soils is derived from studies made on high-Mn materials isolated from black, Mn-rich concretions (Gilkes and McKenzie, 1988). The extremely small crystal size, poor crystallinity, and non-stoichiometric composition of soil Mn minerals make identification in soils complicated (Gilkes and McKenzie, 1988). However, several phases have been identified.

The most common Mn minerals identified in field soils and sediments are birnessite (δ-MnO_2) and cryptomelane (α-MnO_2) (McKenzie, 1989). Only two Mn(III) phases are known to occur in soil: hausmannite (Mn_3O_4) and manganite (γ-MnOOH) (Gilkes and McKenzie, 1988). Manganite has been shown to form as the end product of Mn(II) oxidation in natural waters through a hausmannite intermediate via a dissolution/reprecipitation mechanism (Stumm and Giovanoli, 1976). The pathways of birnessite formation in soils are unclear, however, a dissolution/reprecipitation mechanism is likely involved (Cornell and Giovanoli, 1988). For solid phase Mn(III) oxide minerals such as manganite, disproportionation would be favored at low pH based on the following stoichiometry:

$$2MnOOH\ (s) + 2H^+ \rightarrow Mn(II)\ (aq) + MnO_2\ (s) + 2H_2O \qquad (2)$$

Recent spectroscopic studies have shown that Mn(III) substituted in Na-buserite disproportionates with subsequent Mn(II) release at low pH (Silvester et al., 1997).

1.2.3 Agricultural and Environmental Significance of Mn

Solid phase Mn(III) and Mn(IV) are coordinated by oxo functional groups (O^{2-}, OH^-, H_2O) and widely distributed in soils and sediments as discrete particles and as coatings on other soil/sediment components. Soil Mn oxides are the principal source of available Mn in most soils. In acidic (pH < 5.5) and poorly aerated soils, net reduction of Mn from Mn(III,IV) (hydr) oxides occurs both biotically and abiotically which can give rise to Mn toxicity in plants (Weil et al., 1997). Surface charge properties of Mn(III,IV) (hydr) oxide surfaces are dependent on soil solution pH

(Figure 1.1). Extractants such as DTPA, hydroxylamine hydrochloride (NH_2OH-HCl), and hydroquinone (HYD) are used to identify different pools of Mn and predict Mn availability to plants. Most of the procedures extract water soluble and exchangeable Mn and variable amounts of adsorbed or oxide-bound Mn (Reisenauer, 1988). In addition, Mn extractants such as DTPA show a strong dependence on the pH of the extracting solution (Lindsay and Norvell, 1978) which probably reflects surface properties of the soils and speciation of the extractant. Low correlation coefficients that are typically observed between Mn in the plant and Mn extracted from soils could be due to inefficient extractants and variable solid phase Mn oxides with a range of reactivities. It is evident that the science behind developing Mn extraction methods is not well understood.

Herbicides shown recently to abiotically react with solid phase Mn oxides are atrazine and 2,4-D (Cheney et al., 1996; Cheney et al., 1998). Rates of atrazine dealkylation by birnessite were faster than biotically-mediated dealkylations (Wang et al., 1999). Thus, Mn oxides can contribute significantly to detoxification of organic contaminants.

Carboxylic acid and phenolic functional groups of soil organic matter are common active sites for reactivity (Stevenson, 1994). Tan et al. (1971) identified hydroxyl functionalities which chelated metals in a poultry litter extract using FTIR. Functional groups found in soil organic matter can reduce solid phase Mn(III,IV) (hydr) oxides to the more plant available Mn(II) in a process known as reductive

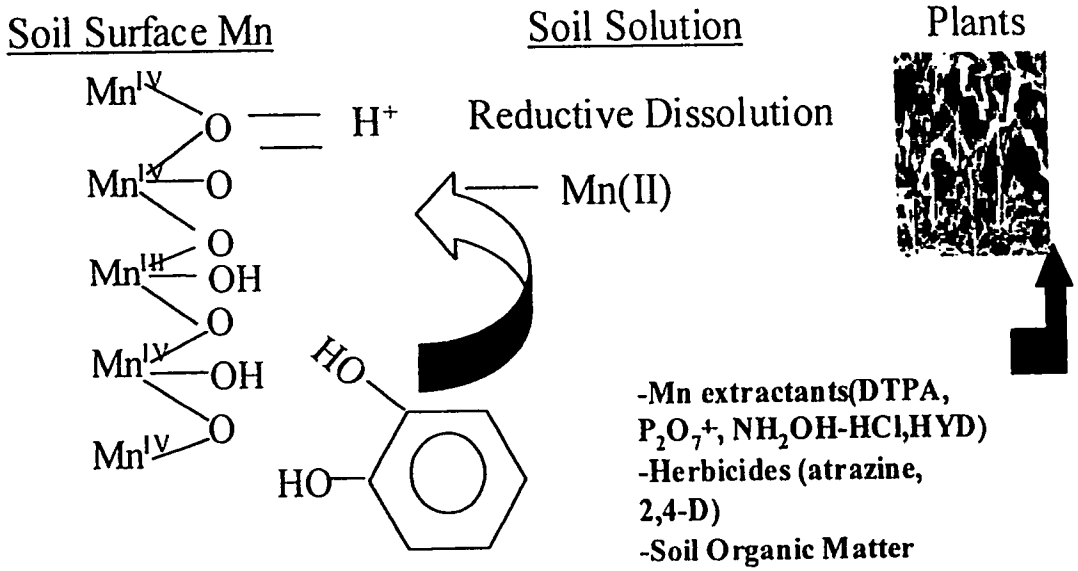

Figure 1.1 A portion of the Mn cycle in soils illustrating the importance of sorption on Mn solubility.

dissolution (Figure 1.1). Numerous investigations have reported that soil organic matter content and organic matter amendments increases Mn availability (Meek et al., 1968; Cheng et al., 1970; Randall et al., 1976). The study by Meek et al. (1968) was particularly striking because addition of organic matter released several times more Mn to solution than untreated controls for a soil with a native pH of 8 (Figure 1.2). One process common to all the reactants present in the soil solution in Figure 1.1 is that they all involve a surface reaction. Thus, a crucial process in the Mn cycle is sorption. However, no direct spectroscopic confirmation of the surface complex formed between entering ligands from the soil solution and the Mn oxide surface is available (Stone et al., 1994).

The reactivity of soil Mn oxides with soil organic matter as shown by Meek et al. (1968) is not well understood at the mechanistic level. A typical E_h-pH diagram was generated describing Mn speciation with birnessite controlling the thermodynamic solubility of Mn(II) and compared with the redox couples of O_2/H_2O and ortho-quinone(o-q)/catechol (1,2-dihydroxybenzene), a representative ligand of soil organic matter (Figure 1.3). It can be seen that one would not predict Mn toxicity until pH < 4, where birnessite would be unstable with respect to oxidation of H_2O. Also, the position of the o-q/catechol couple indicates that only O_2 should oxidize catechol at pH > 6 based on thermodynamic equilibrium calculations. Surprisingly, past investigators have shown that catechol solubilizes birnessite and other solid Mn oxides

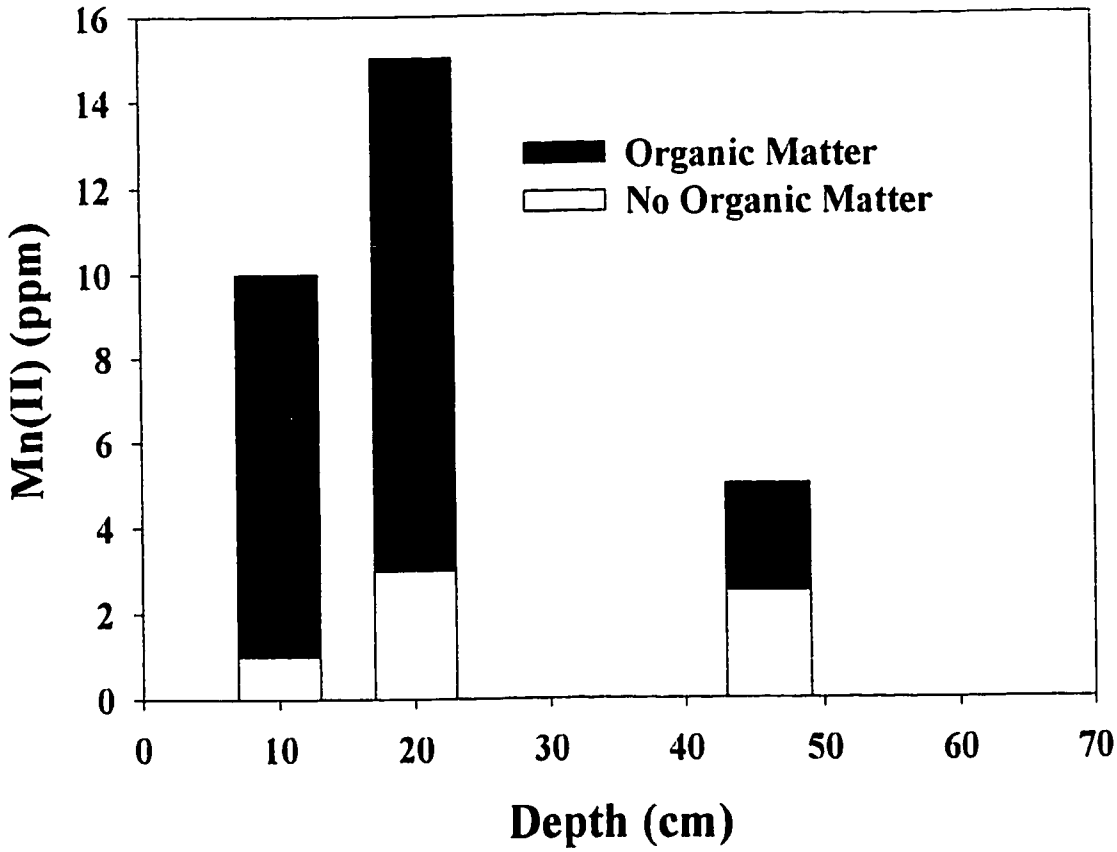

Figure 1.2 Effect of organic matter on soil solution Mn(II) in a silty clay soil at pH 7.8 (Taken from Meek et al., 1968).

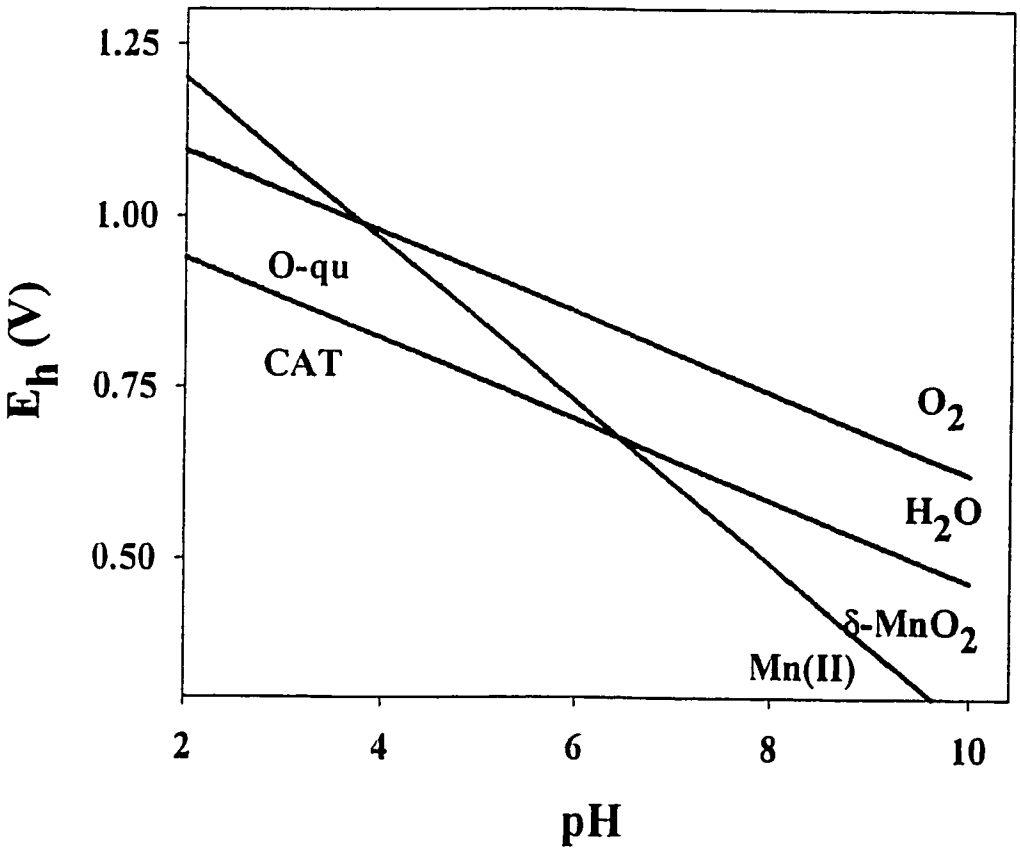

Figure 1.3 An E_h-pH diagram for the O_2 /H_2O, δ-MnO_2 /Mn(II), and the o-quinone(O-qu)/catechol (CAT) couples.

at rapid rates even in the presence of O_2 and high pH (Stone and Morgan, 1984b; McBride, 1989a,b). Also, solid Mn oxides commonly occur in the near surface horizons and would kinetically outcompete O_2 for oxidation of soil organic matter (Luther et al., 1998; see Figure1.2). In practice, there is a disequilibrium in Mn redox chemistry in the presence of soil organic matter. Therefore, as is the case in soil chemical processes, there is a strong need for kinetic studies to measure the reaction rates and deduce mechanisms (Sparks, 1989).

1.3 Research Justification

The ability of Mn(III,IV) (hydr) oxides to catalyze a diverse array of reactions in natural settings prompted this study. There is a lack of *in situ* studies of soil organic matter reactivity on naturally occurring Mn(III,IV) (hydr) oxides. Incomplete understanding of the reductive dissolution mechanism could lead to Mn toxicity in susceptible plants upon application of wastes such as poultry litter. Specifically, no spectroscopic evidence exists for the chemical structure of the sorption complex. In addition, the pronounced disequilibrium in Mn redox reactions prompts the need for kinetic studies.

The study of model systems using small organic ligands with functional groups characteristic of soil organic matter is useful to predict reactivity of the more complex soil organic matter macromolecules. Catechol was the test ligand employed in this research because ortho-type semiquinones have been identified in soil humic

substances (Steelink, 1964), catechols are common intermediates in pesticide degradation pathways (Alexander, 1977), and they have been identified on siderophore molecules (Hersman et al., 1995).

There has been debate over the uptake mechanisms of Pb(II) by Mn(IV) oxides based on the peculiar shape of the pH edges which show nearly complete removal of Pb(II) from solution by birnessite over a wide pH range, which some authors attributed to oxidation of Pb(II) to PbO_2 (Gadde and Laitenen, 1974). Recent studies indicated that Pb(II) was not oxidized based on x-ray absorption fine structure (XAFS) spectra (Morin et al., 1999), but the studies were conducted under a limited set of experimental conditions. There clearly exists a need to revisit this system, particularly in light of recent findings that Pb(II) partitions strongly to solid phase Mn oxides in natural soil environments despite their relative low abundance (Manceau et al., 1997).

In order to understand fate and cycling of Mn at the field scale, one must obtain more direct molecular-level information. The complexity of heterogeneous solid/liquid interfacial reactions coupled with the disequilbrium in Mn redox chemistry suggests that a pragmatic approach for the study of redox reactions promoted by Mn(III,IV) (hydr) oxides is to combine spectroscopic techniques with macroscopic and kinetic investigations, which are necessary to provide mechanistic information (Sparks, 1995).

1.4 Research Objectives

Guided by the above information, the objectives of this study were to:

1) Interrogate the soil organic matter-Mn(III,IV) (hydr) oxide mineral interface through the use of naturally occurring solid phase minerals and catechol as an analogue of soil organic matter;
2) Evaluate the reactivity of catechol on well characterized Mn(III,IV) (hydr) oxide minerals through kinetic studies using *in situ* spectroscopic tools such as electron paramagnetic resonance (EPR) spectroscopy and diffuse reflectance spectroscopy (DRS);
3) Investigate the mechanisms of Pb(II) uptake on birnessite and manganite through thermodynamic, kinetic, and spectroscopic studies employing x-ray absorption fine structure (XAFS) spectroscopy;
4) Provide a predictive framework for Mn and C cycling in natural soil environments and its effect on Pb(II) fate.

1.5 References

Alexander, M. 1977. Introduction to soil microbiology. John Wiley & Sons, New York.

Bartlett, R.J. 1981. Nonmicrobial nitrite-to-nitrate transformation in soils. Soil Sci. Soc.Am. J. 45:1054-1058.

Burns, R.G. 1976. The uptake of cobalt into ferromanganese nodules, soils, and synthetic manganese (IV) oxides. Geochim. Cosmochim. Acta. 40:95-102.

Burns, R.G. 1993. Mineralogical applications of crystal field theory. Cambridge University Press, Cambridge, Great Britain.

Cheney, M. A., G. Sposito, A. E. McGrath and R. S. Criddle. 1996. Abiotic degradation of 2,4-D (dichlorophenoxyacetic acid) on synthetic birnessite: A calorespirometric method. Colloids and Surfaces 107:131-140.

Cheney, M. A., J.Y. Shin, D.E. Crowley, S. Alvey, N. Malengreau, and G. Sposito. 1998. Atrazine dealkylation on a manganese oxide surface. Colloids and Surfaces 137:267-273.

Cheng, B.T., and G.J. Ouellette. 1970. Effect of steam sterilization and organic amendments on the manganese status and associated characteristics of acid soils. Soil Sci. 110:383-388.

Cornell, R.M., and R. Giovanoli. 1988. Transformation of hausmannite into birnessite in alkaline media. Clays Clay Minerals 36:249-257.

Coughlin, R.W., and I. Matsui. 1976. Catalytic oxidation of aqueous Mn(II). J. of Catalysis 41:108-123.

Davies, G. 1969. Some aspects of the chemistry of manganese(III) in aqueous solution. Coor. Chem. Rev. 4:199-224.

Davies, S.H.R., and J.J. Morgan. 1989. Manganese (II) oxidation kinetics on metal oxide surfaces. J. Colloid and Interface Sci. 129:63-77.

Diem, D., and W. Stumm. 1984. Is dissolved Mn^{2+} being oxidized by O_2 in absence of Mn-bacteria or surface catalysis? Geochim. Cosmochim. Acta 48:1571-1573.

Gatte, R.R., and H.A. Laitinen 1974. Studies of heavy metal adsorption by hydrous iron and manganese oxides. Anal. Chem. 46:2022-2026.

Gilkes, R.J., and R.M. McKenzie. 1988. Geochemistry and mineralogy of manganese in soils. p.23-35. *In* R.D. Graham et al. (eds.) Manganese in soil and plants. Kluwer Academic Publishers, The Netherlands.

Godtfredsen, K.L, and A. T. Stone. 1994. Solubilization of manganese dioxide-bound copper by naturally occurring organic compounds. Environ. Sci. Technol. 28:1450-1458.

Hem, J.D. 1978. Redox processes at surfaces of manganese oxide and their effects on aqueous metal ions. Chem. Geol. 21:199-218.

Hersman, L., T. Lloyd, and G. Sposito. 1995. Siderophore-promoted dissolution of hematite. Geochim. Cosmochim. Acta. 59:3327-3330.

Jauregui, M.A., and H.M. Reisenauer. 1982. Dissolution of oxides of manganese and iron by root exudate components. Soil Sci. Soc. Am. J. 46:314-317.

Junta, J.L., and M.F. Hochella Jr. 1996. Manganese(II) oxidation at mineral surfaces: A microscopic and spectroscopic study. Geochim. Cosmochim. Acta. 22:4985-4999.

Kostka, J.E., G.W. Luther III, and K.H. Nealson. 1995. Chemical and biological reduction of Mn(III)-pyrophosphate complexes: Potential importance of dissolved Mn(III) as an environmental oxidant. Geochim. Cosmochim. Acta 59:885-894.

Klewicki, J.E. and J.J. Morgan. 1998. Kinetic behavior of Mn (III) complexes of pyrophosphate, EDTA, and citrate. Environ. Sci. Technol. 32:2916-2922.

Laha, S., and R.G. Luthy. 1990. Oxidation of aniline and other primary aromatic amines by manganese dioxide. Environ. Sci. Technol. 24:363-373.

Lindsay, W.L., and W.A. Norvell. 1978. Development of a DTPA soil test for zinc, iron, manganese, and copper. Soil Sci. Soc. Am. J. 42:421-428.

Luther, G. W. III. 1990. Frontier molecular orbital theory in geochemical processes. p. 173-198. *In* W. Stumm (ed.) Aquatic chemical kinetics: Reaction rates of processes in natural water. Wiley-Interscience, New York.

Luther, G.W. III, B. Sundby, B.L. Lewis, P.J. Brendel, and N. Silverberg. 1997. Interactions of manganese with the nitrogen cycle: alternative pathways to dinitrogen. Geochim. Cosmochim. Acta 61:4043-4052.

Luther, G.W. III, D.T. Ruppel, and C. Burkhard. 1998. Reactivity of dissolved Mn(III) complexes and Mn(IV) species with reductants: Mn redox chemistry without a dissolution step? p. 265-280. *In* D.L. Sparks and T.J. Grundl (eds.) Mineral-water interfacial reactions: Kinetics and mechanisms. ACS Symposium Ser. No. 715, Washington, DC.

Manceau, A. J.C. Harge, C. Bartoli, E. Silvester, J.L. Hazemann, M. Mench, and D. Baize. 1997. Sorption mechanism of zinc and lead on birnessite: Application to their speciation in contaminated soils. p.403-404. *In* I.K. Iskandar et al. (eds.) Fourth International Conference on the Biogeochemistry of Trace Elements. Berkeley, CA.

Meek, B.D., A.J. MacKenzie, and L.B. Grass. 1968. Effects of organic matter, flooding time, and temperature on the dissolution of iron and manganese from soil *in situ*. Soil Sci. Soc. Amer. Proc. 32:634-638.

McBride, M.B. 1989a. Oxidation of dihydroxybenzenes in aerated aqueous suspensions of birnessite. Clays Clay Miner. 37:341-347.

McBride, M.B. 1989b. Oxidation of 1,2- and 1,4-dihydroxybenzene by birnessite in acid aqueous suspension. Clays Clay Miner. 37:470-486.

McKenzie, R. M. 1970. The reaction of cobalt with manganese dioxide minerals. Aust. J. Soil Res. 8:97-106.

Morgan, J.J. 1967. Chemical equilibria and kinetic properties of manganese in natural waters. p. 561-626. *In* S.D. Faust and J.V. Hunter (ed.) Principles and applications of water chemistry. Wiley, New York.

Morin, G., J.D. Ostergren, F. Juillot, P. Ildefonse, G. Calas, and G.E. Brown Jr. 1999. XAFS determination of the chemical form of lead in smelter-contaminated soils and mine tailings: Importance of adsorption processes. Am. Mineral. 84: 420-434.

Naidja, A., P.M Huang, and J.M. Bollag. 1998. Comparison of reaction products from the transformation of catechol catalyzed by birnessite or tyrosinase. Soil Sci. Soc. Am. J. 62:188-195.

Randall, G.W., E.E. Schulte, and R.B. Corey. 1976. Correlation of plant manganese with extractable soil manganese and soil factors. Soil Sci. Soc. Am. J. 40:282-287.

Reisenauer, H.M. 1988. Determination of plant-available soil manganese. p. 87-98. *In* R.D. Graham et al. (eds.) Manganese in soil and plants. Kluwer Academic Publishers, The Netherlands.

Silvester, E., A. Manceau, and V.A. Drits. 1997. Structure of synthetic monoclinic Na-rich birnessite and hexagonal birnessite: II. Results from chemical studies and EXAFS spectroscopy. Am. Mineral. 82:962-978.

Sparks, D.L. 1989. Kinetics of soil chemical processes. Academic Press, New York.

Sparks, D. L. 1995. Environmental soil chemistry. Academic Press, New York.

Steelink, C. 1964. Free radical studies of lignin, lignin degradation products and soil humic acid. Geochim. Cosmochim. Acta. 28:1615-1622.

Stone, A.T., and J. J. Morgan. 1984a. Reduction and dissolution of manganese (III) and manganese (IV) oxides by organics. 1. Reaction with hydroquinone. Environ. Sci. Technol. 18:450-456.

Stone, A.T. and J. J. Morgan. 1984b. Reduction and dissolution of manganese (III) and manganese (IV) oxides by organics. 2. Survey of the reactivity of organics. Environ. Sci. Technol. 18:617-624.

Stumm, W., and R. Giovanoli. 1976. On the nature of particulate manganese in simulated lake waters. Chimia 30:423-425.

Tan, K.H., R.A. Leonard, A.R. Bertrand, and S.R. Wilkinson. 1971. The metal complexing capacity and the nature of the chelating ligands of water extract of poultry litter. Soil Sci. Soc. Amer. Proc. 35:265-269.

Wang, M.C., and P.M. Huang. 1987. Polycondensation of pyrogallol and glycine and the associated reactions as catalyzed by birnessite. Sci. Total Environ. 62:435-442.

Wang, M.C., and P.M. Huang. 1992. Significance of Mn(IV) oxide in the abiotic ring cleavage of pyrogallol in natural environments. Sci. Total Environ. 113:147-157.

Wang, D., J.Y. Shin, M.A. Cheney, G. Sposito, and T.G. Spiro. 1999. Manganese dioxide as a catalyst for oxygen-independent atrazine dealkylation. Environ. Sci. Technol. 33:3160-3165.

Weil, R.R., C.D. Foy, and C.A. Coradetti. 1997. Influence of soil moisture regimes on subsequent soil manganese availability and toxicity in two cotton genotypes. Agron. J. 89:1-8.

White, G. N. and J. B. Dixon. 1996. Iron and manganese distribution in nodules from a young Texas vertisol. Soil Sci. Soc. Am. J. 60:1254-1262.

Xyla, A.G, B. Sulzberger, G.W. Luther III, J.G. Hering, P. van Cappellen, and W. Stumm. 1992. Reductive dissolution of manganese (III,IV) (hydr) oxides by oxalate: The effect of pH and light. Langmuir 8:95-103.

Yamaguchi, K.S., and D.T. Sawyer. 1985. The redox chemistry of manganese (III) and –(IV) complexes. Israel J. of Chem. 25:164-176.

Chapter 2

KINETICS AND MECHANISM OF BIRNESSITE REDUCTION BY CATECHOL

2.1 Abstract

The complex interactions of oxidizable organic ligands with soil Mn(III,IV) (hydr) oxide minerals have received little study by *in situ* spectroscopic techniques. We used a combination of an *in situ* electron paramagnetic resonance stopped-flow (EPR SF) spectroscopic technique and stirred-batch studies to measure the reductive dissolution kinetics of birnessite (δ-MnO_2), a common Mn mineral in soils, by catechol (1,2-dihydroxybenzene). The reaction was rapid, independent of pH, and essentially complete within seconds under conditions of excess catechol at pH 4 to 6. The overall empirical second-order rate equation describing the reductive dissolution rate was $d[Mn(II)]/dt = k[CAT]^{1.0}[SA]^{1.0}$ where $k=4\ (\pm 0.5) \times 10^{-3}$ L m^{-2} s^{-1} and [CAT] and [SA] are the initial concentrations in *M* and m^2 L^{-1}. In the process at early times, catechol was oxidized to the two-electron o-quinone product. The energy of activation (E_a) for the reaction was 59 ($\pm$7) kJ mol^{-1} and the activation entropy ($\Delta S^{\ddagger}$) was -78 $\pm$ 22 J mol^{-1} K^{-1}, suggesting that the reaction was surface-chemical controlled and occurs

by an associative mechanism. Rates of catechol disappearance from solution with simultaneous Mn(II) and o-quinone production were comparable. These data strongly suggest that precursor surface-complex formation is rate-limiting and that electron transfer is rapid. The rapid reductive dissolution of birnessite by catechol has significant implications for C and Mn cycling in soils and the availability of Mn to plants.

2.2 Introduction

Behavior of Mn in soils and geochemical sediments is generally assumed to be mediated by redox reactions. Oxides and hydroxides containing Mn(III) and Mn(IV) can oxidize organic ligands more rapidly than O_2 based on frontier molecular orbital theory (FMOT) considerations (Luther, 1990). Aromatic and nonaromatic ligands have been reported to reductively dissolve Mn(III,IV) (hydr)oxides (Stone and Morgan, 1984a,b) with the formation of polymeric reaction products that resemble soil humic substances (Shindo and Huang, 1982; Shindo and Huang, 1984). Sorbed contaminants can be released into solution following reductive dissolution of solid Mn(III,IV) (hydr)oxides by organic ligands and reactive compounds may be sorbed or coprecipitated as a consequence of hydrolysis of the Mn(II) that is released (Xyla et al., 1992; Godtfredsen and Stone, 1994; Larsen and Postma, 1997). Thus, redox cycling of Mn is dynamic and coupled to geochemical cycling of other metals, C turnover in soils, and N transformations in soils and marine sediments (Hem, 1978; Bartlett, 1981;

Wang and Huang, 1987; Laha and Luthy, 1990; Wang and Huang, 1992; Luther et al., 1997; Naidja et al., 1998).

Pivotal early investigations into oxidizable organic ligand reactions with solid Mn(III,IV) (hydr)oxides reported that the formation of a precursor surface complex is requisite to electron transfer and that inner-sphere electron transfer or reactions involving surface species were rate-limiting (Stone and Morgan, 1984a,b; Xyla et al., 1992). No direct measurements of reductant sorption can be made in most reductive dissolution studies because of the rapid reduction of Mn (III,IV) (hydr)oxides. However, dissolution rates are directly proportional to the concentration of the surface complex (Xyla et al., 1992). The only direct line of evidence in support of an inner-sphere mechanism was the study conducted by Gordon and Taube (1962) using ^{18}O-labeled water. These authors found that the UO_2^{2+} produced by the reaction of MnO_2 with U(IV), derived both oxygen atoms from MnO_2.

Previous EPR spectroscopic measurements showed that initial Mn(II) release from birnessite after reaction with catechol was rapid followed by a slower release over time (McBride, 1989a,b). However, no rate coefficients describing Mn(II) release were measured in these systems. The disequilibrium in aqueous redox reactions commonly observed in the field (Lindberg and Runnels, 1984) underscores the need for kinetic studies (Sparks, 1989; Bartlett and James, 1993; Stone et al., 1994).

Recent investigations have demonstrated that dynamic redox reactivity of Mn(III,IV) (hydr)oxide mineral surfaces catalyzes abiotic degradation of organic pollutants (Ukrainczyk and McBride, 1993a,b; Dec and Bollag, 1994; Pizzigallo et al., 1995; Cheney et al., 1996). In fact, oxidation of catechol to CO_2 by birnessite has been reported and could contribute to significant abiotic degradation of organic contaminants in natural settings (Wang and Huang, 1992; Naidja et al., 1998). This finding is surprising because degradation of organic pollutants has generally been attributed to biological activity.

From this discussion, it is evident that oxidizable organic ligand interactions with Mn(III,IV) (hydr)oxide minerals in soils are complex. Soil Mn oxides are the principal source of plant available Mn(II) and, thus, pathways of reduction influence plant toxicity and disease resistance (Schulze et al., 1995a). Better understanding of the chemistry of these interactions improves our ability to make sound predictions about contaminant fate, cleanup, and plant available Mn(II). Most of the available reductive dissolution kinetics data have been macroscopic measurements (Stone et al., 1994) with few *in situ* spectroscopic studies.

To adequately understand the complex reactivity of Mn(III,IV) (hydr)oxides with organic ligand reductants in soils, however, it is best to begin with simpler model systems and combine *in situ* molecular-level spectroscopic techniques with macroscopic investigations to provide mechanistic kinetic information (Sparks, 1995). In this regard, catechol is a suitable model organic ligand because ortho-type

semiquinones have been identified in soil humic substances (Steelink, 1964), catechols are common intermediates in pesticide degradation pathways (Alexander, 1977), and they have been identified on siderophore molecules (Hersman et al., 1995). Birnessite is a suitable model mineral because it is one of the most commonly identified Mn oxide minerals in soil and geochemical environments (McKenzie, 1989). Our approach to the problem, then, involved a study of the kinetics and mechanism of reductive dissolution of well-characterized birnessite by catechol using *in situ* EPR-SF and stirred-batch techniques.

2.3 Materials and Methods

2.3.1 Birnessite Preparation and Characterization

Birnessite was synthesized according to procedures outlined by McKenzie (1971) by reduction of boiling $KMnO_4^-$ with concentrated HCl. The precipitate was vacuum filtered, dialyzed against deionized water to remove salts, and freeze-dried. Total concentrations of Mn and K were determined by dissolving a known solid weight with 12 *M* HCl and acidified $NH_2OH \bullet HCl$. Powder X-ray diffraction (XRD) analysis revealed that diagnostic d-spacings for birnessite agreed with published values (Table 2.1). Point of zero charge (PZC) was estimated by three different methods: microelectrophoretic mobility measurements, Ca^{2+} sorption experiments, and potentiometric titrations using NaCl as the background electrolyte. Oxidation state was measured iodometrically using a starch end point and standardized thiosulfate

Table 2.1 Selected physical and chemical properties of birnessite.

Property	Birnessite	
Total Mn, %	49.1	± 0.1†
Total K, %	16.0	± 0.1
Crystalline H_2O, %	12.4	
Mean Oxidation State	3.4	± 0.1
BET Surface Area, $m^2 g^{-1}$	40.0	
PZC	2	
$P_2 O_7^{4-}$ Mn(III), %	10.0	
XRD, nm	0.736, 0.362, 0.246, 0.142	

† Standard error of the mean.

solution (Murray et al., 1984; Amonette et al., 1994). Pyrophosphate ($P_2O_7^{4-}$)-extractable Mn(III) was measured by reacting large excesses of $P_2O_7^{4-}$ (50m*M*) with birnessite (~2.7 m*M* Mn_T) at pH 4 and 23°C or 33°C using published procedures (Diebler and Sutin, 1964; Davies, 1969; Kostka et al., 1995). High resolution thermogravimetric analysis (HRTGA, TA Instruments) was used to measure both structural and adsorbed H_2O contents. High resolution ramp mode at a heating rate of 10°C min^{-1} under flowing N_2 was used with Pt crucibles to measure total H_2O content, which is operationally defined as the weight loss after heating to 300°C (Moore et al., 1990).

Birnessite was further characterized using x-ray absorption spectra recorded at beamline X-11A at the National Synchrotron Light Source, Brookhaven National Laboratory, Upton, NY. Beam energy was calibrated to the K-absorption edge of Mn metal foil (6539 eV). The spectra were collected in fluorescence mode using a Lytle detector and compared with a standard Mn(IV) dioxide phase pyrolusite (β-MnO_2). Corundum (α-Al_2O_3) was used as a diluent to minimize self-absorption effects (Schulze et al., 1995b). Comparison of pre-edge XANES spectra of birnessite to reference pyrolusite (iodometric oxidation state of 3.92) showed agreement with published pre-edge energies reported by Manceau et al. (1992). Recent structural refinements of this mineral phase have shown that structural Mn(III) is present in birnessite, often substituted for Mn(IV) in the lattice (Drits et al., 1997; Silvester et al.,

1997). External surface area was measured by the BET procedure using N_2 (g) as the adsorbate (Brunauer et al., 1938).

2.3.2 Stirred-Batch Experiments

Stirred-batch reductive dissolution rate experiments were conducted using a pH-stat (± 0.1 pH units) technique while purging with purified N_2 at 10, 15, 18, and 23° C. Temperature was controlled with a circulating water bath. Birnessite mineral suspensions were dispersed by sonification and pretreated at the experimental pH value and ionic strength prior to catechol addition. Reactions were initiated by addition of a weighed aliquot of catechol stock solution buffered to the desired pH with dilute 0.1 *M* NaOH or 0.1 *M* HCl. Catechol stock solutions were freshly prepared prior to each experimental run. Sample aliquots were removed at increasing time intervals and passed through a 0.2-μm pore-size membrane filter into a tared plastic tube and acid-quenched. Soluble Mn in the filtrates was measured with flame atomic absorption spectrometry (AAS). The UV-VIS spectra of the filtrates in 1-cm cuvettes were recorded to follow formation of products during the reaction sequence using an HP 8452A Diode Array UV-VIS spectrophotometer. Literature values of ε for the o-quinone monomer were taken from Mentasti et al. (1975) as 1460 M^{-1} cm^{-1} at 390 nm. For catechol, Beer's law was obeyed at concentrations ≤ 0.5 m*M* catechol at 276 nm and yielded ε=2380 M^{-1} cm^{-1}. Corrections were made for removal of suspension volume from the batch reactor during sampling in calculating acid consumption.

Mn(II) that was added concurrently with catechol at the beginning of the kinetic run had a negligible influence on the overall reductive dissolution rate. No significant differences were observed between the presence and absence of a N_2 purge.

2.3.3 EPR-SF Kinetic Studies

Reductive dissolution of birnessite by catechol was followed *in situ* using an EPR-SF technique (Klimes et al., 1980; Stach et al., 1985; Fendorf et al., 1993) to measure Mn (II) release and detect possible semiquinone intermediates. The six-line diagnostic EPR spectra confirmed that birnessite was reduced to Mn(II) during the reaction with catechol (Figure 2.1). The hyperfine spectrum of high spin Mn(II) is due to coupling of the electron spin (S=5/2) to the nuclear spin (I=5/2) of the ^{55}Mn ion.

Spectra were recorded at room temperature ($23^{\circ} \pm 0.5^{\circ}$ C) and a microwave frequency of 9.55 GHz (X-band) using a Bruker ESP 300E spectrometer. Mixed samples were injected by the stopped-flow (SF) unit (Update Instruments, Inc., Madison, Wisconsin) into a flow-through quartz flat aqueous cell (Wilmad Glass Co., Buena, NJ) inserted in a TE_{102} resonator. A microwave power attenuation of 30 dB and modulation amplitude of 10^{-3} T were employed and this power rating was checked to ensure that no saturation effects occurred for the highest Mn (II) concentration (Luca and Cardile, 1989). When the entire six-line spectrum for Mn(II) was desired, field-sweep mode was used ($\pm$ 0.05 T). Data processing was done with BRUKER software (WINEPR). Stopped-flow kinetic measurements were made with ms time resolution in time-sweep mode by centering on the *increase* in intensity of the fourth

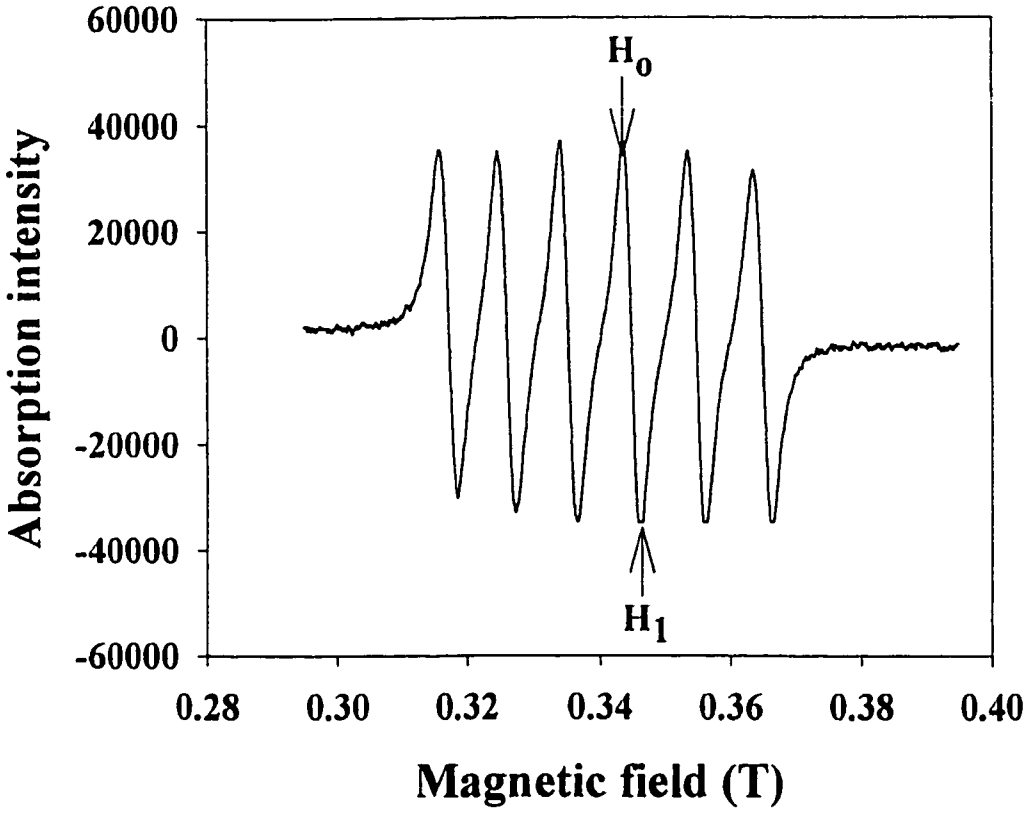

Figure 2.1 Representative room temperature EPR spectrum of 100 μM Mn_T as birnessite (0.45 m^2L^{-1}) reacted with catechol (5×10^{-3} M) depicting the characteristic six-line spectrum of the Mn(II) product. H_0 and H_1 indicate the peak and valley used to quantify Mn(II) concentrations.

downfield resonance peak (H_o in Figure 2.1) at 0.3435 T (g = 1.98) during the reaction sequence. This peak is the most suitable one for quantitative measurements of Mn(II) (Carpenter, 1983). This approach has been used by others in EPR-SF studies (Fendorf et al., 1993). A parallel experiment centering on the "valley" at 0.346 T (H_1 in Figure 2.1) showed a decrease in intensity with time which confirmed that H_0 intensities corresponded to release of Mn(II) following reductive dissolution of birnessite. Signal intensities were converted to concentration using $MnCl_2$ standards prepared in the same suspension matrix as the samples. The same $MnCl_2$ standards were analyzed with flame AAS to intercorrelate the methods. The EPR technique yielded a linear response to Mn(II) between 5 and 200 μM (Figure 2.2).

The SF system consisted of a syringe ram (model 1019), ram controller (model 715), 2-mL syringes, and a Wiskind-grid mixing cell. The mixing cell had a dead volume of 1.6 μL. Details of this system can be found elsewhere (Hubbell et al., 1987). The mixing cell was attached by tubing to the quartz flat aqueous cell located in the EPR cavity. Before starting the reaction, the magnetic field was swept to ensure no residual Mn(II) remained in the flat cell between experimental runs.

Kinetic studies were conducted under pseudo-first-order conditions with either catechol or birnessite in excess. Catechol concentrations ranged from 200 μM-10,000 μM and birnessite suspension surface area concentrations ranged from 0.45 $m^2\ L^{-1}$-4.5 $m^2\ L^{-1}$. Total Mn concentrations as birnessite (100 μM-500 μM) when in defect (catechol in excess) reflect typical environmental concentrations of Mn. Experiments

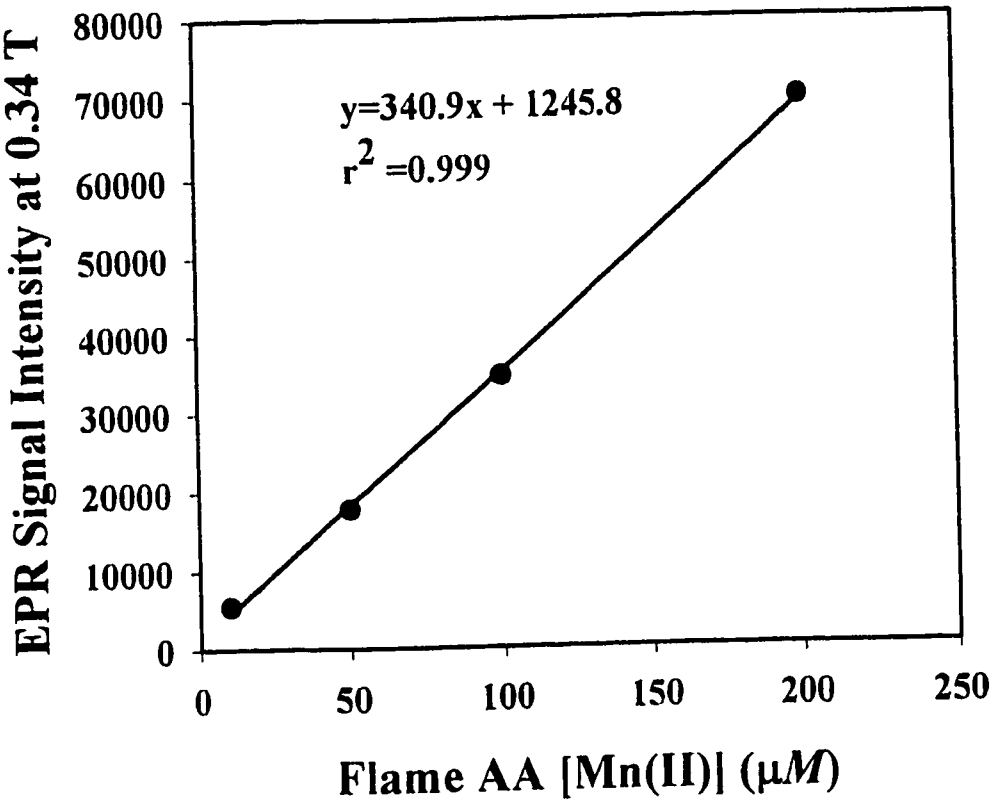

Figure 2.2 Intercalibration standard curve relating EPR signal intensity at the 0.34 T (H_o) peak to flame AAS Mn(II) concentration.

were conducted at initial pH values of 4, 4.5, 5, and 6 as maintained by a 50 m*M* K-acetate buffer. Additional experiments indicated that K-acetate buffer did not significantly influence Mn(II) release rates when compared to the pH-stat method. Adjustments of the buffer to the desired pH were made with aliquots of concentrated HCl and pH was measured with a model 25 pH/ion meter (Fisher-Scientific). Small drifts in pH values (± 0.05) during the reactions were due to the finite capacity of the K-acetate buffer. The low ionic strength coupled with the dilute solids concentration was sufficient to keep birnessite dispersed during the time period of the experimental runs. In addition, birnessite suspensions were sonified prior to filling the inport syringes. Sweep times were set to either 20 or 83s, depending on the experimental conditions, with a temporal resolution of 4096 time steps. The data collection software was configured to automatically trigger a series of field-sweeps of the reacted suspensions immediately after time-sweep mode kinetic measurements to ensure that there were no shifts in the resonance peak and to assist in quantifying final Mn(II) concentrations. The method of initial rates (Lasaga, 1981) was used to ensure that the forward reaction predominated and competing reactions with catechol oxidation products were not operative (Stone, 1987; Sparks, 1995).

2.4 Results and Discussion

2.4.1 EPR-SF Kinetic Studies

Reductive dissolution of birnessite by catechol is favored thermodynamically between pH 4 to 6 (Bricker, 1965; Mihailovic and Cekovic, 1971) assuming the following stoichiometry:

$$\delta\text{-}MnO_2\ (s) + \text{ortho-}C_6H_4(OH)_2 + 2H^+ \rightarrow Mn(II)(aq) + \text{ortho-}C_6H_4O_2\ (aq) + 2H_2O \quad [1]$$

$$\Delta G_r = -50.6\ kJ\ mol^{-1}\ (pH\ 6),\ -96.1\ kJ\ mol^{-1}\ (pH\ 4)$$

Representative EPR-SF kinetics of the reductive dissolution of birnessite by catechol revealed that the reaction was rapid and essentially complete in < 10s when catechol is in excess (Figure 2.3). In a previous study with feitknechtite (Stone and Morgan, 1984a), the rate of Mn(II) production as a function of birnessite concentration, catechol concentration, and pH, was described by

$$d[Mn(II)]/dt = k_{obs}\,[CAT]^a\,[SA]^b\,[H^+]^c \quad [2]$$

where d[Mn(II)]/dt is the rate of Mn(II) production ($M\ s^{-1}$), [CAT] is the initial concentration of catechol (M), [SA] is the surface area concentration of the birnessite suspension ($m^2\ L^{-1}$), $[H^+]$ is the hydrogen ion concentration (M), k_{obs} is the apparent rate constant, and a, b, and c are the reaction orders with respect to the given reactants. The initial rate approach (Lasaga, 1981) was employed to determine the empirical rate equation. The value for d[Mn(II)]/dt was taken from the initial linear slopes when <20% of the reaction had occurred.

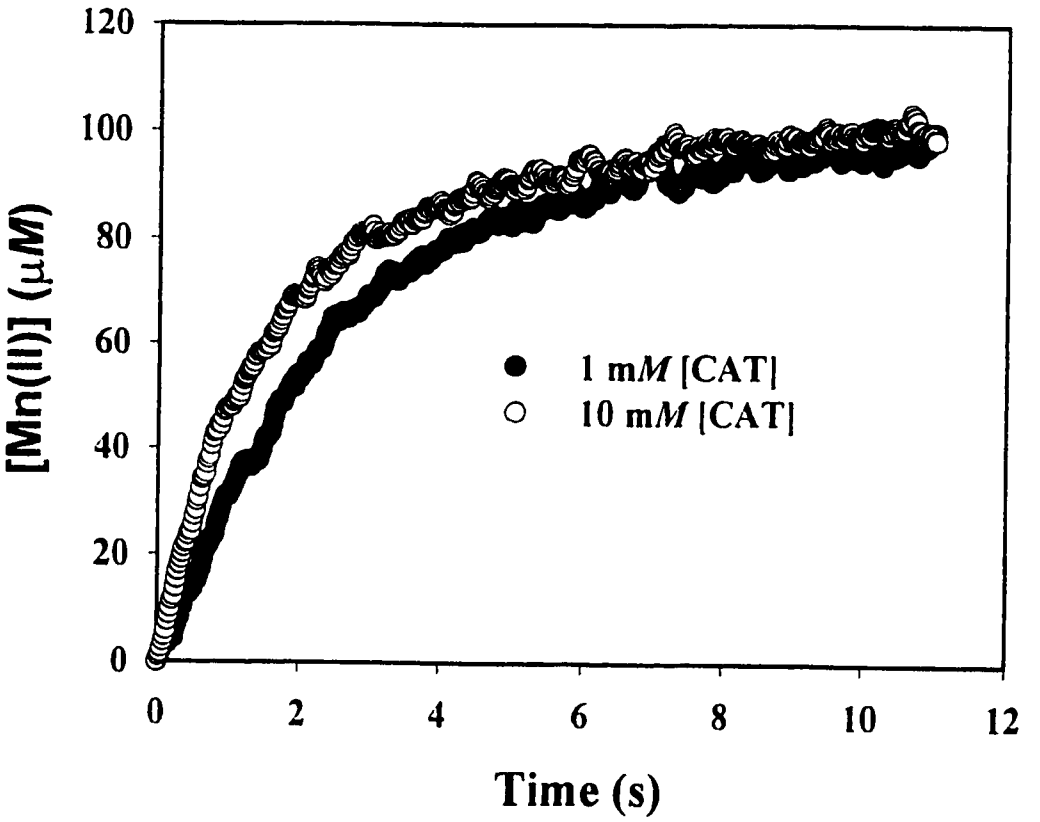

Figure 2.3 Representative EPR-SF kinetics of reductive dissolution of birnessite by catechol at pH 4 as a function of [CAT] conducted at 23°C and 0.45 m^2 L^{-1} [SA].

An initial rate plot of log [Mn(II)] release versus log [CAT] was linear (r^2=0.95) with a slope (a) of 1.06, indicating a first order dependence of the reaction rate on [CAT] at pH 4 (Figure 2.4a). The pseudo-first-order rate coefficient, k', was shown from the y-intercept to be 5×10^{-3} s^{-1}. By considering the nonvaried reactant, the rate constant k_{graph} was calculated by the following relationship

$$k' = k_{graph} [SA]^b \quad [3]$$

resulting in a value of 5.55×10^{-3} L m^{-2} s^{-1}. This value agreed with the average k_{calc} determined from the empirical second-order equation and relevant data in Table 2.2 (average $k_{calc} = 4 \times 10^{-3}$ L m^{-2} s^{-1} for [CAT] of 10^{-3}-10^{-2} *M*, [SA]=0.9 m^2 L^{-1}, $[H^+] = 10^{-4}$ *M*). Similiarly, the initial rate plot for [SA] was linear (r^2=0.95) with a first-order dependence on [SA] (Figure 2.4b). The k_{graph} value obtained from the y-intercept of 2.6×10^{-3} L m^{-2} s^{-1} was in good agreement with the average k_{calc} of 2.6×10^{-3} L m^{-2} s^{-1} (Table 2.2). The initial rate of Mn(II) release from birnessite was virtually independent of pH with a slope near 0 in the pH range 4 to 6 (Figure 2.5). In their studies with feitknechtite, Stone and Morgan (1984a) reported a first-order dependence on both hydroquinone and suspension loading, but a reaction order of 0.46 for $[H^+]$. The overall empirical second-order rate equation describing the reductive dissolution of birnessite by catechol can be written as

$$d[Mn(II)]/dt = k[CAT]^{1.0} [SA]^{1.0} \quad [4]$$

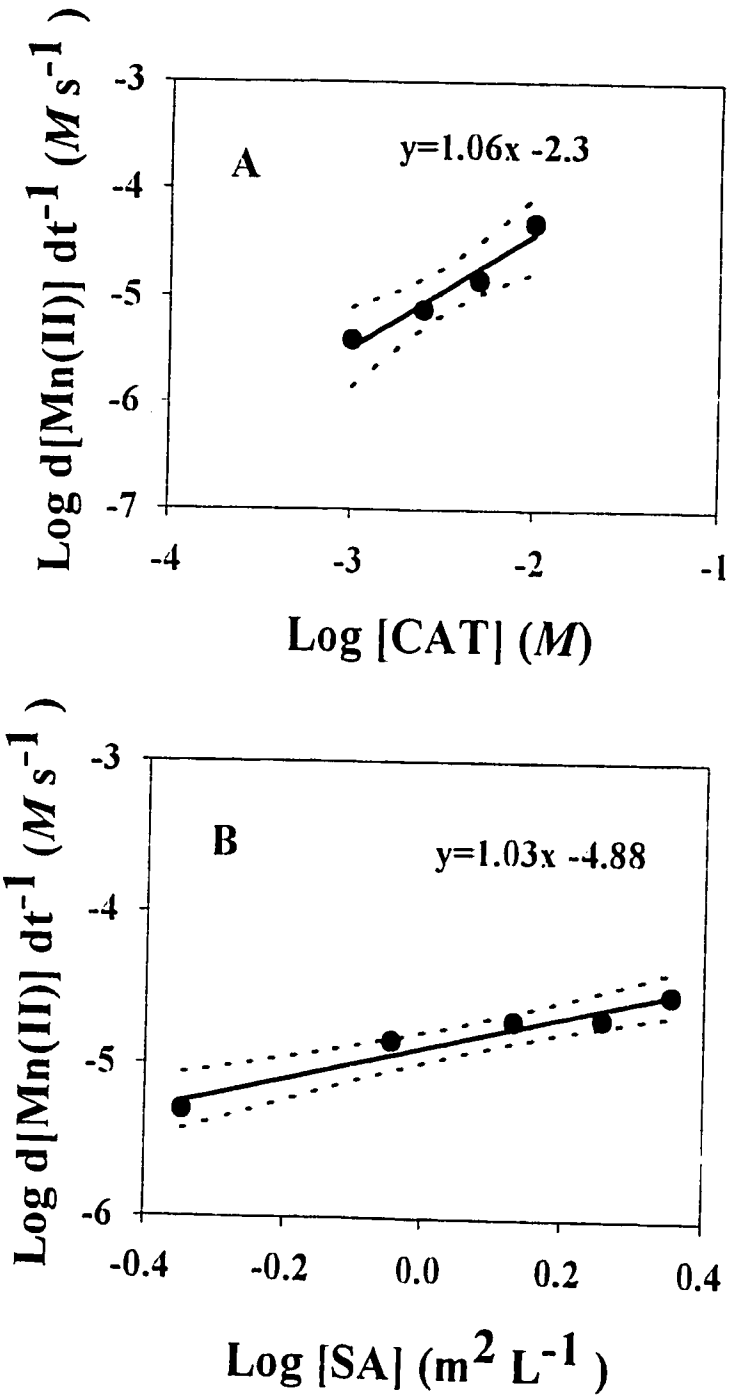

Figure 2.4 Representative initial reaction rates measured by the EPR-SF technique as a function of: (A) [CAT] at pH 4 and 0.90 m^2 L^{-1} [SA] and (B) [SA] at pH 4 and 5×10^{-3} M [CAT]. The dotted lines represent the 95% confidence interval bands.

Table 2.2 Representative experimental conditions used to measure EPR-SF kinetic data.

[CAT]	$[H^+]$	[SA]	k_{calc}	
—— $\times 10^{-2}$ *M* ——		$m^2 L^{-1}$	$\times 10^{-3}$ L m^{-2} s^{-1}	
1.0	10^{-2}	0.9	5.3	± 0.5†
0.5	10^{-2}	0.9	3.2	
0.3	10^{-2}	0.9	3.4	
0.1	10^{-2}	0.9	4.3	± 0.1
1.0	10^{-4}	0.9	4.3	± 0.3
0.5	10^{-4}	0.9	5.6	
0.3	10^{-4}	0.9	4.4	
0.1	10^{-4}	0.9	4.5	± 0.1
0.5	10^{-2}	0.5	2.2	± 0.2
0.5	10^{-2}	1.4	2.8	
0.5	10^{-2}	1.8	2.2	± 0.2
0.5	10^{-2}	2.3	2.6	

†Standard error of the mean.

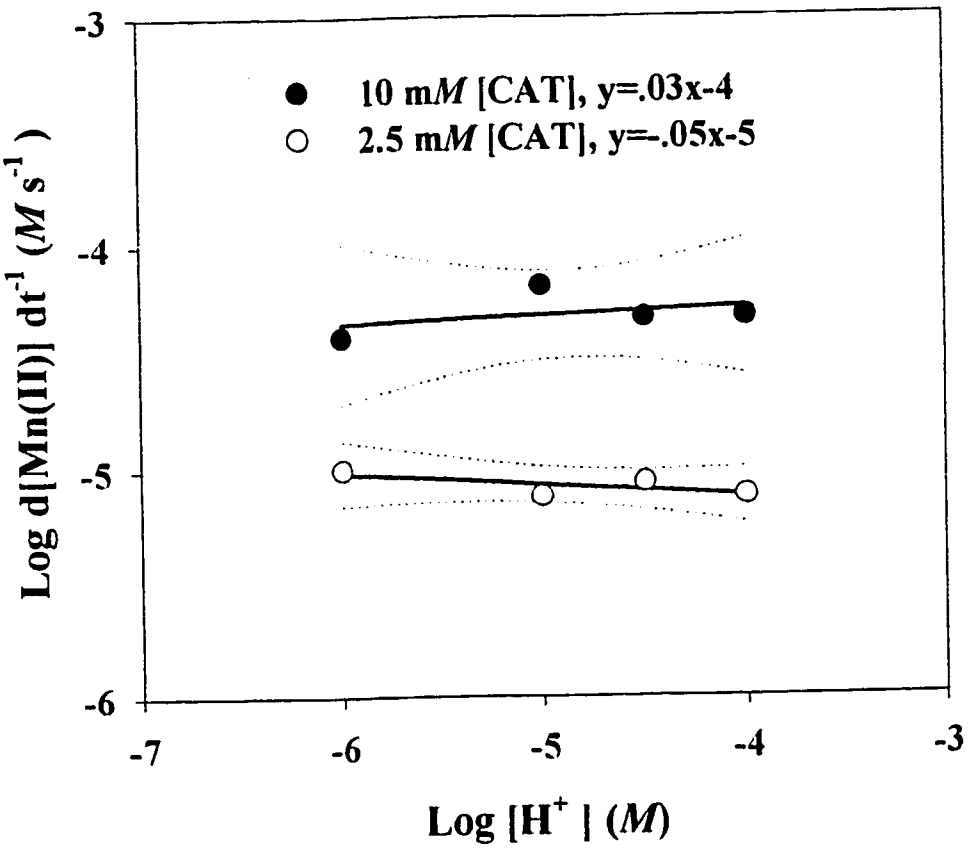

Figure 2.5 Initial reductive dissolution rates measured by EPR-SF as a function of [H^+] and [CAT] at 0.90 m^2 L^{-1} [SA]. The dotted lines represent the 95% confidence intervals.

where k=4 (±0.5) × 10^{-3} L m^{-2} s^{-1} and [CAT] and [SA] are the initial concentrations in *M* and m^2 L^{-1}. The reasonable agreement between the apparent second-order rate constants k_{graph} and k_{calc} provides further support for the proposed rate equation.

It was anticipated that changes in pH might cause changes in the reductive dissolution rate of solid Mn-(III,IV) minerals by oxidizable organic ligands based on previous reports (Stone and Morgan, 1984a; Stone, 1987; Ukrainczyk and McBride, 1992; Xyla et al., 1992) through (1) readsorption of Mn(II) at higher pH; (2) proton-promoted dissolution at lower pH; (3) a change in the thermodynamic driving force for the reaction; (4) increased sorption of catechol on the pH-dependent charged surface of birnessite; and (5) speciation of catechol due to dissociation of the phenolic hydroxyl groups. The general lack of a pH effect may be explained by a combination of the low point of zero charge of the birnessite surface with the following pK'-s (Balistrieri and Murray, 1982):

$$>Mn^{IV}OH_2^+ \leftrightarrow > Mn^{IV}OH + H^+ \qquad pK_{a1} = 2.3 \qquad [5]$$

$$>Mn^{IV}OH \leftrightarrow > Mn^{IV}O^- + H^+ \qquad pK_{a2} = 3.3 \qquad [6]$$

and the low fraction of dissociated catechol (0.02%) calculated at the highest experimental pH (pH=6) based on the pK_{a1}= 9.7 and pK_{a2}= 13.7. The protonated form, the dominant catechol species under our experimental conditions, is generally considered less reactive toward oxidation than the deprotonated catecholate. These

findings imply that the sorption affinity of birnessite for catechol to form a precursor surface complex should remain constant over the pH range employed.

Stability constants for sorption of organic ligands on metal (hydr)oxide surfaces are often proportional to stability constants for the metal-ligand complex in solution (Kummert and Stumm, 1980). Tris-$Mn^{IV}(cat)_3^{2-}$ and bis-$Mn^{III}(cat)_2^-$ complexes form in solution but are better described as $Mn^{II}(semi)_2(cat)^{2-}$ and $Mn^{II}(semi)(cat)^-$ because of internal metal-ligand redox reactions that convert catechol ligands to semiquinone ligands (Richert et al., 1988). The catechol to Mn(IV) ligand-to-metal-charge-transfer (LCMT) band was reported at 585 nm (Hartman et al., 1984) and the catechol to Mn(III) LCMT band between 550 nm and 750 nm (Magers et al., 1978). Chemisorption of catechol in 1:1 bidentate surface chelate complexes (Kummert and Stumm, 1980; McBride and Wesselink, 1988) and 2:1 surface Ti:catechol ratios (Rodriguez et al., 1996) have been invoked and may resemble the surface complex between catechol and surface Mn in this study. Five-membered ring chelates are favored in coordination for steric and entropic reasons (Shriver et al., 1994). The "bite" (O-O) distance in the catecholate ligand of 2.77 Å may be compatible with surface Mn-Mn distances (assuming a 110 cleavage plane) in birnessite of 2.85 Å, suggesting that catechol may also form a binuclear precursor surface complex. The ability of catechol to bind two surface Mn metal centers may explain the observed rapid reductive dissolution rate. It should be pointed out that there is no spectroscopic evidence confirming the structure of the catechol-birnessite

precursor surface complex, but past infrared spectroscopic studies have shown that it is difficult to identify (McBride, 1987). Currently, work in our laboratory is being conducted to observe the LCMT bands on the reacted birnessite using diffuse reflectance spectroscopy. Despite unfavorable sorption interactions between uncharged catechol (pK_{a1}= 9.7, pK_{a2}= 13.7) and the highly negatively-charged birnessite surface (PZC = 2.3), in the pH range of most soils, catechol is extremely efficient at solubilizing Mn.

2.4.2 Stirred-Batch Studies

In the stirred-batch studies, catechol underwent oxidative transformation during reaction with an excess of birnessite (4.5 m^2 L^{-1}) at pH 4 to form o-quinone with concomitant release of Mn(II) (Figure 2.6). Near complete mass balance indicates that the amount of catechol that reacted with birnessite can be accounted for by the production of the o-quinone monomer, the oxidation product expected to form via a two-electron transfer. These results confirm the stoichiometry in Eq. [1]. At longer times (>2 min), competing reactions involving the unstable o-quinone monomer and water are operative (Dawson and Nelson, 1938; Mason, 1949). The less than predicted [H^+] consumption agreed with the lack of direct [H^+] participation in the observed rate equation under our experimental conditions. First order rate plots (data not shown) were linear for catechol disappearance from solution (r^2> 0.99) and yielded a pseudo-first order rate coefficient k_c for catechol disappearance of 0.70

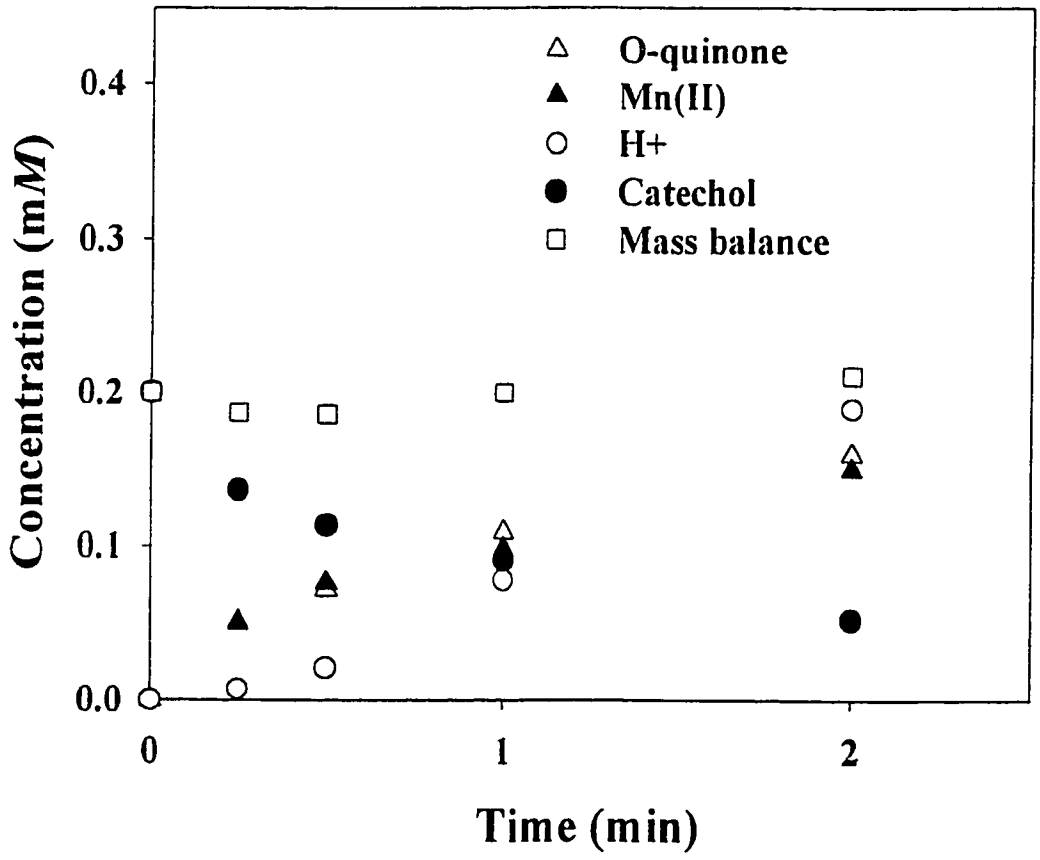

Figure 2.6 Kinetics of catechol oxidation to o-quinone by birnessite and Mn(II) release at 23°C. Experimental conditions were: [CAT] =0.2m*M*, [SA]=4.5 m^2 L^{-1}([Mn_T] =1m*M*), pH 4, I=0.01 *M* NaCl.

(±0.18) min^{-1}. This compares well with the kinetics of o-quinone and Mn(II) appearance (k_o =0.61 min^{-1} and k_m=0.55 min^{-1}) indicating that electron transfer was rapid. These results strongly suggest that catechol sorption to form a precursor surface complex was rate-limiting and product sorption was not affecting the reaction rate.

The suggestion that precursor surface complex formation was rate-limiting is supported by the activation parameters (Table 2.3) derived by Arrhenius and Eyring plots (Figure 2.7). The activation energy (E_a) of 59 (±7) kJ mol^{-1} suggests that the reaction was surface-chemical controlled (Lasaga, 1981; Sparks, 1989; Sparks, 1995) and agrees with previous reductive dissolution studies (Stone and Morgan, 1984a). Other investigators have proposed that electron transfer was the rate-limiting step and have treated precursor complex formation as a preequilibrium step (Stone and Morgan, 1984a; Stone and Morgan, 1987). The high positive value for $\Delta H^{\ddagger}$ (56 ±7 kJ mol^{-1}) and negative value for $\Delta S^{\ddagger}$ (-78 ± 22 J mol^{-1} K^{-1}) suggests the possibility of a bimolecular step which is common to second-order reactions (Espenson, 1995). The observed second-order rate constant measured from EPR-SF studies indicated a more rapid reaction than would be expected from the high activation energy. However, the high activation energy can be compensated for by the large negative $\Delta S^{\ddagger}$ value to yield a fast reaction (Espenson, 1995).

Table 2.3 Activation parameters describing the reductive dissolution of birnessite by catechol.

Parameter	Birnessite/Catechol System	
E_a†, kJ mol^{-1}	58.7	± 6.6§
ln A	21.1	± 2.7
$\Delta H^{\ddagger}$, kJ mol^{-1}	56.2	± 6.6
$\Delta S^{\ddagger}$, J mol^{-1} K^{-1}	-77.9	± 22.4
$\Delta G^{\ddagger}$, kJ mol^{-1}	32.9	± 13.3

†E_a (energy of activation), ln A (pre-exponential factor), $\Delta H^{\ddagger}$(enthalpy of activation), $\Delta S^{\ddagger}$ (entrophy of activation), and $\Delta G^{\ddagger}$ (free energy of activation) were derived from Arrhenius and Eyring plots.
§ Standard error of the mean.

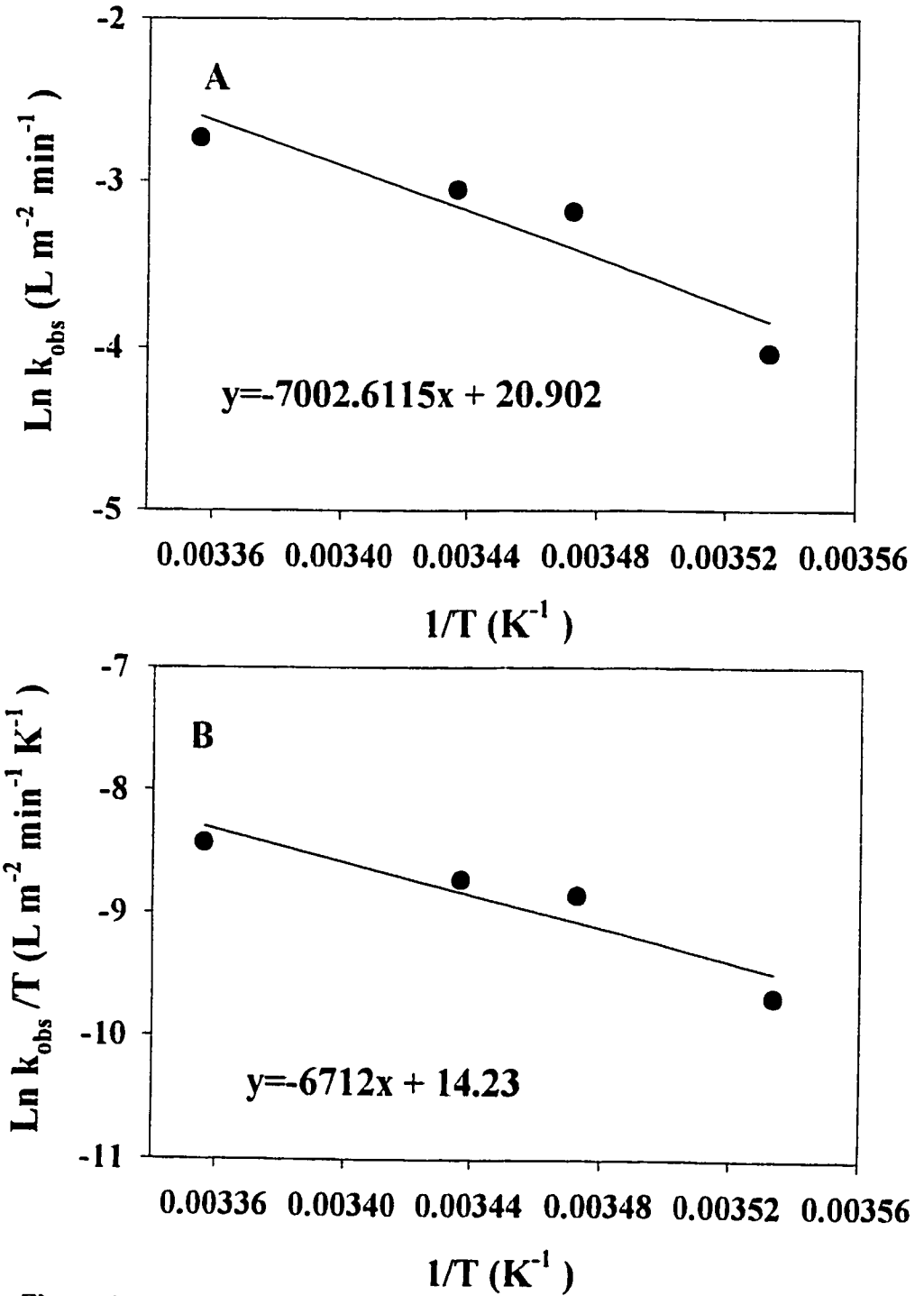

Figure 2.7 Activation parameters derived from (A) Arrhenius and (B) Eyring plots describing the reductive dissolution of birnessite by catechol.

2.4.3 Proposed Reaction Mechanism

These results provide further support for the general reaction mechanism initially proposed by Stone and Morgan (1984a) for reductive dissolution of Mn oxides. Formally, the reaction scheme includes the following steps:

Precursor surface complex formation:

$$C_6H_4(OH)_2\ (aq) + >\delta\text{-}MnO_2\ (s) \underset{k_{-1}}{\overset{k_1}{\leftrightarrow}} >\delta\text{-}MnO_2\text{-}C_6H_4(OH)_2\ (s) \qquad [7]$$

Electron transfer within the surface complex:

$$>\delta\text{-}MnO_2\text{-}C_6H_4(OH)_2\ (s) \underset{k_{-2}}{\overset{k_2}{\leftrightarrow}} >Mn(II)\text{-}C_6H_4O_2\ (s) + 2OH^- \qquad [8]$$

Product release:

$$>Mn(II)\text{-}C_6H_4O_2\ (s) \underset{k_{-3}}{\overset{k_3}{\leftrightarrow}} Mn(II)(aq) + >C_6H_4O_2(s) \qquad [9]$$

$$>C_6H_4O_2(s) \underset{k_{-4}}{\overset{k_4}{\leftrightarrow}} C_6H_4O_2\ (aq) \qquad [10]$$

The activation parameters indicate that the reaction is surface chemical controlled (Table 2.3) suggesting that Eq. [9] and [10] are not rate-limiting. This was illustrated by the simultaneous release of Mn(II) and o-quinone (Figure 2.6) indicating that $k_3 \approx k_4$ and back reactions are negligible ($k_{-3} \approx k_{-4} = 0$). The mass balance results, the pseudo-first order decay in catechol solution concentration, and the immediate product release imply that $k_2 > k_1$ and that precursor surface complex formation as shown in Eq. [7] is rate-limiting. The value for $\Delta S^{\ddagger}$ (-78 J mol^{-1} K^{-1}) supports an associative ligand substitution mechanism in which the E_a is determined primarily by the energy required for bond formation of the entering group (catechol) to the birnessite surface sites (Atwood, 1997). The empirical rate equation further supports an associative mechanism based on the observed first order dependence on [CAT] (see Eq.[4] and Shriver et al., 1994). After precursor surface complex formation, two electrons can be immediately transferred along the bonding axis as an inner sphere process from the filled catechol p orbitals of σ symmetry to the empty e_g (σ^*) orbitals of the Mn(IV) metal centers. Frontier-molecular-orbital-theory (FMOT) predicts a large driving force for electron transfer because of the vacant σ^* orbitals in Mn(IV) (Luther, 1990; Luther et al., 1998). Based on our data, no distinction can be made between two one-electron transfers or a single concerted two-electron transfer nor whether the electrons are transferred as a hydrogen atom (H•) or hydride (H-) ion. The rapid formation of o-quinone, however, would suggest a concerted two-electron transfer step. Perez-Benito et al. (1996) reported a possible direct two-electron transfer from oxalate to Mn(IV) in

soluble MnO_2. Further experiments are being conducted to substantiate the proposed reaction mechanism and verify the chemical structure of the precursor surface complex.

2.5 Conclusions

In this study, mechanisms of reductive dissolution of birnessite by catechol were studied using EPR-SF and stirred-batch techniques. The reaction was rapid and independent of pH under the experimental conditions of this study (pH 4 to 6). Kinetic and thermodynamic results indicate direct attack of aqueous catechol on birnessite by an associative ligand substitution mechanism to form a precursor surface complex with surface Mn oxide sites. Formation of the precursor surface complex is likely the rate-limiting step based on the experimentally determined activation energy of 59 (±7) kJ mol^{-1} and the comparable rates of catechol disappearance and product formation. Our results indicate that catechol could serve as an alternative soil extractant for easily reducible Mn between pH 4 to 6 based on the rapid reductive dissolution kinetics. Excessive levels of catechol in natural soil environments could possibly lead to Mn toxicity in susceptible plants.

2.6 References

Alexander, M. 1977. Introduction to soil microbiology. John Wiley & Sons, New York.

Amonette, J.E., F.A. Khan, A.D. Scott, H. Gan, and J.W. Stucki. 1994. Quantitative oxidation-state analysis of soils. p. 83-113. *In* J.E. Amonette and L.W. Zelazny (ed.) Quantitative methods in soil mineralogy. SSSA Misc. Publ. SSSA, Madison, WI.

Atwood, J.D. 1997. Inorganic and organometallic reaction mechanisms. VCH Publishers, New York.

Balistrieri, L.S., and J.W. Murray. 1982. The surface chemistry of δ-MnO_2 in major ion seawater. Geochim. Cosmochim. Acta. 46:1041-1052.

Bartlett, R.J. 1981. Nonmicrobial nitrite-to-nitrate transformation in soils. Soil Sci. Soc. Am. J. 45:1054-1058.

Bartlett, R.J., and B.R. James. 1993. Redox chemistry of soils. Adv. Agron. 50:151-208.

Bricker, O. 1965. Some stability relations in the system Mn-O_2-H_2O at 25° and one atmosphere total pressure. Am. Mineral. 50:1296-1354.

Brunauer, C.A., P.H. Emmett, and E. Teller. 1938. Adsorption of gases in multi-molecular layers. J. Am. Chem. Soc. 60:309-319.

Carpenter, R. 1983. Quantitative electron spin resonance (ESR) determinations of forms and total amounts of Mn in aqueous environmental samples. Geochim. Cosmochim. Acta. 47:875-885.

Cheney, M. A., G. Sposito, A. E. McGrath and R. S. Criddle. 1996. Abiotic degradation of 2,4-D (dichlorophenoxyacetic acid) on synthetic birnessite: A calorespirometric method. Colloids and Surfaces 107:131-140.

Davies, G. 1969. Some aspects of the chemistry of manganese(III) in aqueous solution. Coor. Chem. Rev. 4·199-224.

Dawson, C.R., and J.M. Nelson. 1938. The influence of catechol on the stability of o-benzoquinone in aqueous solutions. J. Am. Chem. Soc. 60:245-249.

Dec, J., and J.M. Bollag. 1994. Dehalogenation of chlorinated phenols during oxidative coupling. Environ. Sci. Technol. 28:484-490.

Diebler, H., and N. Sutin. 1964. The kinetics of some oxidation-reduction reactions involving manganese(III). J. Phys. Chem. 68:174-180.

Drits, V.A, E. Silvester, A.I. Gorshkov, and A. Manceau. 1997. Structure of synthetic monoclinic Na-rich birnessite and hexagonal birnessite: I. Results from x-ray diffaction and selected-area electron diffraction. Am. Mineral. 82:946-961.

Espenson, J. H. 1995. Chemical kinetics and reaction mechanisms. 2nd ed. McGraw-Hill, Inc., New York.

Fendorf, S.E., D.L. Sparks, J.A. Franz, and D.M. Camaioni. 1993. Electron paramagnetic resonance stopped-flow kinetic study of manganese(II) sorption-desorption on birnessite. Soil Sci. Soc. Am. J. 57:57-62.

Gambrell, R.P. 1996. Manganese. p. 665-682. *In* D.L. Sparks (ed.) Methods of soil analysis. Part 3. SSSA Book Ser. 5. SSSA, Madison, WI.

Godtfredsen, K.L, and A. T. Stone. 1994. Solubilization of manganese dioxide-bound copper by naturally occurring organic compounds. Environ. Sci. Technol. 28:1450-1458.

Gordon, G., and H. Taube. 1962. Oxygen tracer experiments on the oxidation of aqueous uranium(IV) with oxygen-containing oxidizing agents. Inorg. Chem. 1:69-75.

Hartman, J.R., B.M. Foxman, and S. R. Cooper. 1984. Higher valent manganese chemistry. Synthetic, structural, and solution studies on $[Mn(catecholate)_3]^{n-}$ (n=2,3) complexes. Inorg. Chem. 23:1381-1387.

Hem, J.D. 1978. Redox processes at surfaces of manganese oxide and their effects on aqueous metal ions. Chem. Geol. 21:199-218.

Hersman, L., T. Lloyd, and G. Sposito. 1995. Siderophore-promoted dissolution of hematite. Geochim. Cosmochim. Acta. 59:3327-3330.

Hubbell, W.L., W. Froncisz, and J.S. Hyde. 1987. Continuous and stopped flow EPR spectrometer based on a loop gap resonator. Rev. Sci. Instrum. 58:1879-1886.

Klimes, N., G. Lassmann, and B. Ebert. 1980. Time-resolved EPR spectroscopy. Stopped-flow EPR apparatus for biological application. J. Magn. Reson. 37:53-59.

Kostka, J.E., G.W. Luther III, and K.H. Nealson. 1995. Chemical and biological reduction of Mn(III)-pyrophosphate complexes: Potential importance of dissolved Mn(III) as an environmental oxidant. Geochim. Cosmochim. Acta 59:885-894.

Kummert, R., and W. Stumm. 1980. The surface complexation of organic acids on hydrous γ-Al_2O_3. J. Colloid Interface Sci. 75:373-385.

Laha, S., and R.G. Luthy. 1990. Oxidation of aniline and other primary aromatic amines by manganese dioxide. Environ. Sci. Technol. 24:363-373.

Larsen, F., and D. Postma. 1997. Nickel mobilization in a groundwater well field: Release by pyrite oxidation and desorption from manganese oxides. Environ. Sci. Technol. 31:2589-2595.

Lasaga, A.C. 1981. Rate laws of chemical reactions. p. 1-68. *In* A.C. Lasaga and R.J. Kirkpatrick (ed.) Kinetics of geochemical processes. Reviews in mineralogy, Vol. 8. Mineralogical Society of America, Washington, D.C.

Lindberg, R.D., and D.D. Runnells. 1984. Ground water redox reactions: An analysis of equilibrium state applied to E_h measurements and geochemical modeling. Science 225:925-927.

Luca, V., and C.M. Cardile. 1989. Cation migration in smectite minerals: Electron spin resonance of exchanged Fe^{3+} probes. Clays Clay Miner. 37:325-332.

Luther, G. W. III. 1990. Frontier molecular orbital theory in geochemical processes. p. 173-198. *In* W. Stumm (ed.) Aquatic chemical kinetics: Reaction rates of processes in natural water. Wiley-Interscience, New York.

Luther, G.W. III, B. Sundby, B.L. Lewis, P.J. Brendel, and N. Silverberg. 1997. Interactions of manganese with the nitrogen cycle: alternative pathways to dinitrogen. Geochim. Cosmochim. Acta 61:4043-4052.

Magers, K.D., C. G. Smith, and D. T. Sawyer. 1978. Polarographic and spectroscopic studies of the manganese(II), -(III), and –(IV) complexes formed by polyhydroxy ligands. Inorg. Chem. 17:515-523.

Manceau, A., A.I. Gorshkov, and V.A. Drits. 1992. Structural chemistry of Mn, Fe, Co, and Ni in manganese hydrous oxides: Part I. Information from XANES spectroscopy. Am. Miner. 77:1133-1143.

Mason, H.S. 1949. The chemistry of melanin. VI. Mechanism of the oxidation of catechol by tyrosinase. J. Biol. Chem. 181:803-812.

McBride, M.B. 1987. Adsorption and oxidation of phenolic compounds by iron and manganese oxides. Soil Sci. Soc. Am. J. 51:1466-1472.

McBride, M.B. 1989a. Oxidation of dihydroxybenzenes in aerated aqueous suspensions of birnessite. Clays Clay Miner. 37:341-347.

McBride, M.B. 1989b. Oxidation of 1,2- and 1,4-dihydroxybenzene by birnessite in acid aqueous suspension. Clays Clay Miner. 37:470-486.

McBride, M.B., and L.G. Wesselink. 1988. Chemisorption of catechol on gibbsite, boehmite, and noncrystalline alumina surfaces. Environ. Sci. Technol. 22:703-708.

McKenzie, R. M. 1971. The synthesis of birnessite, cryptomelane, and some other oxides and hydroxides of manganese. Mineral. Mag. 38:493-502.

McKenzie, R. M. 1989. Manganese oxides and hydroxides. p. 439-465. *In* J.B. Dixon and S.B Weed (eds.) Minerals in Soil Environments. 2nd ed. SSSA Book Series 1. SSSA, Madison, WI.

Mentasti, E., E. Pelizzetti, E. Pramauro, and G. Giraudi. 1975. Redox reaction of 1,2-dihydroxybenzene in aqueous perchlorate media. Kinetics and mechanism. Inorg. Chim. Acta 12:61-65.

Mihailovic, M.L., and Z. Cekovic. 1971. Oxidation and reduction of phenols. p. 506-581. *In* S. Patai (ed.) The chemistry of the hydroxyl group. Part I. Interscience, London.

Moore, J.N., J.R. Walker, and T.H. Hayes. 1990. Reaction scheme for the oxidation of As(III) to As(V) by birnessite. Clays Clay Miner. 38:549-555.

Murray, J.W., L.S. Balistrieri, and B. Paul. 1984. The oxidation state of manganese in marine sediments and ferromanganese nodules. Geochim. Cosmochim. Acta 48:1237-1247.

Naidja, A., P.M. Huang, and J.M. Bollag. 1998. Comparison of reaction products from the transformation of catechol catalyzed by birnessite or tyrosinase. Soil Sci. Soc. Am. J. 62:188-195.

Perez-Benito, J.F., C. Arias, and E. Amat. 1996. A kinetic study of the reduction of colloidal manganese dioxide by oxalic acid. J. Colloid Interface Sci. 177:288-297.

Pizzigallo, M.D., P.Ruggiero, C.Crecchio, and R. Mininni. 1995. Manganese and iron oxides as reactants for oxidation of chlorophenols. Soil Sci. Soc. Am. J. 59:444-452.

Richert, S.A., P.K.S. Tsang, and D. T. Sawyer. 1988. Ligand-centered oxidation of manganese(II) complexes. Inorg. Chem. 27:1814-1818.

Rodríguez, R., M.A. Blesa, and A.E. Regazzoni. 1996. Surface complexation at the TiO_2 (anatase)/aqueous solution interface: Chemisorption of catechol. J. Colloid Interface Sci. 177:122-131.

Schulze, D.G.,T. McCay-Buis, S.R. Sutton, and D.M. Huber. 1995a. Manganese oxidation states in *Gaeumannomyces*-infested wheat rhizospheres probed by micro-XANES spectroscopy. Phytopathology 85:990-994.

Schulze, D.G., S.R. Sutton, and S. Bajt. 1995b. Determining manganese oxidation state in soils using x-ray absorption near-edge structure (XANES) spectroscopy. Soil Sci. Soc. Am. J. 59:1540-1548.

Shindo, H., and P.M. Huang. 1982. Role of Mn(IV) oxide in abiotic formation of humic substances in the environment. Nature 298:363-365.

Shindo, H., and P.M. Huang. 1984. Catalytic effects of manganese(IV), iron(III), aluminum, and silicon oxides on the formation of phenolic polymers. Soil Sci. Soc. Am. J. 48:927-934.

Shriver, D.F., P. Atkins, and C.H. Langford. 1994. Inorganic chemistry. 2nd ed. W.H. Freeman and Co., New York.

Silvester, E, A. Manceau, and V.A Drits. 1997. Structure of synthetic monoclinic Na-rich birnessite and hexagonal birnessite: II. Results from chemical studies and EXAFS spectroscopy. Am. Mineral. 82:962-978.

Sparks, D.L. 1989. Kinetics of soil chemical processes. Academic Press, New York.

Sparks, D. L. 1995. Environmental soil chemistry. Academic Press, San Diego, CA.

Stach, J., R. Kirmse, W. Dietzsch, G. Lassman, V.K. Belyaeva, and I.N. Marov. 1985. Ligand exchange reactions between copper(II)- and nickel(II)-chelates of different sulfur-and selenium-containing ligands. VI [1]. Kinetics of ligand exchange reactions studied by stopped-flow ESR. Inorg. Chim. Acta 96:55-59.

Steelink, C. 1964. Free radical studies of lignin, lignin degradation products and soil humic acid. Geochim. Cosmochim. Acta. 28:1615-1622.

Stone, A.T. 1987. Reductive dissolution of manganese (III/IV) oxides by substituted phenols. Environ. Sci. Technol. 21:979-988.

Stone, A.T., K.L. Godtfredsen, and B. Deng. 1994. Sources and reactivity of reductants encountered in aquatic environments. p.337-374. *In* G. Bidoglio and W. Stumm (ed.) Chemistry of aquatic systems: Local and global perspectives. ECSC, The Netherlands.

Stone, A.T., and J. J. Morgan. 1984a. Reduction and dissolution of manganese (III) and manganese (IV) oxides by organics. 1. Reaction with hydroquinone. Environ. Sci. Technol. 18:450-456.

Stone, A.T. and J. J. Morgan. 1984b. Reduction and dissolution of manganese (III) and manganese (IV) oxides by organics. 2. Survey of the reactivity of organics. Environ. Sci. Technol. 18:617-624.

Stone, A.T. and J. J. Morgan. 1987. Reductive dissolution of metal oxides. p.221-254. *In* W. Stumm (ed.) Aquatic surface chemistry: Chemical processes at the particle-water interface. Wiley, New York.

Ukrainczyk, L. and M.B. McBride. 1992. Oxidation of phenol in acidic aqueous suspensions of manganese oxides. Clays Clay Minerals 40:157-166.

Ukrainczyk, L. and M.B. McBride. 1993a. The oxidative dechlorination reaction of 2,4,6-trichlorophenol in dilute aqueous suspensions of manganese oxides. Environ. Toxicol. Chem. 12:2005-2014.

Ukrainczyk, L. and M.B. McBride. 1993b. Oxidation and dechlorination chlorophenols in dilute aqueous suspensions of manganese oxides: Reaction products. Environ. Toxicol. Chem. 12:2015-2022.

Wang, M.C., and P.M. Huang. 1987. Polycondensation of pyrogallol and glycine and the associated reactions as catalyzed by birnessite. Sci. Total Environ. 62:435-442.

Wang, M.C., and P.M. Huang. 1992. Significance of Mn(IV) oxide in the abiotic ring cleavage of pyrogallol in natural environments. Sci. Total Environ. 113:147-157.

Xyla, A.G, B. Sulzberger, G.W. Luther III, J.G. Hering, P. van Cappellen, and W. Stumm. 1992. Reductive dissolution of manganese (III,IV) (hydr)oxides by oxalate: The effect of pH and light. Langmuir 8:95-103.

Chapter 3

SPECTROSCOPIC AND KINETIC INVESTIGATION OF THE DYNAMIC ROLE OF STRUCTURAL Mn(III) IN OXIDATION OF SOIL ORGANIC MATTER

3.1 Abstract

There is a paucity of mechanistic information available describing the reactivity of soil organic matter on naturally occurring Mn(III,IV) (hydr) oxide minerals. Reactivity studies were conducted using catechol as an analogue of soil organic matter and following the reductive dissolution of solid phase Mn minerals using electron paramagnetic resonance (EPR) spectroscopy, diffuse reflectance spectroscopy (DRS), and ultraviolet-visible (UV-VIS) spectroscopy. The adsorption of catechol was inner-sphere on manganite (γ-MnOOH) and birnessite (δ-MnO_2) with broad ligand-to-metal-charge-transfer (LMCT) bands identified at energies of 12674 cm^{-1} and 10812 cm^{-1} that decreased in intensity over time. The initial reductive dissolution rates (R) by catechol decreased in the order birnessite > manganite > pyrolusite and were not attributed to differences in surface area or thermodynamic driving force for the reduction reactions. However, approximately 95% of the variation in R was described by available Mn(III) extracted by the Mn(III)-specific ligand pyrophosphate. These results indicate that the coordination environment of

structural Mn(III) in naturally occurring Mn(III,IV) (hydr) oxide minerals affects its availability and role in C cycling.

3.2 Introduction

Solid Mn(III,IV) (hydr) oxide minerals are powerful oxidants in soils and geochemical environments because of the vacant orbitals of sigma (σ^*) symmetry that impart significant surface reactivity (Luther, 1990). The rapid estimated water exchange rate (k_{H2O}) for $Mn(III)_{aq}$ in solution of 1×10^6 s^{-1} (Davies, 1969) can be explained by its d^4 electronic configuration, which, in an octahedral ligand field, is distorted to tetragonal symmetry due to the Jahn-Teller effect. In contrast, Mn(IV) has a d^3 electronic configuration and, like Cr(III), is inert to ligand substitution reactions with an estimated k_{H2O} on the order of 10^{-6} s^{-1} (Margerum et al., 1978). Therefore, one would expect Mn(III) solid phases to be more kinetically reactive than Mn(IV). This hypothesis has not been tested, particularly on naturally occurring Mn oxides where measuring water exchange rates is experimentally difficult.

Few studies have evaluated adsorption mechanisms using solid phase oxides which differ in the electronic configuration of the metal center. Yates and Healy (1975) compared α–FeOOH (d^5, labile) with α-Cr_2O_3 (d^3, inert) which differ only in their ability to undergo ligand substitution reactions with phosphate, nitrate, and sulfate and were able to distinguish inner-sphere from outer-sphere surface complexes based on rates and extent of adsorption. Previously, we reported that reductive dissolution of birnessite by catechol was rapid between pH 4 to 6 (Matocha et al.,

2000). This phase is nonstoichiometric, with Mn(III) substituted in lattice vacancy sites (Drits et al., 1997; Silvester et al., 1997). This structural Mn(III) may give rise to the rapid kinetics observed in birnessite, which has traditionally been regarded as a Mn(IV) dioxide (δ-MnO_2).

The sorption of soil organic matter on solid Mn(III,IV) (hydr) oxide minerals is not well understood, although soil organic matter levels are correlated with release of Mn to soil solution (Reisenauer, 1988). Previous research has shown that carboxylic acid functional groups are operative in adsorption of natural organic matter on Fe- and Al-oxides at low pH, while hydroxyl groups adsorb strongly at high pH (Gu et al., 1995; Filius et al., 1999). There is evidence to suggest that catechol forms inner sphere surface complexes with Mn oxides (Stone and Morgan, 1984a, b; McBride, 1989a, b), however, there is practically no information available probing the chemical structure of the surface complex formed between Mn(III,IV) (hydr) oxide minerals and soil organic matter because mostly macroscopic studies have been conducted on these systems (Stone et al., 1994).

This study was undertaken to: 1) test the hypothesis that the lability of Mn(III) predicted by frontier molecular orbital theory in solution affects the reductive dissolution kinetics of solid Mn(III,IV) (hydr) oxide minerals by comparing several phases with varying levels of structural Mn(III) in their reactivity with catechol, a model organic ligand of soil organic matter (Evanko and Dzombak, 1998); 2) identify characteristics of the precursor surface complex formed between catechol and

Mn(III,IV) minerals using *in situ* spectroscopic techniques. The chemical nature of the precursor surface complex will undoubtedly play a significant role in the ability of solid phase Mn(III,IV) (hydr)oxide minerals to degrade organic contaminants and influence C cycling.

3.3 Materials and Methods

3.3.1 Materials

Birnessite (δ-MnO_2) was synthesized according to procedures outlined by McKenzie (1971). Boiling $KMnO_4$ was reduced with concentrated HCl and the resulting birnessite precipitate was vacuum filtered, dialyzed against deionized water to remove salts, and freeze-dried. Manganite (γ-MnOOH) was synthesized by oxidizing Mn(II) (as $MnSO_4$) with 30% H_2O_2 and forcing precipitation with 0.2M NH_3 (Giovanoli and Leuenberger, 1969). The product was filtered, washed and dialyzed to remove salts, and dried over P_2O_5 in a vacuum dessicator. The pyrolusite (β-MnO_2) phase employed was reagent grade. These solid Mn(III,IV) mineral phases were characterized by powder x-ray diffraction, total Mn by complete dissolution, mean oxidation state by iodometric titration, BET surface area, and point of zero charge (PZC) was estimated by microelectrophoretic mobility measurements, Ca^{2+} sorption experiments, and potentiometric titrations. A nice comparison can be drawn from the results of manganite and pyrolusite because they are formally isostructural with the only difference being oxidation state giving rise to a tetragonally distorted geometry in manganite.

3.3.2 Reductive Dissolution Rates

Reductive dissolution of Mn(III,IV) oxide solid phases by catechol was studied in stirred batch systems with a pH stat and *in situ* using the EPR-SF technique to quantify the increase in Mn(II) concentration over time (Matocha et al., 2000). Temperature was controlled with a circulating water bath in the stirred batch studies. Corrections were made for removal of suspension volume from the batch reactor during sampling in calculating acid consumption. The EPR-SF experiments were conducted using 50 m*M* K-acetate buffered between pH 4 to 6 with dilute HCl.

3.3.3 Available Mn(III)

The ligand pyrophosphate ($P_2O_7^{4-}$) stabilizes Mn(III) in solution with O ligating atoms to lower the reduction potential (Diebler and Sutin, 1964; Davies, 1969):

$$Mn(III)(aq) + e^- \rightarrow Mn(II)(aq) \qquad E^o=1.5\ V \qquad [1]$$

$$Mn(III)HP_2O_7(aq) + e^- \rightarrow Mn(II)HP_2O_7 \qquad E^o=1.2\ V \qquad [2]$$

The major complex species of the Mn(III) pyrophosphate complexes are not well understood (Klewicki and Morgan, 1998), but these complexes still behave as powerful environmental oxidants (Kostka et al., 1995). Interaction of pyrophosphate with solid phase Mn mineral phases has received less attention, although it has been defined as extracting organically bound Mn in soil (McKeague, 1967; Sims et al., 1979; Khan and Fenton, 1996). Initial rates of pyrophosphate-extractable Mn(III) nonreductive dissolution were used as an operationally defined measure of available

Mn(III). Extractable Mn(III) was measured by reacting large excesses of pyrophosphate (50m*M*) with each of the solid phases at pH 4 and 6.5 at 296 K in a stirred batch reactor. The excess ligand was used to control pH. The Mn(III)-pyrophosphate complexes were measured by UV-VIS spectrophotometry in 1-cm cuvettes using an HP 8452A Diode Array UV-VIS spectrophotometer. Reagent grade Mn(III) acetate (Alfa) and $Na_4H_4P_2O_7$ (Aldrich) were used to prepare Mn(III)-pyrophosphate standards. Micromolar concentrations of Mn(III)-pyrophosphate complexes were measured in the UV region at 210 and 260 nm and m*M* concentrations at 480 nm as described previously (Kostka et al., 1995). The molar absorptivities (ε) for the Mn(III)- pyrophosphate complex were 1.72×10^{-4} M^{-1} cm^{-1} at pH 6.5 and 1.86×10^{-4} M^{-1} cm^{-1} at pH 4.5.

3.3.4 Spectroscopic Characterization

Catechol reacted solid phases were analyzed *in situ* using diffuse reflectance spectroscopy (DRS) at 296 K on a Lambda 9 spectrophotometer using a Spectralon standard (Labsphere) as a background calibration. Spectra were recorded from 1000 to 250 nm in 1 nm steps at a scan speed of 130 nm min^{-1}. The response time was 2 s with a NIR gain setting of 2. Unreacted Mn solid phases were removed from the stirred batch reactor after preequilibration and prior to catechol addition and scanned immediately. Catechol was added at concentrations ranging between 1 and 10 m*M* buffered at pH 4 to 0.3 g L^{-1} of the solid phases. The pH was controlled using a Brinkmann pH-stat automatic titrator. Reacted samples were pulled at increasing time

intervals from the stirred batch reactor and the wet pastes were placed in an aluminum sample holder 10 mm in diameter and immediately scanned in a vertical orientation. The Kubelka-Munk function was calculated from all spectra (Wendlandt and Hecht, 1966) and spectral processing was performed using the software package GRAMS/386 (Galaxy Industrial Corp.). Spectral fitting was performed with PEAKSOLVE (Galactic Industies Corp.).

3.4 Results and Discussion

3.4.1 Reductive Dissolution Experiments

Previously, it was shown that reduction of birnessite by catechol was a surface chemical controlled reaction and followed an empirical pH-independent rate expression:

$$d[Mn(II)]/dt = 4\ (\pm 0.5) \times 10^{-3}\ L\ m^{-2}\ s^{-1}\ [CAT]^{1.0}\ [SA]^{1.0} \qquad [3]$$

that was measured using an EPR-SF kinetic technique (Matocha et al., 2000). The value of 4×10^{-3} L m^{-2} s^{-1} represents the empirical rate constant, k_{cat}, for the reaction. The lack of a pH effect between the experimental pH range of 4 to 6 was surprising based on the consumption of H^+ measured in stirred batch studies (Figure 3.1) and the commonly held belief that organic acids like catechol sorb on metal oxide surfaces predominantly at greater pH values (Filius et al., 1999).

It was hypothesized that structural Mn(III) located in birnessite may contribute to the observed rapid kinetics because of its rapid k_{H2O} in solution because surface complexation would be difficult at inert Mn(IV) sites. Thus, the EPR-SF technique

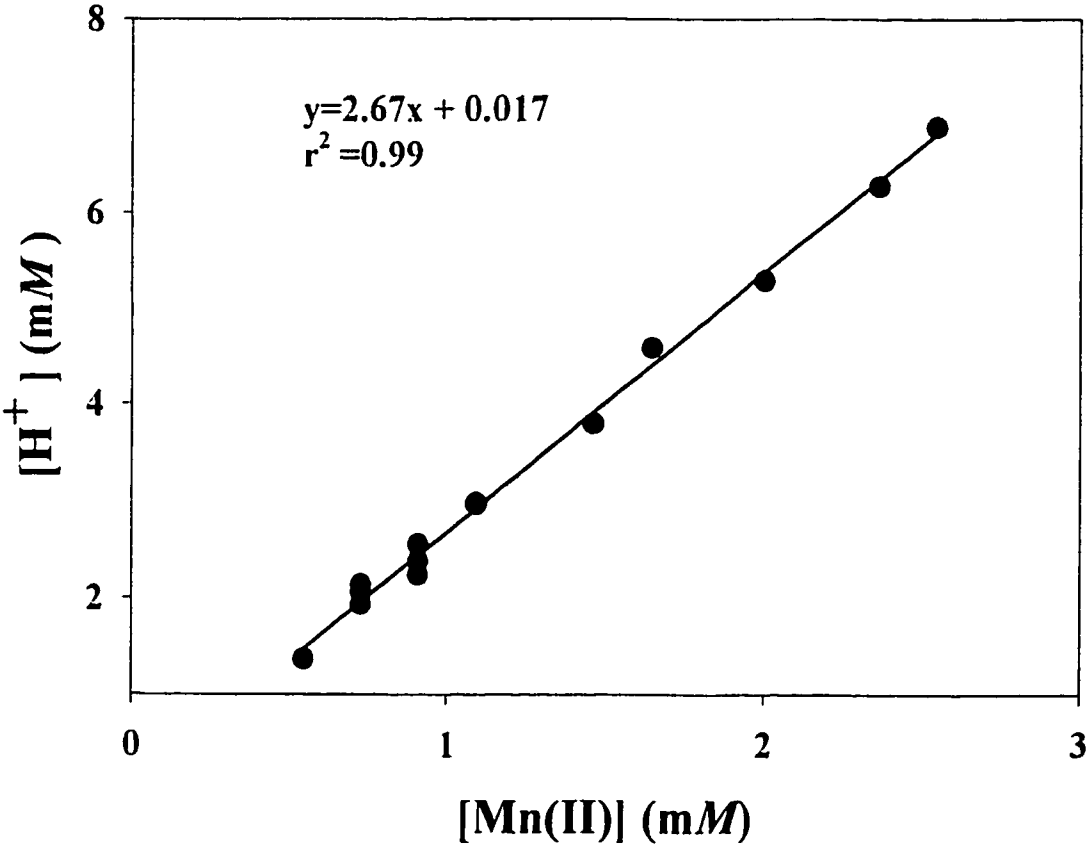

Figure 3.1 Representative stoichiometry of the reductive dissolution of birnessite by catechol.

and stirred batch techniques were used to measure the reactivity of a pristine solid Mn(III) phase (manganite) and a Mn(IV) phase (pyrolusite) by catechol. Approximately 2.4 H^+ were consumed per Mn(II) produced in the reaction of manganite with catechol (Figure 3.2) to confirm the stoichiometry:

$$2\gamma\text{-MnOOH} + C_6H_4(OH)_2 + 4H^+ \rightarrow 2Mn(II)(aq) + C_6H_4O_2\ (aq) + 4H_2O \qquad [4]$$

Like birnessite, there was little dependence on ionic strength which indicates that charged species were not involved and suggests inner sphere surface complexation of catechol to the manganite surface (Figure 3.3). In contrast to birnessite, the ability of catechol to reduce manganite was strongly pH dependent (Figure 3.4). The overall rate expression was derived as:

$$d[Mn(II)]/dt = 3\ (\pm 0.5) \times 10^{-5}\ L\ m^{-2}\ s^{-1}\ [CAT]^{0.2}\ [SA]^{1.7}\ [H^+]^{0.5} \qquad [5]$$

The fractional order dependence on [CAT] was consistent with previous reports on this same mineral (Xyla et al., 1992) where the authors showed for example, a 33% increase in the rate with a 10-fold increase in oxalate concentration. The greater rate of Mn(II) release from manganite at low pH was influenced by charging properties of the manganite surface with a PZC of 6.1. For example, at pH 4, the manganite surface functional groups will be protonated forming Mn(III)-H_2O bonds which are labile to ligand substitution reactions (Luther et al., 1998) favoring surface complexation of catechol with surface Mn(III). The complex rate expression suggests multiple electron pathways, most likely one-electron transfers, although no ortho-semiquinone species

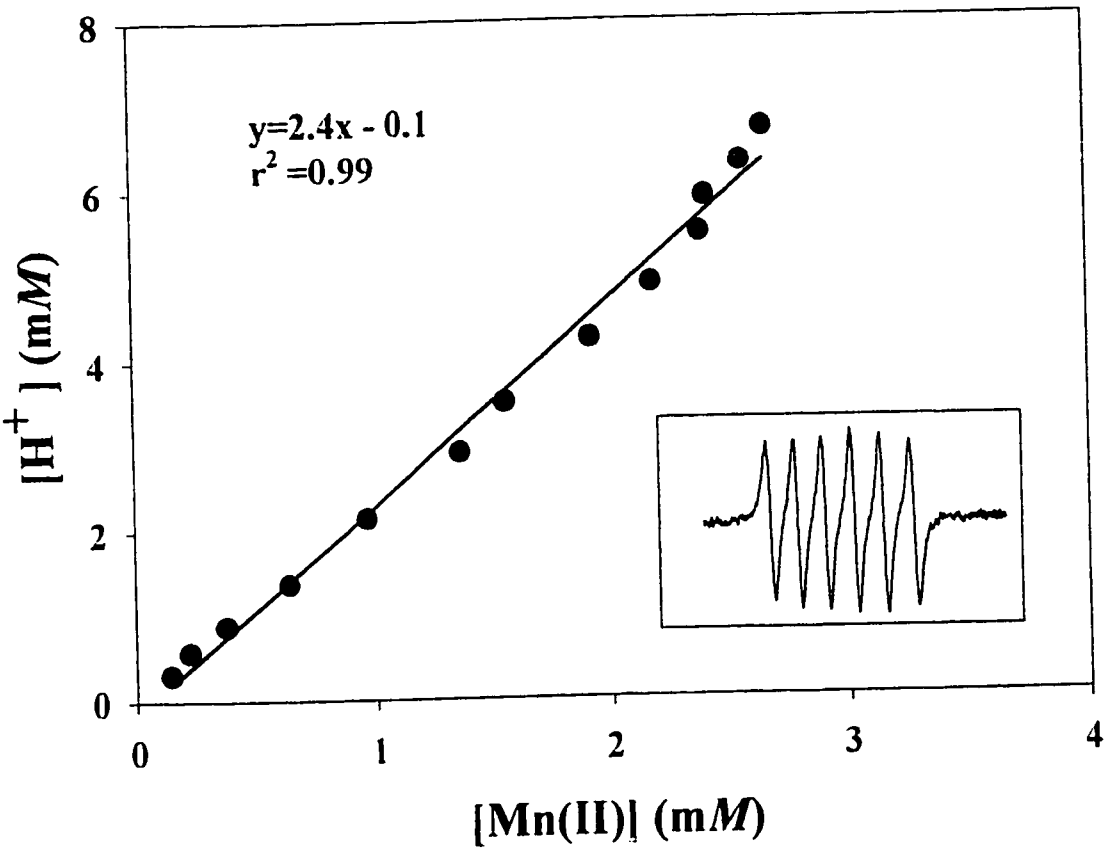

Figure 3.2 Stoichiometry of the reductive dissolution of manganite by catechol. The inset confirmed that manganite was reduced to the Mn(II) product based on the diagnostic EPR six-line spectrum.

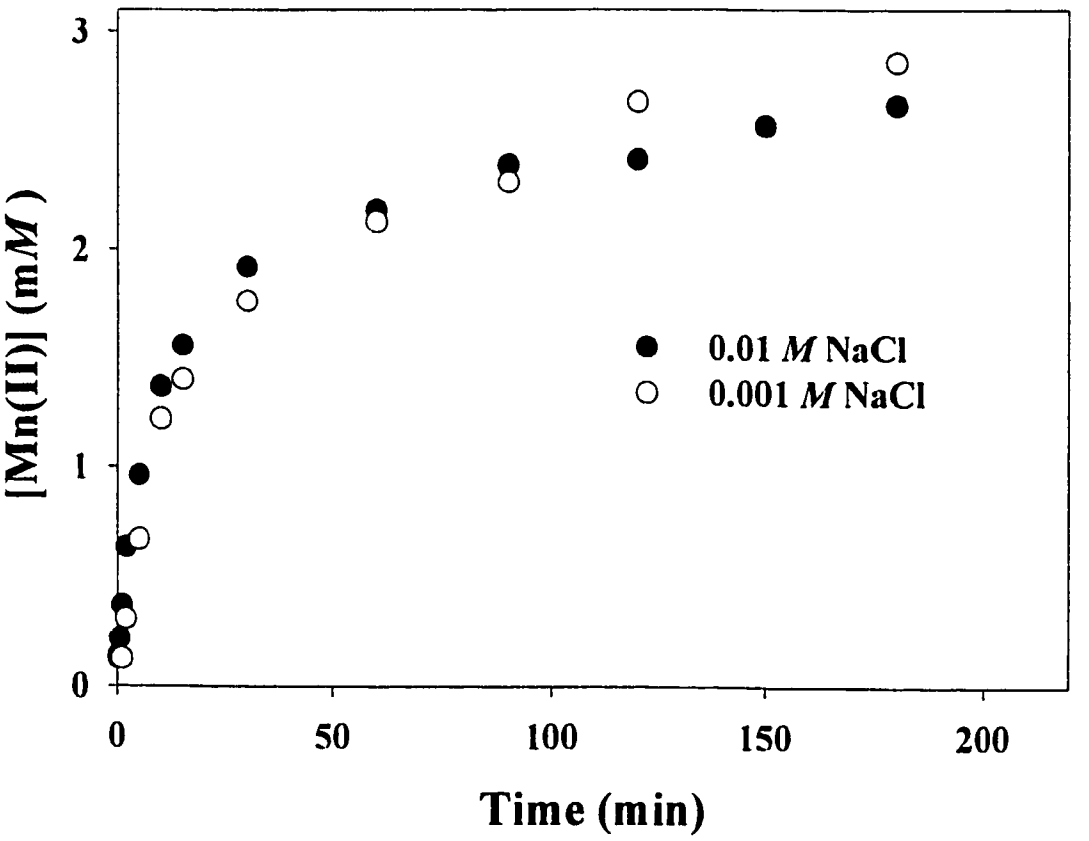

Figure 3.3 Reductive dissolution of manganite by catechol in stirred-batch studies as a function of ionic strength.

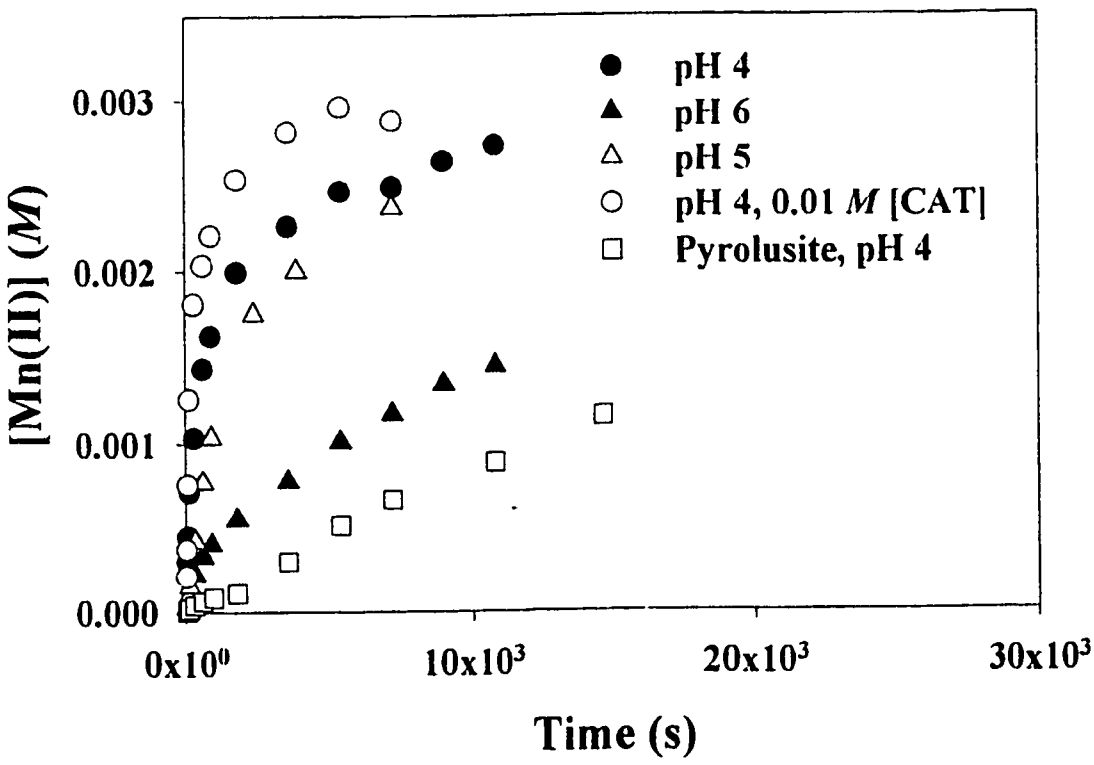

Figure 3.4 Reductive dissolution rate of manganite (3m*M* Mn_T) as a function of pH at 1 m*M* [CAT] and 10 m*M* [CAT] . Included is the reduction rate of pyrolusite (3m*M* Mn_T) at 1 m*M* [CAT] and pH 4.

were identified with EPR, probably due to the instability of these free radicals at low pH (Pedersen, 1973).

It is intriguing to note the reductive dissolution rate differences between birnessite and manganite, with experimental k_{cat} values differing by almost two orders of magnitude. The $[H^+]$ term does not enter in directly into the rate expression for birnessite, but it does for manganite. The reductive dissolution rate shuts down at or above the point of zero charge (PZC) for manganite, while the reaction is rapid on birnessite at pH values well above its PZC of about 2. In addition, the pristine manganite phase was dissolved at an overall slower rate when compared to birnessite despite the greater concentration of presumably labile and reactive Mn(III). The Mn(IV) solid phase pyrolusite which differs from manganite only in oxidation state, behaves as FMOT would predict, with a slower reductive dissolution rate (Figure 3.4) which reflects the relative inertness of Mn(IV) metal centers discussed previously. Initial reductive dissolution rates (R) of the three solid Mn(III,IV) minerals by catechol under identical experimental conditions normalized with respect to surface area decreased in the order birnessite > manganite > pyrolusite (Table 3.1). It is apparent that factors other than mineral surface area and thermodynamic driving force explain the differences in reductive dissolution rates between the three Mn(III,IV) (hydr) oxide minerals.

Table 3.1 Comparison of initial reductive dissolution rates (R) by catechol with thermodynamic driving force.

Parameter	Birnessite	Manganite	Pyrolusite
R (μmol m^{-2} min^{-1})	142	32	3.55
ΔG_r (kJ mol^{-1})†	93	100	87

†Calculated from Nernst equation for concentrations of [Mn(II)]= 10^{-5} *M* and $[H^+]=10^{-4}$ *M*.

3.4.2 Structural Mn(III) in Mn(III,IV) (Hydr) Oxides

Assuming an octahedral (O_h) crystal field, the high spin d^4 Mn(III) cation has a $t_{2g}^3 e_g^1$ ground state electronic configuration and only one spin-allowed $t_{2g} \rightarrow e_g$ electronic transition, corresponding to the $^5E_g \rightarrow {}^5T_{2g}$ spectroscopic transition, would be expected at an energy near 20,000 cm^{-1} (500 nm) based on molecular orbital calculations for MnO_6^{9-} clusters and experimental data (Sherman, 1984; Sherman and Vergo, 1988). More than one band is usually observed because Mn(III) lowers its symmetry to increase stability of its coordination site from O_h to tetragonal (D_{4h}) due to the Jahn-Teller effect giving rise to three absorption bands (Lever, 1984). Kubelka-Munk converted diffuse reflectance spectra (DRS) for untreated birnessite and manganite samples were deconvoluted using a minimum of Gaussian bands on a constant baseline with unconstrained fitting parameters. For birnessite, typically three absorption bands were detected at 13398, 17840, and 21449 cm^{-1} based on Gaussian model fits (Figure 3.5). Absorption band energies and assignments determined from the fitting routine are listed in Table 3.2 with a corresponding diagram depicting the 3d orbital energy levels for the different symmetries (Figure 3.6). The low energy bands for birnessite at 13398 and 17840 cm^{-1} confirmed the presence of Mn(III) because Mn(IV) transitions are found at higher energies. Geschwind et al. (1962) observed the $^4A_2 \rightarrow {}^4T_2$ transition at 21300 cm^{-1} for Mn(IV) doped into an oxo system (Al_2O_3), lower than the calculated value of 26860 cm^{-1} (Sherman, 1984). Similiarly, bands attributed to Mn(IV) have also been observed at 22000 and 28000 cm^{-1} in MnF_6^{2-}

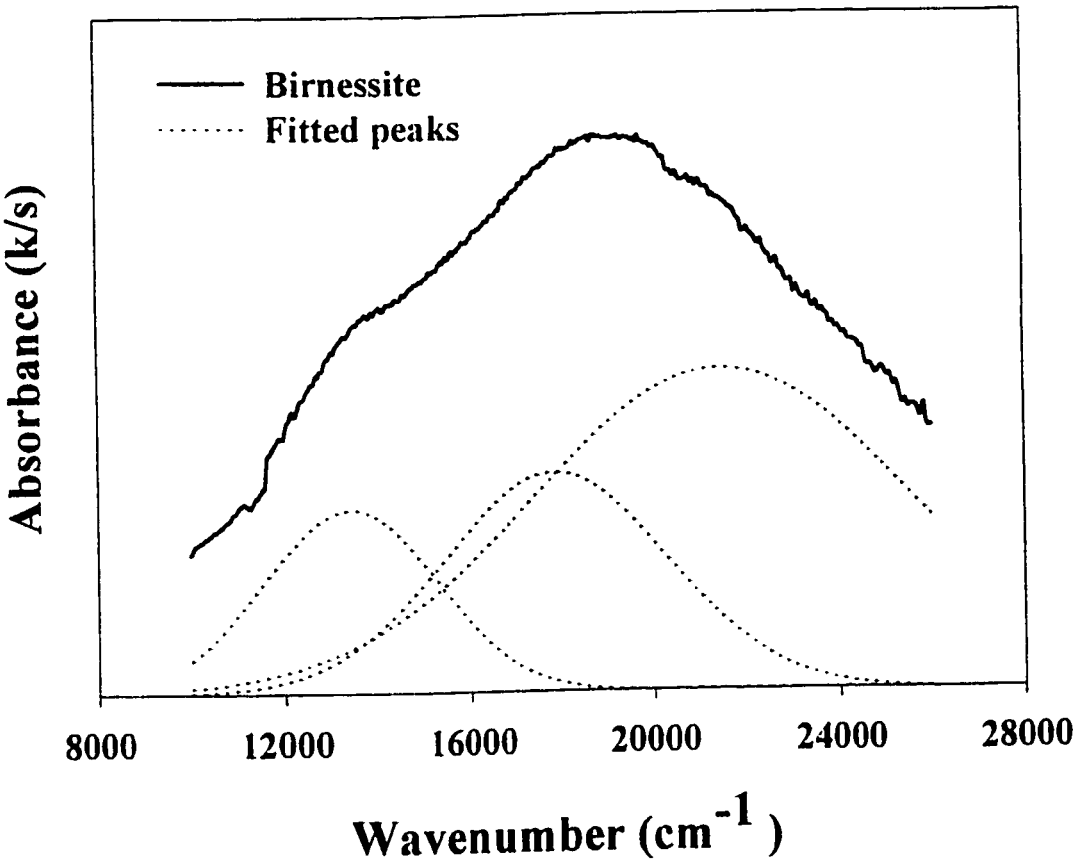

Figure 3.5 Diffuse reflectance spectrum and model deconvolution of unreacted birnessite.

Table 3.2 Assignments and energies of Mn(III) ligand-field bands determined by Gaussian decomposition in DRS spectra of unreacted birnessite and manganite.

Mineral	$^5B_{1g} \rightarrow {}^5A_{1g}$	$^5B_{1g} \rightarrow {}^5B_{2g}$	$^5B_{1g} \rightarrow {}^5E_g$
Birnessite	13398	17840	21449
Manganite	12624	16785	22934
Mn(III)-Montmorrillonite†	10400	18800	22400

†Taken from Sherman and Vergo (1988).

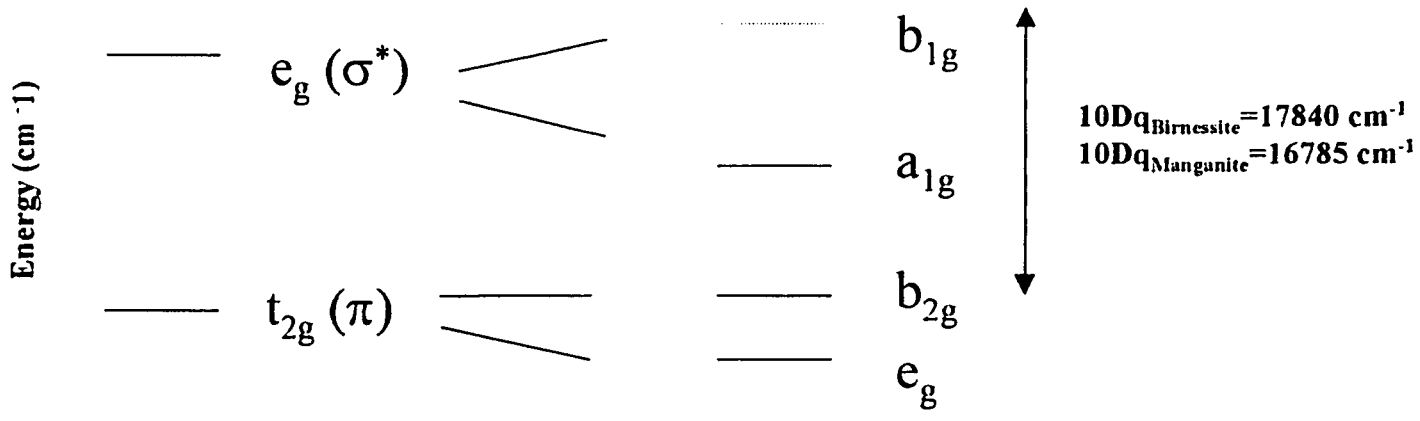

Figure 3.6 Energy levels of 3d orbitals for Mn(III) cation in different symmetries. The ligand field parameter 10Dq in D_{4h} symmetry is defined by the b_{1g}-b_{2g} orbital energy separation.

(Lever, 1984). The possibility that the feature at 21449 cm^{-1} in birnessite may be due to Mn(IV) transitions cannot be ruled out. Untreated manganite contained absorption bands corresponding to Mn(III) ligand field theory bands in D_{4h} symmetry at 12624, 16785, and 22934 cm^{-1} based on the reasonable agreement with literature values for Mn(III) in other oxo systems (Table 3.2). In D_{4h} symmetry, the ligand field theory parameter 10Dq corresponds to the $^5B_{1g} \rightarrow {}^5B_{2g}$ spectroscopic transition energy, represented by the b_{1g} - b_{2g} orbital energy separation in Figure 3.6. The 10Dq parameter was greater in birnessite than manganite, but both were lower in energy than the value of the free aquocomplex of 21000 cm^{-1} (Orgel, 1966). For our purposes, it can be assumed that structural Mn(III) in manganite and birnessite may have different levels of availability based on the positions of the Mn(III) ligand field bands.

3.4.3 Spectroscopic Characteristics of Catechol-Mn Oxide Interface.

Implicit in the reductive dissolution mechanism first proposed by Stone and Morgan (1984a,b) and described again recently (Stone et al., 1994) is the direct interaction of reductant with the Mn oxide surface followed by electron transfer and Mn(II) release. No direct confirmation of the nature of the precursor surface complex has been reported. Diffuse reflectance spectroscopy allowed for the *in situ* investigation of the catechol-Mn oxide water interface. The DRS difference spectra of manganite and birnessite reacted with catechol were compared with catechol reacted with anatase (TiO_2), a d^0 metal cation that forms strong inner-sphere complexes with catechol in

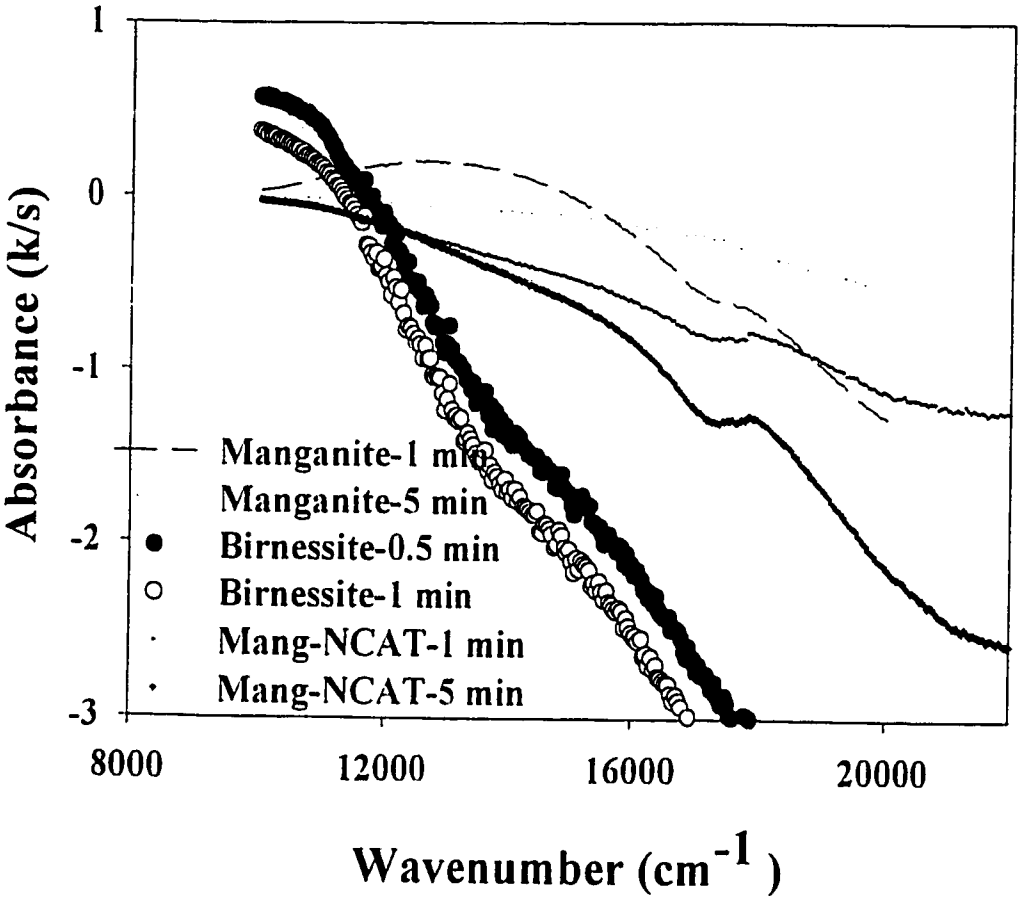

Figure 3.7 Diffuse reflectance difference spectra showing the LMCT bands for catechol reacted with manganite and birnessite at [CAT] =1m*M*, [SA] =10 m^2 L^{-1} , and pH 4 over time. The LMCT for CAT on birnessite and manganite was verified by the systematic shift in the LMCT band to 17900 cm^{-1} for 4-nitrocatechol (NCAT) on manganite.

solution (Borgias et al, 1984). Catechol adsorption was inner-sphere on manganite with a broad ligand-to-metal-charge-transfer (LMCT) band centered at 12674 cm^{-1} after 1 min of reaction time followed by a decrease in intensity after 5 min (Figure 3.7). The decrease in intensity of the LMCT band over time reflected the dissolution of the solid phase. An interesting shoulder appeared initially in the manganite difference spectrum at 17524 cm^{-1}, but apparently disappeared after 5 min. This could be due to a catechol reaction product interacting with the available surface sites on manganite because under the experimental conditions (pH 4, 1 m*M* [CAT]: 3 m*M* Mn_T), an excess of surface sites would be present. The LMCT band on manganite agrees with previous studies which have shown that oxo chelating ligands form charge transfer complexes with Mn(III) as broad bands in the 5000-15000 cm^{-1} region (Dingle, 1966).

The LMCT band identified in the difference spectrum for birnessite indicated that catechol was adsorbed as an inner-sphere complex. However, the position of the LMCT band was red shifted to about 10812 cm^{-1} for birnessite and decreased in intensity over time (Figure 3.7). The higher energy LMCT band in manganite was ascribed to the greater energy separation between Mn(III) and oxo donors of catechol when compared to birnessite which contains both structural Mn(III) and Mn(IV) (Figure 3.8). The vacant σ^* molecular orbitals for surface Mn(III) and Mn(IV) metal centers allow for significant electron overlap with the oxygen lone pairs of σ symmetry (p_z) on catechol, which are in the ring plane (Figure 3.8), so electron transfer occurs on

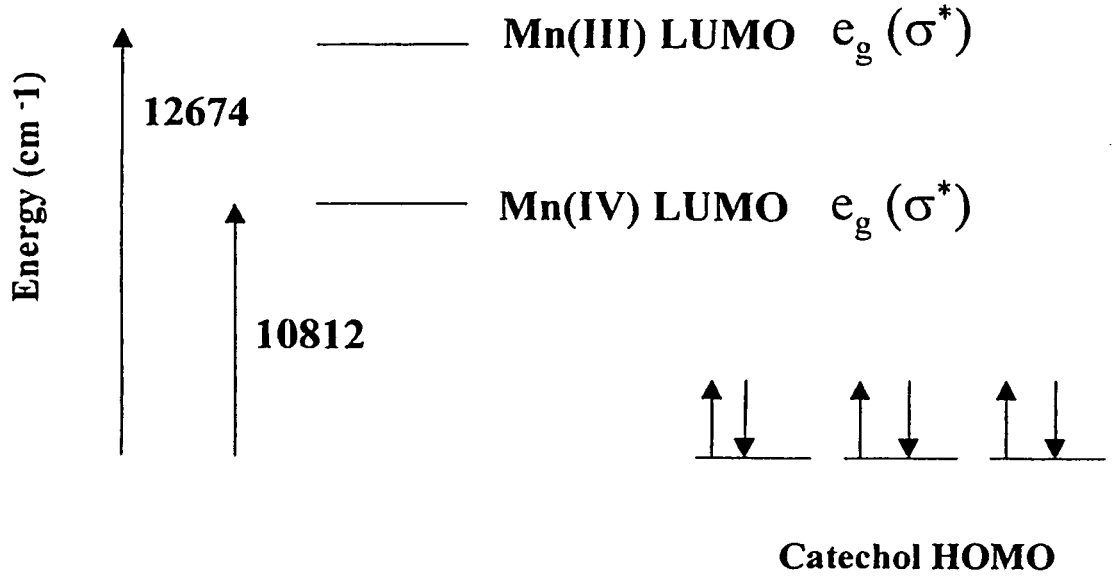

Figure 3.8 Simplified energy level diagram of 3d orbitals for Mn(III) and Mn(IV) and frontier orbitals of catechol illustrating the energy differences of LMCT bands measured with DRS.

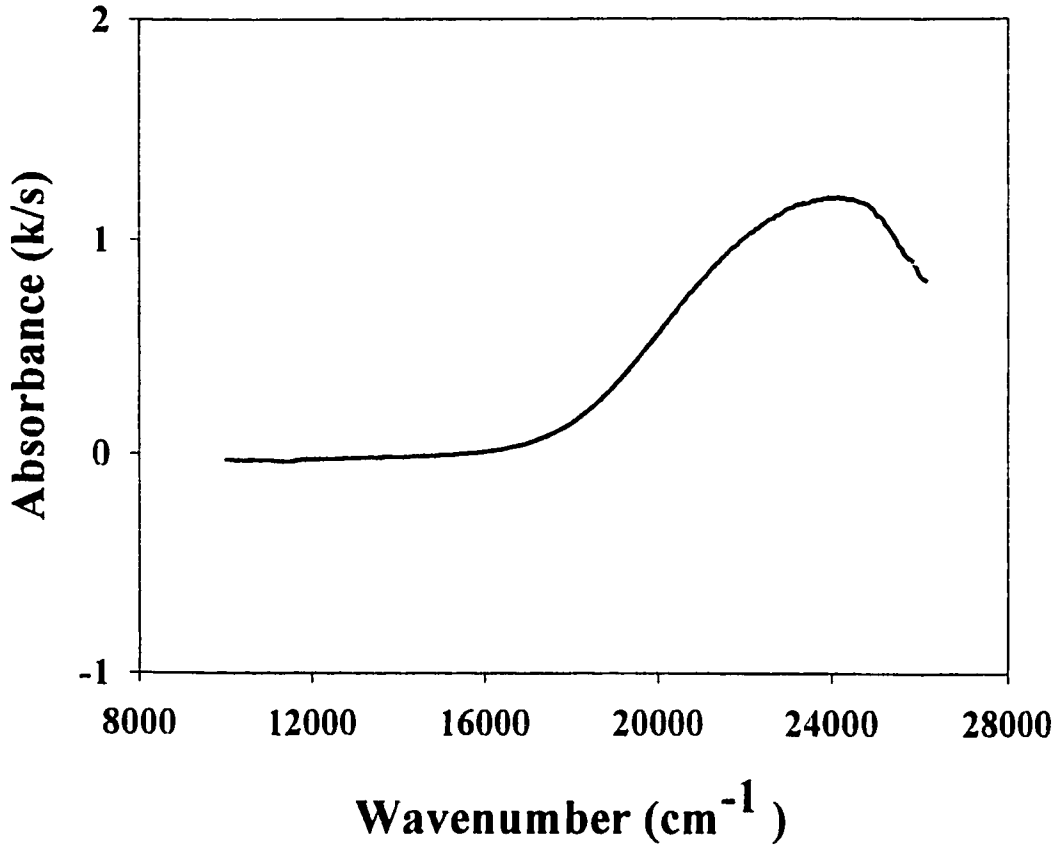

Figure 3.9 Diffuse reflectance difference spectrum of anatase (TiO_2) reacted with 1 m*M* [CAT] at pH 4.

the bonding axes as was the case for reductive dissolution by oxalate (Xyla et al.,1992). Tris-$Mn^{IV}(cat)_3^{2-}$ and bis-$Mn^{III}(cat)_2^-$ complexes form in solution but are better described as $Mn^{II}(semi)_2(cat)^{2-}$ and $Mn^{II}(semi)(cat)^-$ because of internal metal-ligand redox reactions that convert catechol ligands to semiquinone ligands (Richert et al., 1988). The catechol to Mn(IV) LCMT band was reported at 585 nm (Hartman et al., 1984) and the catechol to Mn(III) LCMT band between 550 nm and 750 nm (Magers et al., 1978) in solution and are blue shifted when compared to the LMCT bands for the surface complexes. Similarly, a broad LMCT band centered at 24000 cm^{-1}(425 nm) was observed by reacting catechol with TiO_2 indicating inner-sphere coordination of catechol on TiO_2 (Figure 3.9), and this band was red shifted when compared to $Ti(cat)_3$ solution complexes identified at 389 nm (Borgias et al., 1984).

This is the first direct spectroscopic evidence for the precursor surface complex in the reactions of solid Mn(III,IV) (hydr) oxide minerals with oxidizable organic ligands.

3.4.4 Role of Available Mn(III) in C Cycling. Pyrophosphate reacted directly with the surface of birnessite to extract structural Mn(III) to form a stable Mn(III)-pyrophosphate complex with UV-VIS peaks at 480, 260, and 218 nm which increased in intensity over time (Figure 3.10). The initial rate of Mn(III) extraction from birnessite by pyrophosphate was more rapid than manganite and pyrolusite at pH 6.5 (Figure 3.11). The stoichiometry of the pyrophosphate-extracted Mn(III) was not determined, however, a forty μM sample of the Mn(III)-pyrophosphate complex from

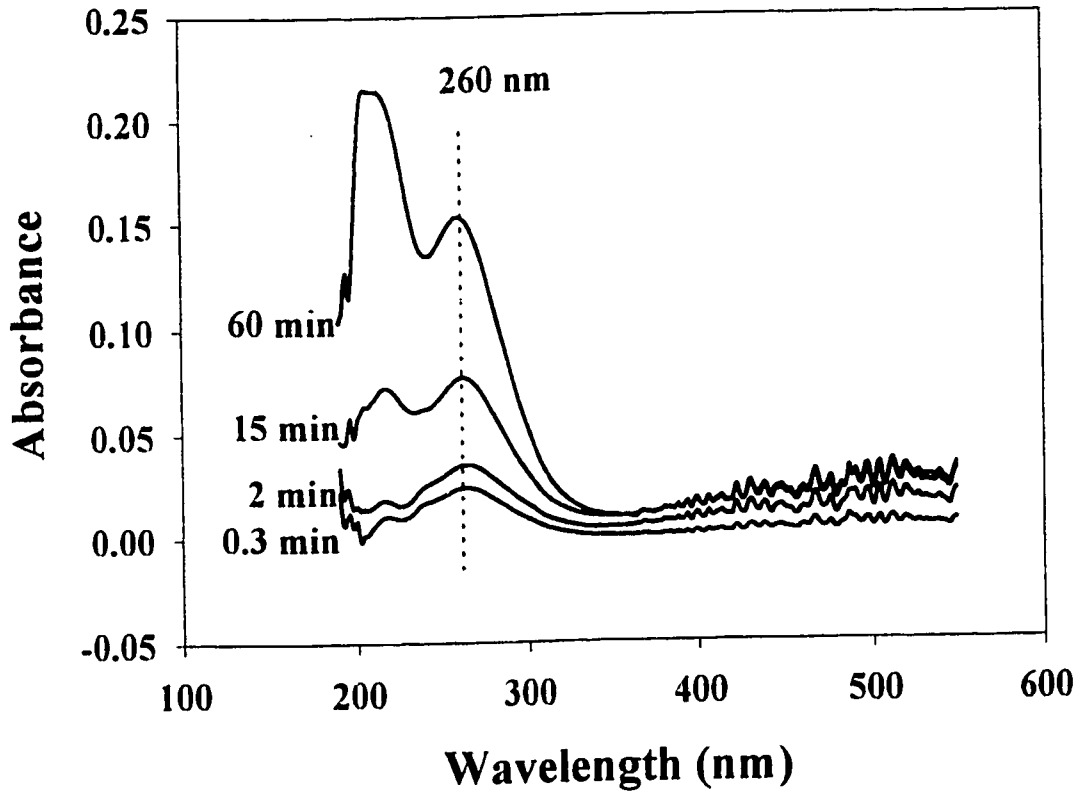

Figure 3.10 UV-VIS spectra indicating the production of soluble Mn(III)-pyrophosphate complex over time during the reaction of birnessite with 50 mM pyrophosphate at pH 6.5. The dotted line represents the wavelength used for quantification of initial Mn(III) extraction rates by pyrophosphate.

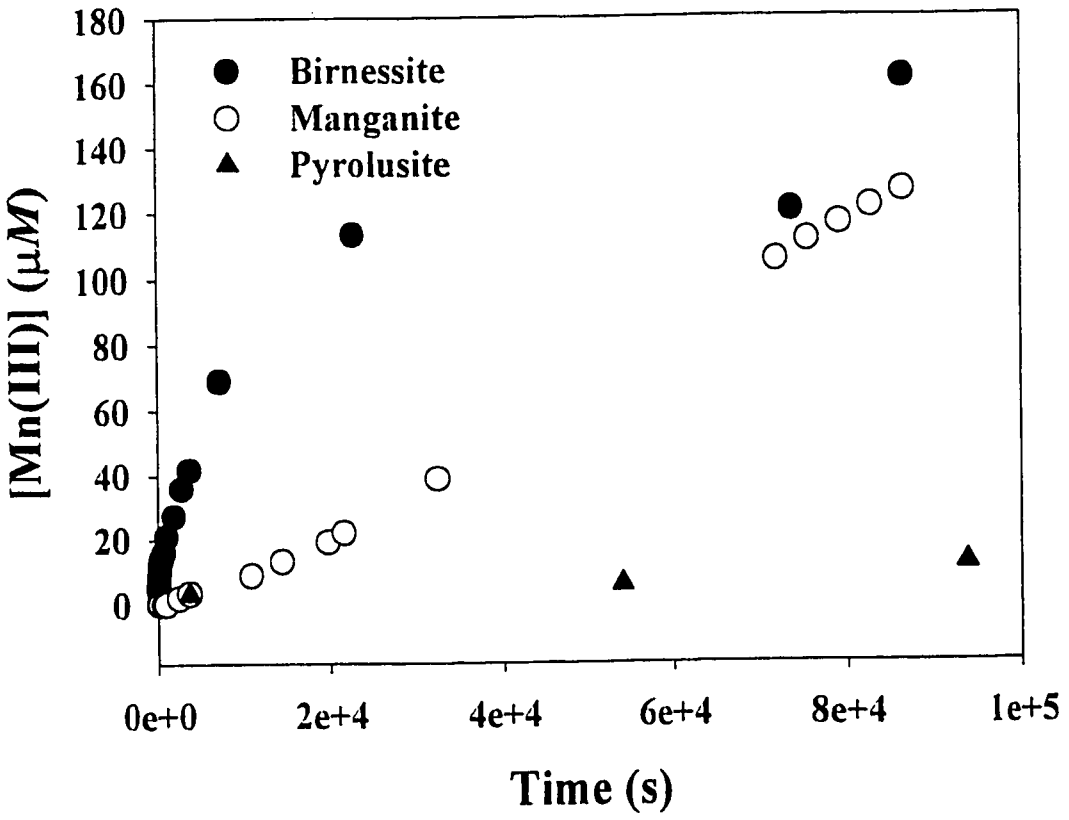

Figure 3.11 Rates of Mn(III) extraction from birnessite, manganite, and pyrolusite by 50 mM pyrophosphate at pH 6.5.

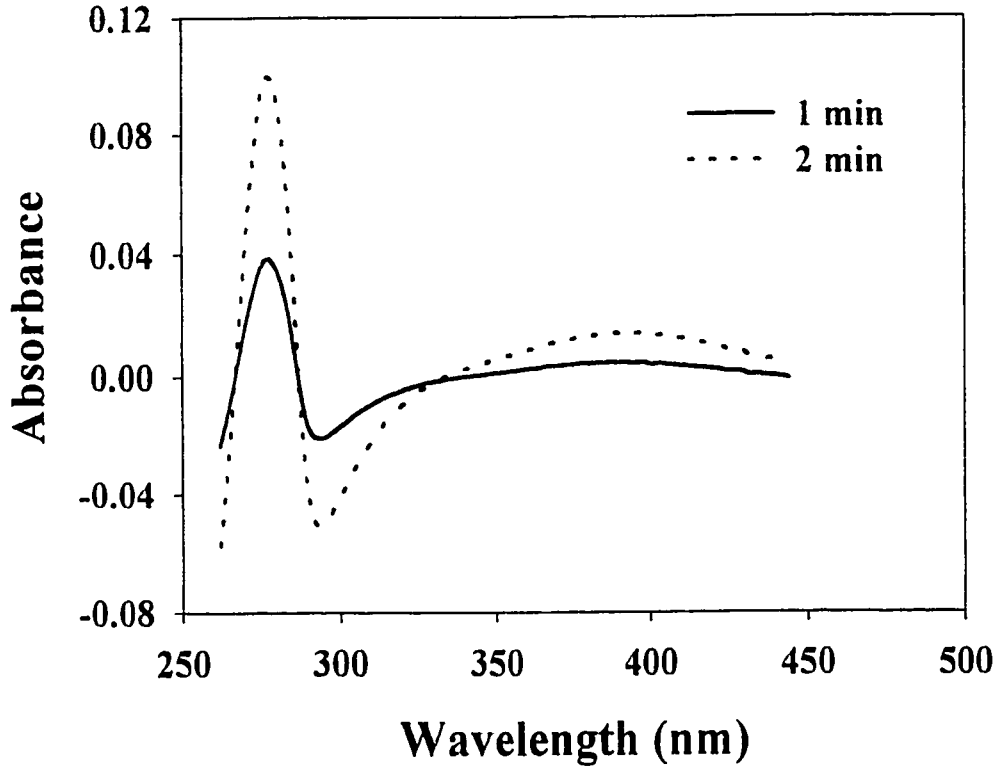

Figure 3.12 UV-VIS spectra of a 40 μ*M* sample of Mn(III)-pyrophosphate reacted with 98 μ*M* [CAT] at pH 6.5. The increase in intensity around the catechol parent peak of 275 nm was due to product formation and occurred because Mn(III)-pyrophosphate complex was used as the blank

birnessite was reactive towards 98 μM of catechol in solution based on rapid formation of catechol reaction products at 236, 292, and a broad band at 400 nm (Figure 3.12). The fact that the Mn(III)-pyrophosphate complex reacted with catechol in solution was an interesting finding because past researchers observed no reactivity using pyruvate and oxalate as reductants (Kostka et al., 1995).

No correlation existed between the initial reductive dissolution rates (R) of the three phases by catechol and the thermodynamic driving force (see Table 3.1). In contrast, a linear trend existed between R and the initial rate of Mn(III) extraction by pyrophosphate (r) with 95% of the variation in the reduction rate described by available Mn(III) (Figure 3.13). It is interesting that despite differences in structure between the three mineral phases, with pyrolusite and manganite representing crystalline end members of the rutile structure type and birnessite consisting of a disordered layer structure, the reductive dissolution rate by catechol can be adequately described by available Mn(III) within the mineral.

3.5 Conclusions

In this study, the reactivity of three different Mn oxide minerals were compared with respect to their reduction by catechol, a model analogue of soil organic matter, using kinetic and *in situ* spectroscopic studies. Structural Mn(III) in birnessite and manganite was characterized using diffuse reflectance spectroscopy (DRS) and revealed band positions at energies indicative of different coordination environments. Catechol adsorbed as an inner-sphere surface complex prior to electron transfer on

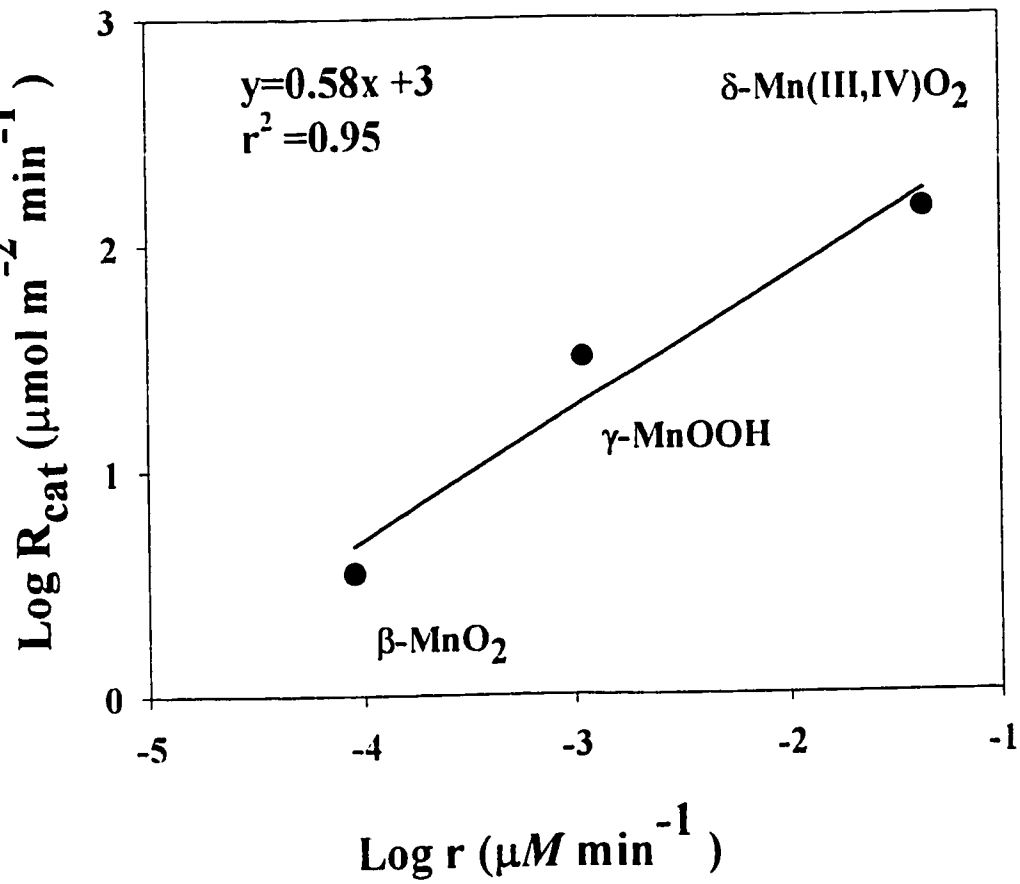

Figure 3.13 Relationship between the initial rate of Mn(III) extraction by pyrophosphate, defined as available Mn(III), and the the reductive dissolution rate by catechol.

manganite and birnessite based on ligand-to-metal-charge transfer (LMCT) bands located by difference spectra at energies of 10812 cm^{-1} for birnessite and 12674 cm^{-1} for manganite. Kinetics of the reduction of the solid phases by catechol were measured using electron paramagnetic resonance (EPR) spectroscopy and stirred batch studies. Surface area-normalized initial reductive dissolution rates decreased in the order birnessite > manganite > pyrolusite. The differences in the rates were not correlated with the thermodynamic driving force for the respective half reactions, but were linearly related by available structural Mn(III). Therefore, the role of Mn(III) in different coordination environments merits special attention in abiotic cycling of soil organic matter and Mn cycling.

3.6 References

Borgias, B.A., S.R. Cooper, Y.B. Koh, and K.N. Raymond. 1984. Synthetic, structural, and physical studies of titanium complexes of catechol and 3,5-Di-*tert*-butylcatechol. Inorg. Chem. 23:1009-1016.

Burns, R.G. 1993. Mineralogical applications of crystal field theory. Cambridge University Press, Cambridge, Great Britain.

Davies, G. 1969. Some aspects of the chemistry of manganese(III) in aqueous solution. Coor. Chem. Rev. 4:199-224.

Diebler, H., and N. Sutin. 1964. The kinetics of some oxidation-reduction reactions involving manganese(III). J. Phys. Chem. 68:174-180.

Dingle, R. 1966. The visible and near infrared spectrum of manganese(III) complexes. Acta Chem. Scand. 20:33-44.

Drits, V.A, E. Silvester, A.I. Gorshkov, and A. Manceau. 1997. Structure of synthetic monoclinic Na-rich birnessite and hexagonal birnessite: I. Results from x-ray diffraction and selected-area electron diffraction. Am. Mineral. 82:946-961.

Evanko, C.R., and D.A. Dzombak. 1998. Influence of structural features on sorption of NOM-analogue organic acids to goethite. Environ. Sci. Technol. 32: 2846-2855.

Filius, J.D., D.G. Lumsdon, J.C.L Meeussen, T. Hiemstra, and W.H.V. Riemsdijk. 1999. Adsorption of fulvic acid on goethite. Geochim. Cosmochim. Acta. 64:51-60.

Geschwind, S., P. Kislink, M.P. Klein, J.P. Remeika, and D.L. Wood. 1962. Sharp-line fluorescence, electron paramagnetic resonance and thermoluminescence of Mn(IV) in α-Al_2O_3. Phys. Rev. 126:1684-1686.

Giovanoli, R., and U. Leuenberger. 1969. Über die oxydation von manganoxidhydroxid. Helv. Chim. Acta 52:2333-2340.

Gu, B., J. Schmitt, Z. Chen, L. Liang, and J.R. McCarthy. 1995. Adsorption and desorption of different organic matter fractions on iron oxide. Geochim. Cosmochim. Acta. 59:219-229.

Hartman, J.R., B.M. Foxman, and S. R. Cooper. 1984. Higher valent manganese chemistry. Synthetic, structural, and solution studies on $[Mn(catecholate)_3]^{n-}$ (n=2,3) complexes. Inorg. Chem. 23:1381-1387.

Khan, F.A., and T.E. Fenton. 1996. Secondary iron and manganese distributions and aquic conditions in a mollisol catena of central Iowa. Soil Sci. Soc. Am. J. 60:546-551.

Klewicki, J.K., and J.J. Morgan. 1998. Kinetic behavior of Mn(III) complexes of pyrophosphate, EDTA, and citrate. Environ. Sci. Technol. 32:2916-2922.

Kostka, J.E., G.W. Luther III, and K.H. Nealson. 1995. Chemical and biological reduction of Mn(III)-pyrophosphate complexes: Potential importance of dissolved Mn(III) as an environmental oxidant. Geochim. Cosmochim. Acta 59:885-894.

Lever, A.P.B. 1984. Inorganic electron spectroscopy. Elsevier, Amsterdam.

Luther, G. W. III. 1990. Frontier molecular orbital theory in geochemical processes. p. 173-198. *In* W. Stumm (ed.) Aquatic chemical kinetics: Reaction rates of processes in natural water. Wiley-Interscience, New York.

Luther, G.W. III, D.T. Ruppel, and C. Burkhard. 1998. Reactivity of dissolved Mn(III) complexes and Mn(IV) species with reductants: Mn redox chemistry without a dissolution step? p. 265-280. *In* D.L. Sparks and T.J. Grundl (ed.) Mineral-water interfacial reactions: Kinetics and mechanisms. ACS Symposium Ser. No. 715, Washington, DC.

Magers, K.D., C. G. Smith, and D. T. Sawyer. 1978. Polarographic and spectroscopic studies of the manganese(II), -(III), and –(IV) complexes formed by polyhydroxy ligands. Inorg. Chem. 17:515-523.

Margerum, D.W., G.R. Cayley, D.C. Weatherburn, and G.K. Pagenkopf. 1978. Kinetics and mechanisms of complex formation and ligand exchange. Am. Chem. Soc. Monogr. 174:1-220.

Matocha, C.J., D.L. Sparks, J.E. Amonette, and R.V. Kukkadapu. 2000. Kinetics and mechanism of birnessite reduction by catechol. Soil Sci. Soc. Am. J. In review.

McBride, M.B. 1989a. Oxidation of dihydroxybenzenes in aerated aqueous suspensions of birnessite. Clays Clay Miner. 37:341-347.

McBride, M.B. 1989b. Oxidation of 1,2- and 1,4-dihydroxybenzene by birnessite in acid aqueous suspension. Clays Clay Miner. 37:470-486.

McKeague, J.A. 1967. An evaluation of 0.1M pyrophosphate and pyrophosphate-dithionite in comparison with oxalate as extractants of the accumulation products in podzols and other soils. Can. J. Soil Sci. 47: 95-99.

McKenzie, R. M. 1971. The synthesis of birnessite, cryptomelane, and some other oxides and hydroxides of manganese. Mineral. Mag. 38:493-502.

Orgel, L.E. 1966. An introduction to transition metal chemistry: Ligand field theory. Methuen, London.

Pedersen, J.A. 1973. Electron spin resonance studies of oxidative processes of quinones and hydroquinones in alkaline solution: Formation of primary and secondary semiquinone radicals. J.C.S. Perkin II 2: 424-431.

Reisenauer, H.M. 1988. Determination of plant-available soil manganese. p.87-98. *In* R.D. Graham et al. (eds.) Manganese in soil and plants. Kluwer Academic Publishers, The Netherlands.

Richert, S.A., P.K.S. Tsang, and D. T. Sawyer. 1988. Ligand-centered oxidation of manganese(II) complexes. Inorg. Chem. 27:1814-1818.

Sherman, D.M. 1984. The electronic structures of manganese oxide minerals. Am. Mineral. 69:788-799.

Sherman, D.M. and N. Vergo. 1988. Optical spectrum, site occupancy, and oxidation state of Mn in montmorrilonite. Amer. Mineral. 73:140-144.

Shriver, D.F., P. Atkins, and C.H. Langford. 1994. Inorganic chemistry. 2nd ed. W.H. Freeman and Co., New York.

Silvester, E, A. Manceau, and V.A Drits. 1997. Structure of synthetic monoclinic Na-rich birnessite and hexagonal birnessite: II. Results from chemical studies and EXAFS spectroscopy. Am. Mineral. 82:962-978.

Sims, J.L., P. Duangpatra, J.H Ellis, and R.E. Phillips. 1979. Distribution of available manganese in Kentucky soils. Soil Sci. 127:270-274.

Stone, A.T., K.L. Godtfredsen, and B. Deng. 1994. Sources and reactivity of reductants encountered in aquatic environments. p.337-374. *In* G. Bidoglio and W. Stumm (ed.) Chemistry of aquatic systems: Local and global perspectives. ECSC, The Netherlands.

Stone, A.T., and J. J. Morgan. 1984a. Reduction and dissolution of manganese (III) and manganese (IV) oxides by organics. 1. Reaction with hydroquinone. Environ. Sci. Technol. 18:450-456.

Stone, A.T., and J. J. Morgan. 1984b. Reduction and dissolution of manganese (III) and manganese (IV) oxides by organics. 2. Survey of the reactivity of organics. Environ. Sci. Technol. 18:617-624.

Wendlandt, W.M., and H. Hecht. 1966. Reflectance spectroscopy. InterScience, New York.

Xyla, A.G, B. Sulzberger, G.W. Luther III, J.G. Hering, P. van Cappellen, and W. Stumm. 1992. Reductive dissolution of manganese (III,IV) (hydr)oxides by oxalate: The effect of pH and light. Langmuir 8:95-103.

Yates, D.E., and T.W. Healy. 1975. Mechanism of anion adsorption at the ferric and chromic oxide/water interfaces. J. Colloid Interface Sci. 52: 222-228.

Chapter 4

REACTIVITY OF Pb(II) AT THE Mn(III,IV) (HYDR)OXIDE-WATER INTERFACE

4.1 Abstract

In this study, the reactivity of Pb(II) on naturally occurring Mn(III,IV) (hydr)oxide minerals was evaluated using kinetic, thermodynamic, and spectroscopic investigations. Pb(II) was more strongly adsorbed to birnessite (δ-MnO_2) than manganite (γ-MnOOH) under all experimental conditions. This was reflected in the greater estimated ΔG°_{chem} value for birnessite (–83.6 kJ mol^{-1}) than manganite (ΔG°_{chem}=-66.6 kJ mol^{-1}). The kinetic studies, adsorption isotherms, and ionic strength and pH edges suggested the existence of inner-sphere surface complexes between Pb and both Mn minerals. The isoteric heat of adsorption (ΔH_{Γ}) describing Pb adsorption on birnessite was 94 kJ mol^{-1} at 1.1 mmol g^{-1}, and decreased with increasing adsorption density. This indicated that adsorption was an endothermic process and that birnessite possessed varying sites of reactivity for Pb. X-ray absorption fine structure (XAFS) spectroscopic characteristics of inner-sphere surface complexes were identified between Pb-birnessite and Pb-manganite with no evidence to suggest surface precipitation or oxidation as operative sorption mechanisms. Significant differences in the intensity of the second coordination shell at $R_{Pb\text{-}Mn}$=3.74 Å between birnessite and

manganite at similar surface loadings of 3.5 and 4.4 μmol m^{-2} indicated a difference in the type of adsorption complex between the two phases as reflected in the higher coordination number (N=3) for birnessite. The similarity between Zn-birnessite and Pb-birnessite XAFS spectra based on the second shell peak indicated that Pb and Zn were adsorbed to similar sites, namely above and below structural vacancies in the interlayer. The different adsorption complexes agreed with estimated thermodynamic parameters and led to contrasting desorption behavior. These results have significant implications for Pb partitioning in soils containing solid phase Mn(III,IV) (hydr)oxides.

4.2 Introduction

Environmental concerns over Pb(II) contamination in soils, sediments, and aquatic settings has given rise to the development of remediation strategies targeted at reducing the solubility and toxicity of Pb(II). Since Pb(II) is generally associated with insoluble mineral phases or bound through sorption processes in contaminated soils (Sauvé et al., 1998), the proposed strategies have focused on decreasing the solubility of Pb(II) through partitioning to solid phase minerals (Ainsworth et al., 1994; Ma et al., 1994; Ford et al., 1997; Martinez and McBride, 1998; Strawn et al., 1998) and through phytoremediation (Huang et al., 1997). Understanding the reactivity of soil components with Pb is necessary to predict the fate and transport of Pb in the environment and optimize remediation efforts. This requires combining macroscopic and spectroscopic techniques to obtain mechanistic information (Sparks, 1995).

Sorption mechanisms of Pb on clays and oxides are complex. Strawn et al.(1998), employing XAS, noted that Pb sorbed as an inner-sphere bidentate surface complex on γ-Al_2O_3 with no evidence to suggest surface precipitation. Bargar et al. (1996) conducted grazing-incidence XAS studies and showed that both outer-sphere and inner-sphere surface complexes occur between Pb and surface functional groups on α-Al_2O_3 depending on the specific surface site exposed. The uptake of Pb on goethite was enhanced in the presence of Cl^- due to Pb-Cl^--Fe(s) ternary complex formation based on XAFS-derived Pb-Fe distances (Bargar et al., 1998). Other studies using 2:1 phyllosilicate minerals with fixed structural charge have reported metal exchange on basal planes and inner-sphere surface complexation at edge sites for Pb depending on ionic strength and pH (Strawn and Sparks, 1999).

The reactivity of Pb at the Mn(III,IV) (hydr)oxide-water interface is not clearly understood. The phyllomanganates or the birnessite group minerals are nonstoichiometric, possess low points of zero charge (PZC), and are typified by high specific surface areas, which endow them with significant surface reactivity (McKenzie, 1989). Thus, they can drastically affect surface charge characteristics of bulk field soils (Chorover and Sposito, 1995). It has been shown that birnessite has a disproportionately high sorption capacity for Pb, despite its low relative abundance in soils (Jenne, 1968; Gatte and Laitinen, 1974; McKenzie, 1980). Gatte and Laitenen (1974) suggested that the high affinity of Pb for hydrous manganese dioxide over a wide pH range was attributed to oxidation of Pb(II) to Pb(IV) (as PbO_2) by MnO_2

despite the unfavorable thermodynamics ($\Delta G = 32$ kJ mol^{-1}). Cronan (1974) reported that Pb present in marine Mn nodules exists as Pb(IV). Hem (1978) discussed that Pb(IV) can be substituted in the Mn oxide structure because it has a compatible ionic radius (r=0.77 Å) with high-spin species of Mn(II) (0.82 Å) and Mn(III) (0.65 Å) when compared to the much larger Pb(II) ion (1.20 Å). McKenzie (1980) argued that strong specific (inner-sphere) binding accounted for Pb(II) sorption behavior on birnessite and suggested the possibility of the formation of Pb-Mn minerals such as coronadite. Biogenically produced Mn oxides were found to adsorb several times more Pb than abiotically prepared Mn oxide (Nelson et al., 1999). In most of these studies, only macroscopic observations were reported. It is possible that the layer type birnessite minerals contain multiple sorption sites with a range of reactivities for Pb(II). Manceau et al. (1992) first explored the surface complex between Pb and birnessite using XAS and reported Pb(II) as a backscatterer in the second coordination shell. They concluded that Pb formed multinuclear surface complexes with birnessite. However, recent XAS investigations reported Mn as a next nearest neighbor in the second coordination shell after reacting Pb with birnessite (Manceau et al., 1997; Morin et al., 1999). The Pb sorption mechanism was explained as inner-sphere by sharing edges with surface MnO_6 octahedra at low surface coverages, while at greater surface coverages, Pb sorbed above or below lattice vacancies as tridentate complexes. These studies were conducted under a limited set of experimental conditions.

To our knowledge, there is little information available linking spectroscopic with kinetic and thermodynamic studies of the Pb-birnessite interface which is necessary because birnessite is the most commonly identified Mn oxide mineral in soils (McKenzie, 1989). The reactivity of a naturally occurring solid Mn(III) mineral with Pb(II), such as manganite (γ-MnOOH), has not been investigated although it has a greater reduction potential than birnessite at pH< 6. The present study was undertaken to reconcile differences in the literature by further interrogation of Pb(II) reactivity at the Mn(III,IV) (hydr)oxide-water interface employing a combination of thermodynamic, kinetic, and spectroscopic studies.

4.3 Materials and Methods

4.3.1 Materials

The birnessite (δ-MnO_2) solid phase mineral was prepared according to procedures outlined by McKenzie (1971) by reduction of closed shell Mn(VII) (as boiling $KMnO_4$) with concentrated HCl. The precipitate was vacuum filtered, dialyzed against deionized water to remove excess salts, and freeze-dried. Measured BET surface area of birnessite was 40 $m^2\ g^{-1}$, iodometrically-determined oxidation state was 3.44, and powder x-ray diffraction d-spacings confirmed the presence of synthetic birnessite. Total concentrations of Mn and K were 49% and 16% as measured by dissolving a known solid weight with 12 *M* HCl and acidified $NH_2OH{\bullet}HCl$. The pH at the point of zero charge (PZC) was estimated by microelectrophoretic mobilities, potentiometric titrations in NaCl background, and

Ca^{2+} sorption experiments and revealed an extrapolated PZC of 2. Manganite (γ-MnOOH) was synthesized by oxidizing Mn(II) (as $MnSO_4$) with 30% H_2O_2 and forcing precipitation with 0.2*M* NH_3 (Giovanoli and Leuenberger, 1969). The product was filtered, washed and dialyzed to remove salts, and dried over P_2O_5 in a vacuum dessicator. This procedure produced a crystalline manganite based on sharp XRD peaks with 55% total Mn, mean oxidation state of 3.02, BET surface area of 32 $m^2\ g^{-1}$, and estimated PZC of 6.25.

4.3.2 Reactivity Experiments

Lead sorption kinetic studies were conducted in batch using the pH-stat technique under a N_2 purge to remove CO_2. For birnessite, rate studies were conducted at pH 3.5 in 0.01 *M* $NaClO_4$, an initial Pb concentration of 1.9 m*M*, and 1.0 g L^{-1}. Under these conditions, MINEQL$^+$ indicates the predominant Pb species to be 98.4% free Pb^{2+}(aq) and 1.6% $PbHCO_3^+$ (aq). Aliquots of Pb were added from a 0.1 *M* $Pb(ClO_4)_2$ stock solution. Release rates of Mn were also followed to check for metal-promoted dissolution of the solid phase.

The pH-edge experiments were conducted at ionic strengths of 0.1 *M* and 0.01 *M* $NaClO_4$ in a glovebox (to prevent possible precipitation of $PbCO_3$) under N_2 with boiled DI water at 296 K and 1 g L^{-1} birnessite and 0.1 g L^{-1} manganite. Adsorption isotherms of Pb on birnessite were determined using the batch equilibration method at 278 and 296 K using 1 g L^{-1} at pH 3.5. Isotherms describing Pb adsorption were measured on 0.1 g L^{-1} manganite in the glovebox. Both sorbents were preequilibrated

at the desired pH in 0.01 *M* $NaClO_4$ overnight before aliquots were transferred to centrifuge tubes and spiked with appropriate aliquots of a 0.1 *M* Pb stock solution to achieve initial Pb concentrations ranging from 9.6×10^{-6} to 1.5×10^{-3} *M*. The strong pH dependence of Pb uptake on manganite necessitated the use of 5 m*M* MES [2-(N-morpholino)ethane sulfonic acid] buffer, adjusted to pH 6.7. This buffer did not complex Pb(II) or react with the manganite surface (no release of soluble Mn) under the experimental conditions employed. Aliquots were removed after 3 h of reaction time and filtered through 0.2 μm pore size membrane filters and quenched with 12 μL of concentrated HNO_3. Concentrations of Pb and Mn in solution were measured using flame atomic absorption spectrometry (AAS) with detection limits of 4.8 μ*M* and 5.5 μ*M* and under certain cases, graphite furnace AAS was employed for Pb with a lower detection limit of 0.24 μ*M*.

Desorption experiments were conducted at 298 K by removing the equilibrium supernatant solution, replacing the solution with an equal volume of $NaClO_4$ background solution, and resuspending the Mn oxide-solution mixture for the same reaction time as the adsorption isotherm experiments (3 h).

The change in free energy of adsorption under standard conditions, ΔG^o_{ads}, is a combination of the change in coulombic energy (ΔG^o_{coul}), solvation energy (ΔG^o_{solv}), and chemisorption or specific adsorption energy (ΔG^o_{chem}) (Stumm et al., 1970; James and Healy, 1972; Parks, 1975)

$$\Delta G^o_{ads} = \Delta G^o_{chem} + \Delta G^o_{coul} + \Delta G^o_{solv} \qquad [1]$$

If specific adsorption accompanies the overall adsorption process, then at the estimated PZC, the electrostatic term ΔG^{o}_{coul} reduces to zero and it can be assumed that $\Delta G^{o}_{chem} > \Delta G^{o}_{solv}$ which reduces [1] to

$$\Delta G^{o}_{ads} \cong \Delta G^{o}_{chem} \quad [2]$$

and allows one to estimate ΔG^{o}_{chem} using the Grahame equation

$$\Gamma_{Pb} = 2rC_{Pb} \exp(-\Delta G^{o}_{ads}/RT) \quad [3]$$

where Γ_{Pb} is the surface coverage of Pb (mol cm^{-2}) in the Stern plane, r is the radius of the adsorbed Pb (cm), C_{Pb} is the equilibrium Pb concentration (mol cm^{-3}), R is the molar gas constant (J mol^{-1} K^{-1}), and T is the absolute temperature (K). This approach has been used by others to estimate ΔG^{o}_{chem} (James and Healy, 1972; Murray, 1975).

The mean isoteric heat of adsorption at a given surface adsorption density, ΔH_{Γ} (kJ mol^{-1}), was estimated with the Clausius-Clapeyron equation (Chiou and Shoup, 1985):

$$\Delta H_{\Gamma} = R \ln[(C_2/C_1)]/(1/T_2 - 1/T_1) \quad [4]$$

where R is the molar gas constant (kJ mol^{-1} K^{-1}), C_2 (mol dm^{-3}) is the equilibrium concentration of an ion at absolute temperature T_2 (K); C_1 (mol dm^{-3}) is the equilibrium concentration of an ion at absolute temperature T_1 (K).

4.3.3 XAFS Analysis

X-ray absorption fine structure (XAFS) spectra were collected at beamline X-11A at the National Synchrotron Light Source (NSLS) at Brookhaven National Laboratory, Upton, NY, to explore the chemical nature of the Pb-reacted birnessite and

manganite samples. The electron beam energy was 2.5 GeV and Pb L_{III}-edge (13055 eV) spectra were collected in fluorescence mode using a Stern-Heald detector filled with Kr and an As filter to minimize elastic scattering of the samples and six sheets of Reynolds aluminum foil to minimize Mn-K_α background fluorescence. Samples were prepared in the glovebox using 10 g L^{-1} birnessite and manganite, with initial concentrations of Pb to yield approximately similar loadings on the surface. A minimum of three scans were collected per sample with the following scan settings: -200 to –30 eV (relative to the Pb edge) in 10 eV steps and 1 s resolution; -30 to 30 in 0.5 eV steps at 1 s resolution; 30 eV to 6 $Å^{-1}$ in 0.07 $Å^{-1}$ steps at 2 s resolution; 6 $Å^{-1}$ to 11 $Å^{-1}$ in 0.07 $Å^{-1}$ steps at 5 s resolution. Data reduction steps were performed using WinXAS 97 1.1. In extracting the $\chi(k)$ function, the XAFS signal was isolated from the absorption edge background by using a cubic spline function fit with eleven segments. The k^3-weighted $\chi(k)$ function was then Fourier-transformed over k= 2-10 $Å^{-1}$ to yield the radial structure function (RSF). Data fitting was done in k space with a multishell fit routine. Theoretical scattering paths were generated by FEFF 7.02 (Rehr et al., 1991), using an input file based on a model of α-PbO (Leciejewicz, 1961) generated with the program ATOMS. Lead was substituted in birnessite and manganite structural refinements to get the scattering paths.

4.4 Results and Discussion

4.4.1 Adsorption Kinetics

The kinetics of Pb sorption on birnessite were rapid, with 55% sorbed within 15 s and 82% sorbed after 3 h (Figure 4.1). The sorption reaction slowly continued, with 86% removed from solution after 24 h. The adsorption of Pb on manganite was rapid and essentially complete after 3 h with no detectable release of Mn to solution (data not shown). Rapid sorption of Pb by metal oxides followed by slower uptake over time is well documented in the literature (Benjamin and Leckie, 1981; Strawn et al., 1998). Mechanistic explanations for the slower Pb uptake on birnessite include diffusion into micropores of solids followed by sorption to interior sites, surface precipitation, or binding to lower energy sites (Strawn and Sparks, 1998). More Pb was sorbed on birnessite at 23^{O}C than 5 ^{O}C throughout the entire reaction period suggesting an endothermic reaction. Manganese(II) release from solid phase birnessite was concurrent with Pb sorption, totaling 1% of the total Mn added. Birnessite consists of edge-sharing Mn(IV)O_6 octahedra interlayered with sheets of water molecules and one of six octahedral sites is unoccupied. The charge on the sheets generated by these vacancies is compensated for by Mn(II) and Mn(III) situated above and below the interlayer vacancies octahedrally coordinated by oxygens in the Mn(IV)O_6 octahedral sheet and water molecules in the interlayer (Giovanoli et al., 1970; Golden et al., 1986). The Mn(II), present as a charge balancing cation in the interlayer vacancy sites of birnessite, was likely displaced from the structure by sorbed

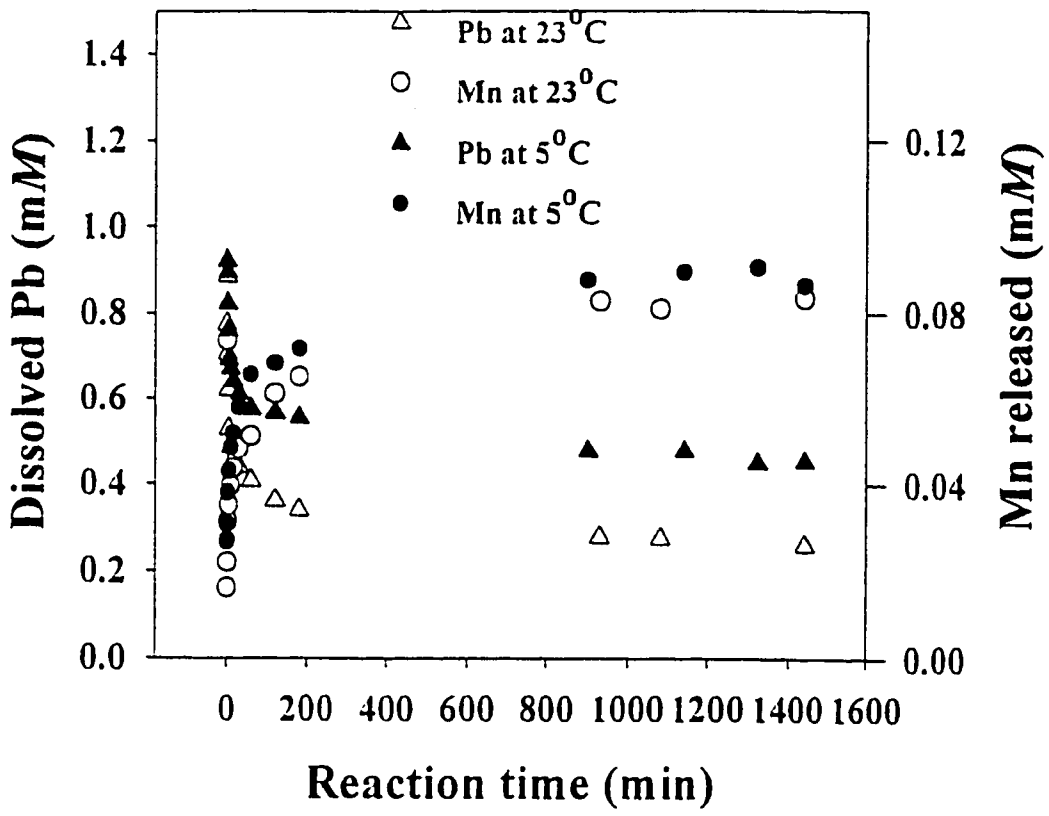

Figure 4.1 Pb(II) sorption kinetics and Mn(II) release on 1 g L^{-1} birnessite suspension at pH 3.5, I=0.01 M $NaClO_4$, and $[Pb_T]$=1.9 mM, as a function of temperature.

Pb. Thus, the diffusion of Pb in the interlayer must occur to displace structural Mn(II) which is consistent with an endothermic process.

The rapid rates of Pb adsorption on birnessite and manganite are closely related to the fast water exchange rates from the primary hydration sphere of the labile Pb ion, with log k_{H2O} of 10 s^{-1} (Burgess, 1988). Previous investigations have demonstrated a linear relationship between the intrinsic adsorption rate constant k_{ads}(int) for labile metal ions (measured with relaxation methods) on metal oxide surfaces and k_{H2O} (Hachiya et al., 1984; Hayes and Leckie, 1986; Grossl et al., 1994) suggesting inner-sphere adsorption.

4.4.2 Ionic Strength Edges, pH Edges, and Isotherms

Strong sorption of Pb on birnessite was demonstrated by the high affinity over a wide pH range of 1.5-7.5 and the independence of ionic strength (Figure 4.2a). These findings agree with previous studies (Gatte and Laitinen, 1974; McKenzie, 1980) for Pb reactivity on birnessite and suggest inner-sphere surface complexation. Additional experiments at lower pH and higher initial Pb concentration indicated substantial sorption at and below the PZC of birnessite (Figure 4.2b). In contrast, a pH dependence was observed for Pb sorption on manganite, with a pH_{50} of ~6.0 which is near the PZC of the surface indicating that Pb may be sorbing to deprotonated surface functional groups (Figure 4.3). The lack of a pronounced ionic strength effect and sorption below the PZC also suggest inner-sphere surface complexation of Pb on manganite.

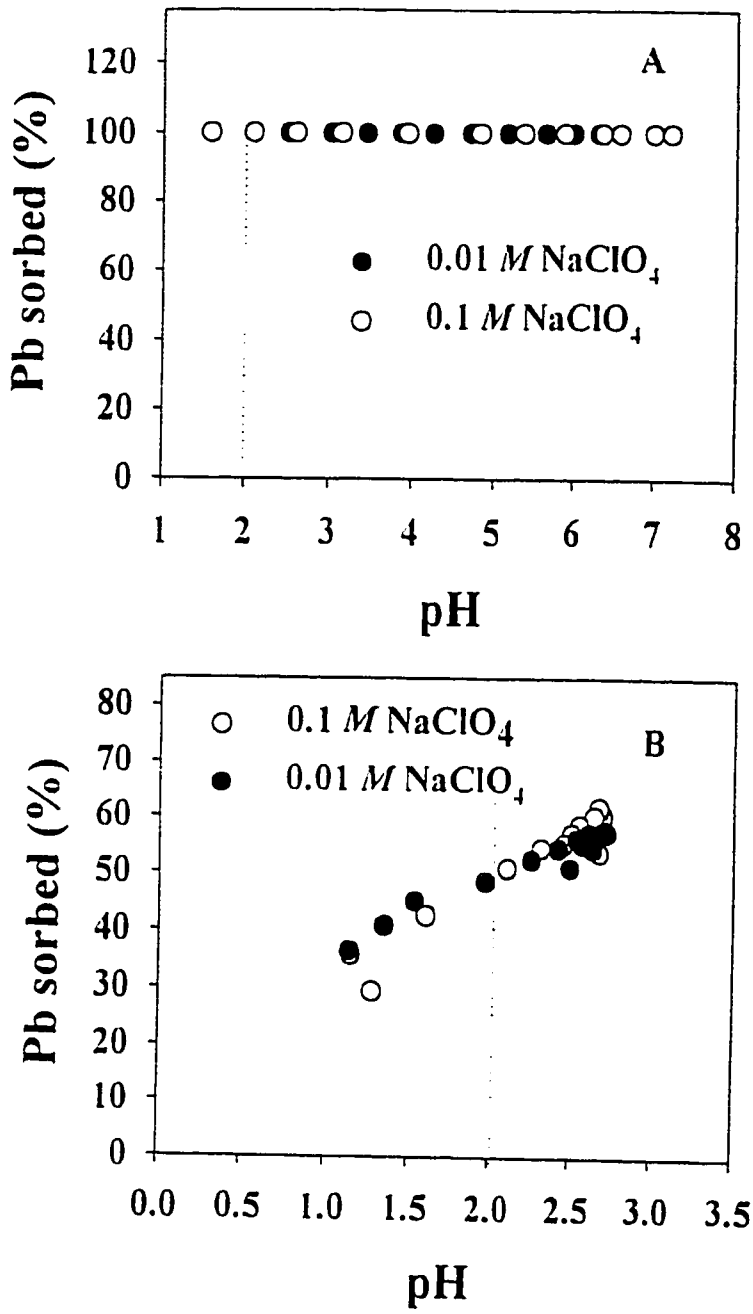

Figure 4.2 Ionic strength and pH edges at 296 K describing Pb(II) adsorption on (A) 1 g L^{-1} birnessite and initial [Pb_T]=0.14m*M* and (B) 1 g L^{-1} birnessite and [Pb_T]=2.74 m*M*. The dotted lines are a guide to indicate the PZC of birnessite.

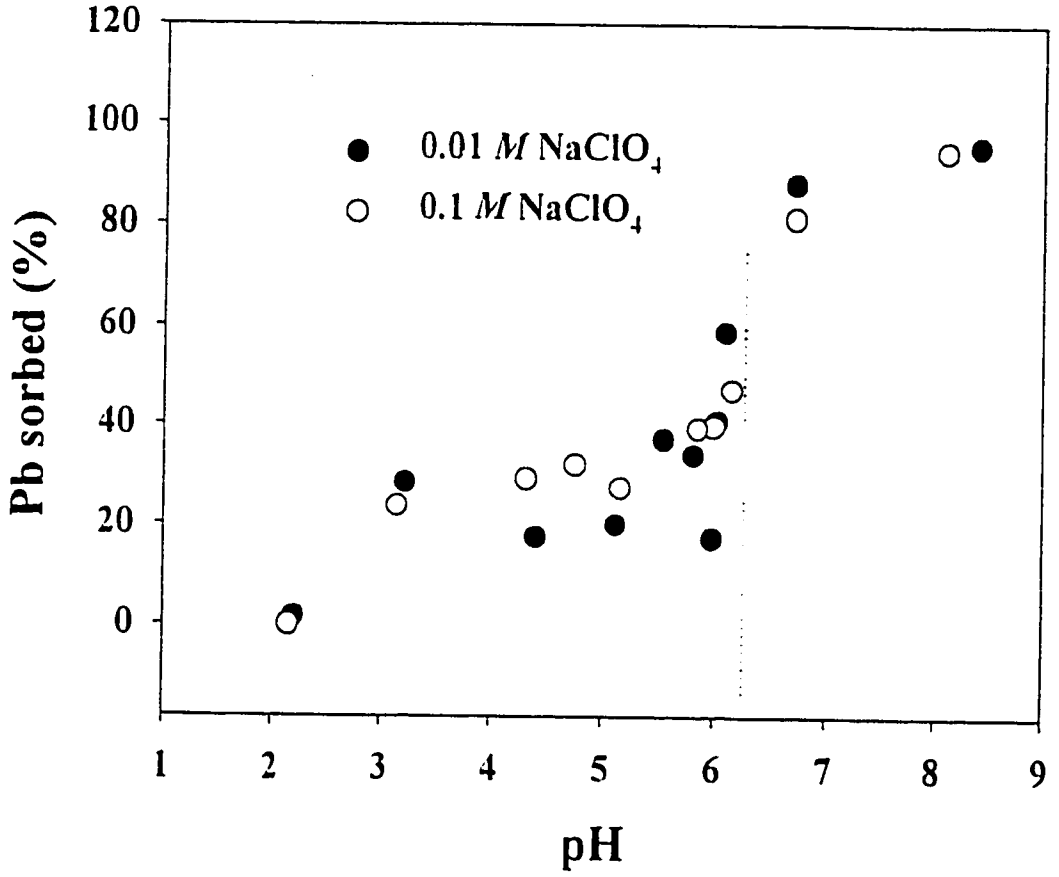

Figure 4.3 Ionic strength and pH edge of 0.1 g L^{-1} manganite suspension concentration and initial [Pb_T]=14μM. The dotted line is a guide to the PZC of manganite.

Representative adsorption isotherms describing Pb sorption on birnessite indicate a high affinity isotherm, resembling the H- or L-type isotherm with an adsorption maximum of 0.2 mol_{Pb} mol^{-1}_{Mn} (Figure 4.4a). In contrast, the Pb sorption isotherm was approximately linear (r^2=0.97) for manganite (Figure 4.4b) demonstrating the higher affinity of birnessite for Pb. More Pb was sorbed at 23° C than 5° C on birnessite in agreement with the kinetic data. The estimated isoteric heat of adsorption (ΔH_Γ) value of 94 kJ mol^{-1} at 1.1 mmol g^{-1} indicated the overall adsorption process was endothermic, driven by an increase in entropy, and the decrease in ΔH_Γ with increasing adsorption density suggested that birnessite has heterogeneous adsorption sites for Pb(II) (inset, Figure 4.4a). These sites of varying reactivity could be deprotonated surface functional groups and surface and interlayer sites situated above and below vacancies located at every sixth position in the $Mn(IV)O_6$ octahedral sheet in birnessite. Titration and modeling results of surface charge point to an active interlayer in birnessite (McKenzie, 1981) while manganite has a structure of corner-sharing $Mn(III)O_6$ octahedra with no interlayer (McKenzie, 1989). It can be anticipated that the high energy sites on birnessite could be the interlayer vacancy sites, because of the need to compensate for charge imbalance. Benjamin and Leckie (1981) proposed the heterogeneous site binding model for amorphous iron oxyhydroxide and stated that the high energy sites were occupied first, followed by lower energy sites with a decrease in binding ability of the surface at higher adsorption densities. Modeling results by Catts and Langmuir (1986)

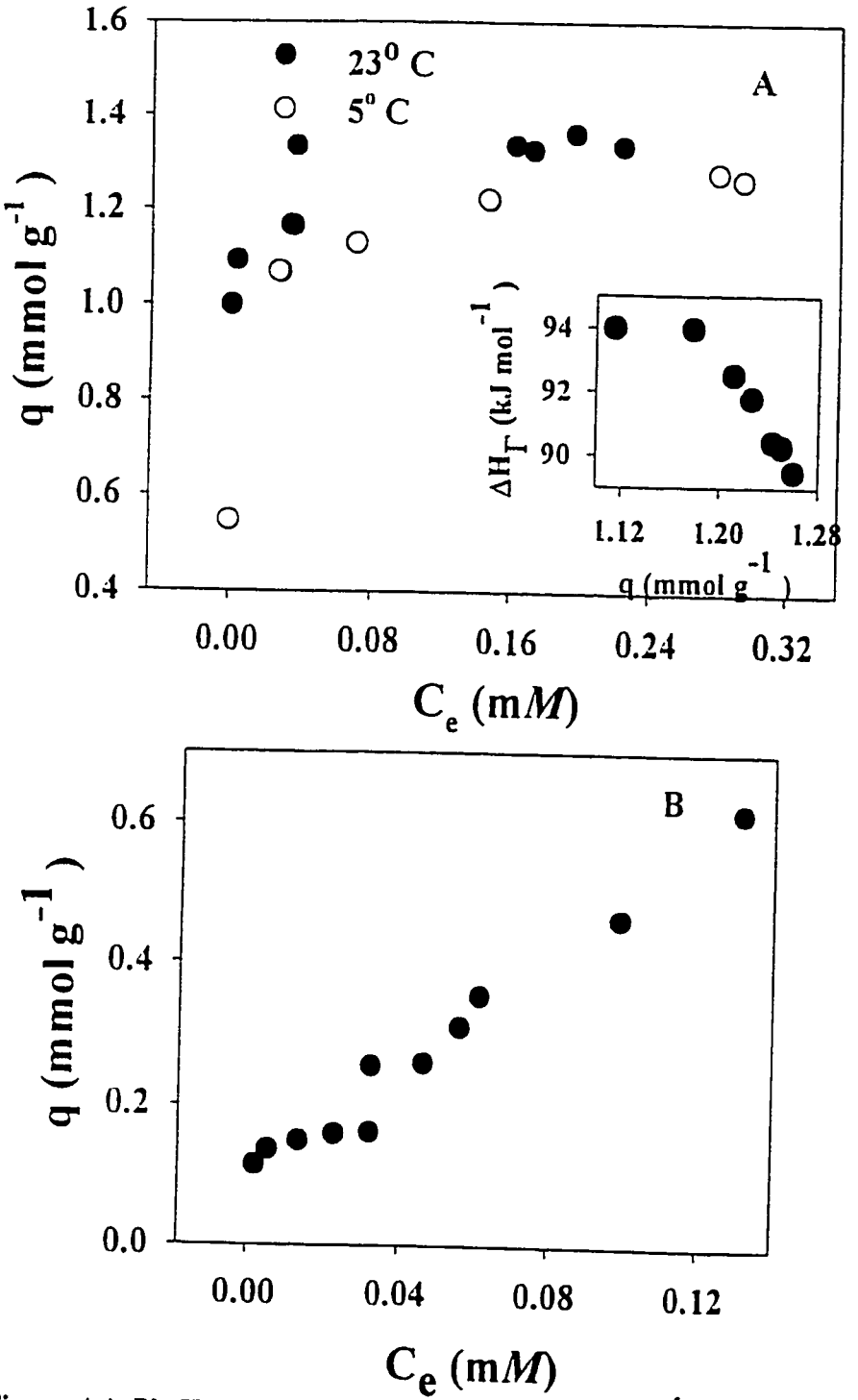

Figure 4.4 Pb(II) adsorption isotherms on (A) 1 g L^{-1} birnessite as a function of temperature, with inset showing isoteric heat of adsorption (ΔH_Γ) as a function of surface loading and (B) 0.1 g L^{-1} manganite.

describing Pb adsorption on birnessite indicated that birnessite possessed heterogeneous surface sites with a spectrum of binding energies for Pb, with the highest energy sites saturated at surface coverages of <1%. Recent XAS results demonstrated that Pb partitions to different surface sites on Al oxide surfaces as outer sphere and inner sphere surface complexes (Bargar et al., 1996). It could be that Pb(II) diffused to the interlayer vacancy sites in birnessite in the early stages of the reaction based on the concurrent release of Mn(II) during endothermic Pb(II) adsorption.

The release of Mn(II) during Pb adsorption on birnessite was concentration dependent (Table 4.1). Lead adsorption was very strong on birnessite with <1% desorbed by background $NaClO_4$ at the highest loading. More Pb was released from manganite than birnessite at ~0.1 mmol g^{-1}. The tight binding of Pb on birnessite could be ascribed to an increase in the activation energy required to break the Pb-birnessite bond (Strawn and Sparks, 1998). McKenzie (1980) reported very little desorption of Pb from birnessite using a more aggressive extractant (2.5% acetic acid) with >90% nonextractable Pb after 1 d, and 95% after 28 weeks. Desorption of Pb from hydrous iron oxide and goethite was reported to be reversible with respect to pH with no apparent residence time effect (Ainsworth et al., 1994; Eick et al., 1999). Despite spectroscopic confirmation of a bidentate inner-sphere bonding mechanism between Pb and Al oxide surfaces, desorption of Pb was nearly complete when desorption was allowed to reach equilibrium (Strawn et al., 1998). It is intriguing that

Table 4.1 Representative Pb adsorption and desorption studies and estimated thermodynamic parameters for birnessite at pH 3.7 and manganite at pH 6.7.

Solid Phase Mineral	Pb Adsorbed (mmol g^{-1})	Mn(II) Released (mM)	Pb Desorbed (%)	ΔG_{chem}^{0} (kJ mol^{-1})
Birnessite	0.1	0	0	
	0.96	0.04	0	-83.6
	1.33	0.09	0.3	
Manganite	0.14	0	6.2	
	0.26	0	100	-66.6

a labile metal ion such as Pb would be so resistant to desorption from birnessite. Additional desorption studies for longer reaction times would be useful to further characterize Pb desorption behavior.

The thermodynamic driving force for Pb adsorption was greater on birnessite than manganite based on the estimated magnitude of ΔG^{o}_{chem} (Table 4.1) and this was reflected in the stronger Pb adsorption on birnessite observed in the pH edge and isotherm experiments. The ΔG^{o}_{chem} values for Pb on birnessite and manganite exceeded those in previous investigations for Co(II), Mn(II), Ni(II), Zn(II), and Cu(II) adsorption on hydrous manganese dioxide, which ranged from –8 kJ mol^{-1} for Ni(II) to -20 kJ mol^{-1} for Co(II) (Murray et al., 1968; Murray,1975). Direct *in situ* spectroscopic evidence was obtained to explore the chemical nature of the adsorbed Pb and help explain the slow release rate of Pb.

4.4.3 XAFS

The radial structure functions (RSFs) describing Pb reacted with birnessite and manganite were fitted and compared to a β-PbO_2 standard and a Zn-reacted birnessite (Figure 4.5) because Zn has been shown to be adsorbed at structural vacancies on birnessite (Manceau et al., 1997). The RSFs have peaks characteristic of radial distances (uncorrected for phase shift) between Pb and next nearest neighbors. The best fits of the RSFs for birnessite and manganite were achieved by fitting O in the first shell and Mn in the second shell. Fitted bond lengths indicated that Pb reacted

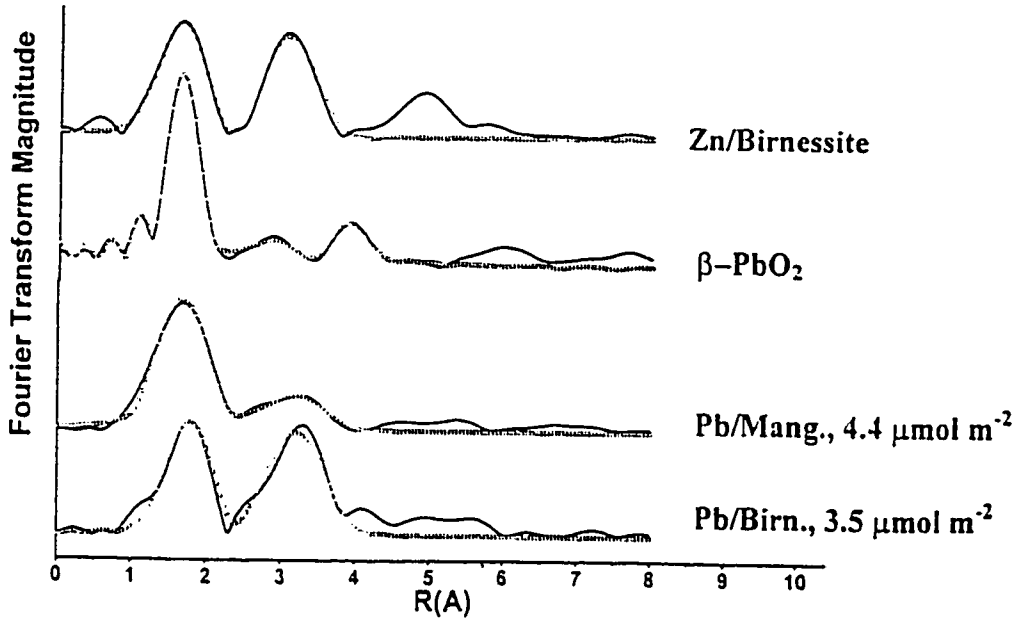

Figure 4.5 Radial structure functions (RSFs) derived from XAFS spectral analysis for Pb(II) reacted with manganite and birnessite at 296 K and I=0.01 *M* $NaClO_4$ compared to RSFs for Zn reacted with birnessite and β-PbO_2. The open symbols represent the multishell fits to the experimental data (solid lines). For Zn/birnessite and β-PbO_2 spectra, the scale is different because the first Me-O coordination shell is octahedral with N=6.

with birnessite and manganite was coordinated to surface groups with O as the ligating atom (O^{2-}, OH^-, or H_2O) in the first coordination shell with R_{Pb-O}=2.29-2.34 Å (Table 4.2). These values were consistent with Pb-O distances observed in previous studies of Pb reacted on Fe and Al oxides (Bargar et al., 1997a, b; Strawn et al., 1998). The shell appearing at about 3.5 Å in the RSFs was fit with Mn as a backscattering atom in the second shell with R_{Pb-Mn}=3.74 Å. This feature was more intense for birnessite than manganite at similar surface loadings of 3.5 and 4.4 μmol m^{-2}, indicating a difference in the adsorption complex between the two phases as reflected in the higher coordination number (N=3) for birnessite. The similarity between Zn-birnessite and Pb-birnessite spectra with respect to second shell Mn scattering indicated that Pb and Zn were adsorbed to similar sites, namely above and below structural vacancies in the interlayer. For the Pb-birnessite sample, the feature remained unchanged from 15 min to 24 h reaction time (data not shown) suggesting that Pb may have entered the interlayer sites to displace Mn(II) initially with continued uptake at similar sites over time.

Attempts to fit Pb in the second shell were unsuccessful which demonstrated that surface precipitation and oxidation were not operative mechanisms of Pb(II) uptake on birnessite and manganite under these experimental conditions. The lack of Pb(II) oxidation was further confirmed by comparison with the XAFS data of β-PbO_2 (Figure 4.5 and Table 4.2). The shorter bond distance for β-PbO_2 in the first

Table 4.2 Structural parameters derived from XAFS analyses.

	Me-O Shell			Me-Mn Shell			Pb-Pb Shell		
Sample	R(Å)†	N‡	σ^2(Å^2)§	R(Å)	N	σ^2(Å^2)	R(Å)	N	σ^2(Å^2)
Pb/Birnessite	2.34	3.1	0.01	3.73	3.0	0.007			
Pb/Manganite	2.29	2.7	0.01	3.74	1.5	0.012			
β-PbO_2	2.15	5.8	0.003				3.38	2.3	0.004
							3.87	5.8	0.006
Zn/Birnessite	2.07	5.4	0.005	3.50	6.3	0.006			

† Interatomic distance.
‡ Coordination number.
§ Debye-Waller factor.

coordination shell (R_{Pb-O}=2.15 Å) was consistent with differences in the ionic radius for Pb(II) and Pb(IV). These results agreed with previous findings that Pb(II) was not oxidized on birnessite but adsorbed as a tridentate inner-sphere complex at vacancies in the birnessite structure (Manceau et al., 1997; Morin et al., 1999). Differences in the chemical structure of adsorbed Pb on birnessite and manganite agreed with estimated thermodynamic parameters and led to contrasting desorption behavior. These findings have significant implications for Pb partitioning in the environment, particularly in soils containing solid phase Mn(III,IV) (hydr)oxides.

4.5 References

Ainsworth, C.C., J.L. Pilon, P.L. Gassman, and W.G. Van Der Sluys. 1994. Cobalt, cadmium, and lead sorption to hydrous iron oxide: Residence time effect. Soil Sci. Soc. Am. J. 58:1615-1623.

Bargar, J.R., S.N. Towle, G.E. Brown, Jr., and G.E. Parks. 1996. Outer-sphere Pb(II) adsorbed at specific sites on single crystal α-alumina. Geochim. Cosmochim. Acta. 60:3541-3547.

Bargar, J.R.,G.E. Brown, Jr., and G.E. Parks. 1997a. Surface complexation of Pb(II) at oxide-water interfaces: I. XAFS and bond-valence determination of mononuclear and polynuclear Pb(II) sorption products on aluminum oxides. Geochim. Cosmochim. Acta 61: 2617-2637.

Bargar, J.R., G.E. Brown, Jr., and G.E. Parks. 1997b. Surface complexation of Pb(II) at oxide-water interfaces: II. XAFS and bond-valence determination of mononuclear Pb(II) sorption products and surface functional groups on iron oxides. Geochim. Cosmochim. Acta 61: 2639-2652.

Bargar, J.R., G.E. Brown, Jr., and G.E. Parks. 1998. Surface complexation of Pb(II) at oxide-water interfaces: III. XAFS determination of Pb(II) and Pb(II)-chloro adsorption complexes on goethite and alumina. Geochim. Cosmochim. Acta. 62: 193-207.

Benjamin, M.M. and J.O. Leckie. 1981. Multiple-site adsorption of Cd, Cu, Zn, and Pb on amorphous iron oxyhydroxide. J. Colloid Interface Sci. 79: 209-221

Burgess, J. 1988. Ions in solution. Ellis Horwood, Chichester.

Catts, J.G., and D. Langmuir. 1986. Adsorption of Cu, Pb and Zn by δMnO_2: applicability of the site binding-surface complexation model. Appl. Geochem. 1: 255-264.

Chiou, C.T., and T.D. Shoup. 1985. Soil sorption of organic vapors and effects of humidity on sorptive mechanism and capacity. Environ. Sci. Technol. 19:1196-1200.

Chorover, J., and G. Sposito. 1995. Surface charge characteristics of kaolinitic tropical soils. Geochim. Cosmochim. Acta. 59: 875-884.

Cronan, D.S. 1974. Authigenic minerals in deep-sea sediments. p.491-525. *In* The Sea; E.D. Goldberg, (Ed.); Wiley, New York.

Drits, V.A., E. Silvester, A.I. Gorshkov, and A. Manceau. 1997. Structure of synthetic monoclinic Na-rich birnessite and hexagonal birnessite: I. Results from x-ray diffraction and selected-area electron diffraction. Am. Mineral. 82: 946-961.

Eick, M.J., J.D. Peak, P.V. Brady, and J.D. Pesek. 1999. Kinetics of lead adsorption/desorption on goethite: Residence time effect. Soil Sci. 164: 28-39.

Ford, R.G., P.M. Bertsch, and K.J. Farley. 1997. Changes in transition and heavy metal partitioning during hydrous iron oxide aging. Environ. Sci. Technol. 31:2028-2033.

Gatte, R.R., and H.A. Laitinen 1974. Studies of heavy metal adsorption by hydrous iron and manganese oxides. Anal. Chem. 46:2022-2026.

Giovanoli, R., and U. Leuenberger. 1969. Über die oxydation von manganoxidhydroxid. Helv. Chim. Acta 52:2333-2340.

Giovanoli, R., E. Stähli, and W. Feitknecht. 1970. Uber Oxihydoxide des vierwertigen Mangans mit Schichtengitter. 1. Natrium-Mangan(II,III) Manganat(IV). Helv. Chim. Acta 53: 209-220.

Golden, D.C., J.B. Dixon, and C.C. Chen. 1986. Ion exchange, thermal transformations, and oxidizing properties of birnessite. Clays Clay Miner. 34: 511-520.

Grossl, P.R., D.L. Sparks, and C.C. Ainsworth. 1994. Rapid kinetics of Cu(II) adsorption/desorption on goethite. Environ. Sci.. Technol. 28:1422-1429.

Hachiya, K., M. Sasaki, T. Ikeda, N. Mikami, and T. Yasunaga. 1984. Static and kinetic studies of adsorption-desorption of metal ions on the γ-Al_2O_3 surface. J. Phys. Chem. 88: 27-31.

Hayes, K.F. and J.O. Leckie. 1986. Mechanism of lead ion adsorption at the goethite-water interface. p. 114-141. *In* J.A. Davis and K.F. Hayes (ed.) Geochemical processes at mineral surfaces. America Chemical Society, Washington, D.C.

Hem, J.D. 1978. Redox processes at surfaces of manganese oxide and their effects on aqueous metal ions. Chem. Geol. 21: 199-218.

Huang, J.W., J. Chen, W.R. Berti, and S.D. Cunningham. 1997. Phytoremediation of lead-contaminated soils: Role of synthetic chelates in lead phytoextraction. Environ. Sci. Technol. 31: 800-805.

James, R.O., and T.W. Healy. 1972. Adsorption of hydrolysable metal ions at the oxide-water interface. J. Colloid Interface Sci. 40: 65-81.

Jenne, E.A. 1968. Controls on Mn, Fe, Co, Ni, Cu, and Zn concentrations in soils and water: The significant role of hydrous Mn and Fe oxides. Adv. Chem. Ser. 67: 337-387.

Leciejewicz, J. 1961. On the crystal structure of tetragonal (red) PbO. Acta Crystallogr. 14:1304.

Ma, Q.O., T.J. Logan, S.J. Traina, and J.A. Ryan. 1994. Effects of NO_3^-, Cl^-, F^-, SO_4^{2-}, and CO_3^{2-} on Pb^{2+} immobilization by hydroxyapatite. Sci. Technol. 28:408-418.

Manceau, A., L. Charlet, M.C. Boisset, B. Didier, and L. Spadini. 1992. Sorption and speciation of heavy metals on hydrous Fe and Mn oxides. From microscopic to macroscopic. Appl. Clay Sci. 7:201-223.

Manceau, A., J.C. Harge, C. Bartoli, E. Silvester, J.L. Hazemann, M. Mench, and D. Baize. 1997. Sorption mechanism of zinc and lead on birnessite: Application to their speciation in contaminated soils. p.403-404. *In* I.K. Iskandar et al. (eds.) Biogeochemistry of Trace Elements. Berkeley, CA.

Martínez, C.E., and M.B. McBride. 1998. Solubility of Cd^{2+}, Cu^{2+}, Pb^{2+}, and Zn^{2+} in aged coprecipitates with amorphous iron hydroxides. Environ. Sci. Technol. 32:743-748.

McKenzie, R. M. 1971. The synthesis of birnessite, cryptomelane, and some other oxides and hydroxides of manganese. Mineral. Mag. 38:493-502.

McKenzie, R.M. 1980. The adsorption of lead and other heavy metals on oxides of manganese and iron. Aust. J. Soil Res. 18: 61-73.

McKenzie, R.M. 1981. The surface charge on manganese oxides. Aust. J. Soil Res. 19: 41-50.

McKenzie, R. M. 1989. Manganese oxides and hydroxides. p. 439-465. *In* J.B. Dixon and S.B Weed (ed.) Minerals in Soil Environments. 2nd ed. SSSA Book Series 1. SSSA, Madison, WI.

Morin, G.; J.D. Ostergren, F. Juillot, P. Ildefonse, G. Calas, and G.E. Brown Jr. 1999. XAFS determination of the chemical form of lead in smelter-contaminated soils and mine tailings: Importance of adsorption processes. Am. Mineral. 84: 420-434.

Murray, D.J., T.W. Healy, and D.W. Fuerstenau. 1968. The adsorption of aqueous metal on colloidal hydrous manganese oxide. Adv. Chem. Ser. 79: 74-81.

Murray, J.W. 1975. The interaction of metal ions at the manganese dioxide-solution interface. Geochim. Cosmochim. Acta. 39:505-519.

Nelson, Y. M., L.W. Lion, W.C. Ghiorse, and M.L. Shuler. 1999. Production of biogenic Mn oxides by *Leptothrix discophora* SS-1 in a chemically defined growth medium and evaluation of their Pb adsorption characteristics. Appl. Environ. Micro. 65:175-180.

Parks, G.A. 1975. Adsorption in the marine environment. p 241-308. *In* Chemical Oceanography. J.P. Riley and G. Skirrow (eds.) Academic Press, London.

Post, J.E., and D.R. Veblen. 1990. Crystal structure determinations of synthetic sodium, magnesium, and potassium birnessite using TEM and the Rietveld method. Am. Mineral. 75:477-489.

Rehr, J.J., J. Mustre de Leon, S. Zabinsky, and R.C. Albers. 1991. Theoretical x-ray absorption fine-structure standards. J. Amer. Chem. Soc. 113:5135-5140.

Sauvé, S., M.B. McBride, and W. Hendershot. 1998. Soil solution speciation of lead (II): Effects of organic matter and pH. Soil Sci. Soc. Am. J. 62: 618-621.

Sparks, D.L. 1995. Environmental Soil Chemistry. Academic Press, San Diego.

Sparks, D.L. 1999. Kinetics and mechanisms of chemical reactions at the soil mineral/water interface. p.135-192. *In* Soil Physical Chemistry. D.L Sparks (ed.) CRC Press, Boca Raton, FL.

Strawn, D.G., A.M. Scheidegger, and D.L. Sparks. 1998. Kinetics and mechanisms of Pb(II) sorption and desorption at the aluminum oxide-water interface. Environ. Sci. Technol. 32: 2596-2601.

Strawn, D.G., and D.L. Sparks. 1998. Sorption kinetics of trace elements in soils and soil materials. p.1-28. *In* I.K. Iskandar et al. (eds.) Biogeochemistry of Trace Elements. Berkeley, CA.

Strawn, D.G., and D.L. Sparks. 1999. The use of XAFS to distinguish between inner- and outer-sphere lead adsorption complexes on montmorillonite. J. Colloid Interface Sci. 216:257-269.

Stumm, W., C.P. Huang, and S.R. Jenkins. 1970. Specific chemical interaction affecting the stability of dispersed system. Croat. Chem. Acta. 42:223-245.

Chapter 5

CONCLUSIONS

5.1 Summary

The research presented in this dissertation attempted to develop a mechanistic framework for understanding Mn redox cycling in the presence of soil organic matter using naturally occurring Mn(III,IV) (hydr) oxide minerals and catechol as an analogue for soil organic matter. The most commonly identified Mn mineral, birnessite, was shown to be the most reactive towards catechol. An electron paramagnetic resonance stopped-flow kinetic technique was successfully employed to measure the reduction of birnessite by catechol because the rapid rates precluded the use of standard batch methods. The precursor surface complex formed between catechol and Mn(III,IV) (hydr) oxides was identified for the first time *in situ* using diffuse reflectance spectroscopy.

Additional solid Mn phases were studied to elucidate the rapid reductive dissolution kinetics of birnessite by catechol. It was found that the availability of structural Mn(III) in the Mn oxide minerals was linearly related to oxidation of catechol and solubilization of solid phase Mn minerals. This finding is novel because Mn(II) and Mn(IV) have received the most attention in aquatic chemistry (Morgan, 1967) until recently, where it has been recognized that disproportionation of Mn(III) is

kinetically controlled and solid Mn(III) oxides and soluble Mn(III) complexes have been shown to be environmentally significant oxidants (Stone and Morgan, 1984; Kostka et al., 1995; Klewicki et al., 1998; Luther et al., 1998). Recent x-ray absorption near edge structure spectra strongly suggested the presence of Mn(III) in both air-dried and saturated soils (Schulze et al., 1995). Apparently, all "Mn(III) is not created equal", in other words, Mn(III) coordinated in layer structure Mn minerals like birnessite is more reactive than Mn(III) in tunnel structures (manganite, pyrolusite) that are linked by edge-shared MnO_6 octahedra. There is a strong potential that the increase in land application of animal wastes with electron-donating and chelating functional groups to soils could solubilize native Mn oxide minerals, particularly those containing structural Mn(III) in "reactive" coordination environments, thus influencing the global Mn and C cycles.

5.2 Future Research Needs

The role of Mn(III) in different coordination environments may provide the link to explain the ability of birnessite to abiotically produce CO_2 from catechol (Naidja et al., 1998), a pathway not well understood because it has been ascribed to biological activity in past studies. One important question still to address is to better characterize solid phase Mn minerals in natural field settings and perform reactivity experiments on these phases. They often occur tightly associated with phyllosilicate minerals and other occluded soil materials. The ability to structurally define the solid

phase Mn mineral controlling solubility of plant available Mn(II) would be very useful.

Another need is to investigate *in situ* the water exchange rates of different soil components, particularly those containing structural Mn(III). Currently, nuclear magnetic resonance coupled with isotopic labelling is used to measure water exchange. It goes without saying that measuring water exchange rates in soils, albeit ambitious, would allow one to better predict fate of a contaminant or nutrient once applied to soils or sediments and even aid in nutrient management systems which would benefit production agriculture, the general public, and preserve environmental quality.

5.3 References

Klewicki, J.K., and J.J. Morgan. 1998. Kinetic behavior of Mn(III) complexes of pyrophosphate, EDTA, and citrate. Environ. Sci. Technol. 32:2916-2922.

Kostka, J.E., G.W. Luther III, and K.H. Nealson. 1995. Chemical and biological reduction of Mn(III)-pyrophosphate complexes: Potential importance of dissolved Mn(III) as an environmental oxidant. Geochim. Cosmochim. Acta 59:885-894.

Luther, G.W. III, D.T. Ruppel, and C. Burkhard. 1998. Reactivity of dissolved Mn(III) complexes and Mn(IV) species with reductants: Mn redox chemistry without a dissolution step? p. 265-280. *In* D.L. Sparks and T.J. Grundl (ed.) Mineral-water interfacial reactions: Kinetics and mechanisms. ACS Symposium Ser. No. 715, Washington, DC.

Morgan, J.J. 1967. Chemical equilibria and kinetic properties of manganese in natural waters. p. 561-626. *In* S.D. Faust and J.V. Hunter (ed.) Principles and applications of water chemistry. Wiley, New York.

Naidja, A., P.M. Huang, and J.M. Bollag. 1998. Comparison of reaction products from the transformation of catechol catalyzed by birnessite or tyrosinase. Soil Sci. Soc. Am. J. 62:188-195.

Schulze, D.G., S.R. Sutton, and S. Bajt. 1995. Determining manganese oxidation state in soils using x-ray absorption near-edge structure (XANES) spectroscopy. Soil Sci. Soc. Am. J. 59:1540-1548.

Stone, A.T., and J. J. Morgan. 1984. Reduction and dissolution of manganese (III) and manganese (IV) oxides by organics. 1. Reaction with hydroquinone. Environ. Sci. Technol. 18:450-456.

Appendix A

SUPPLEMENTARY MATERIAL FOR CHAPTER 2

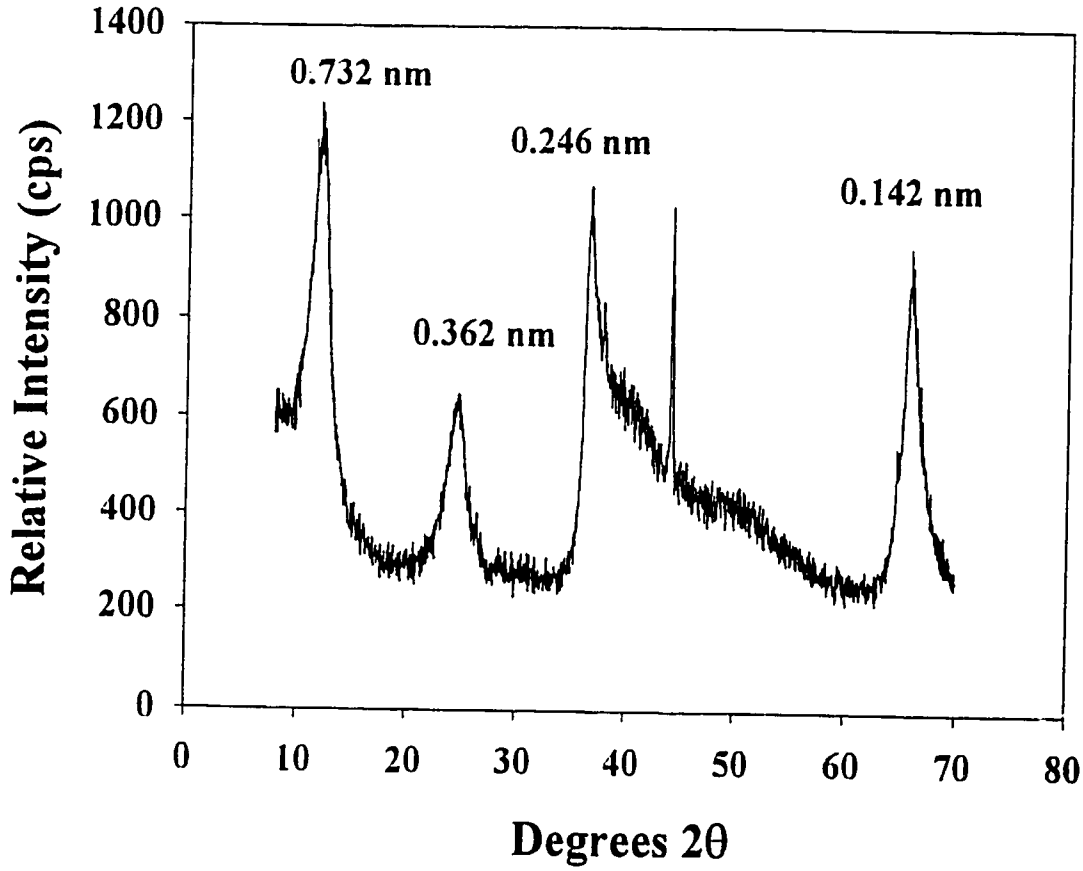

Figure A.1 X-ray diffractogram of untreated birnessite. Scans were taken using CuKα radiation with Al sample holders and a step size of 0.03 ° 2θ at 22 s/step.

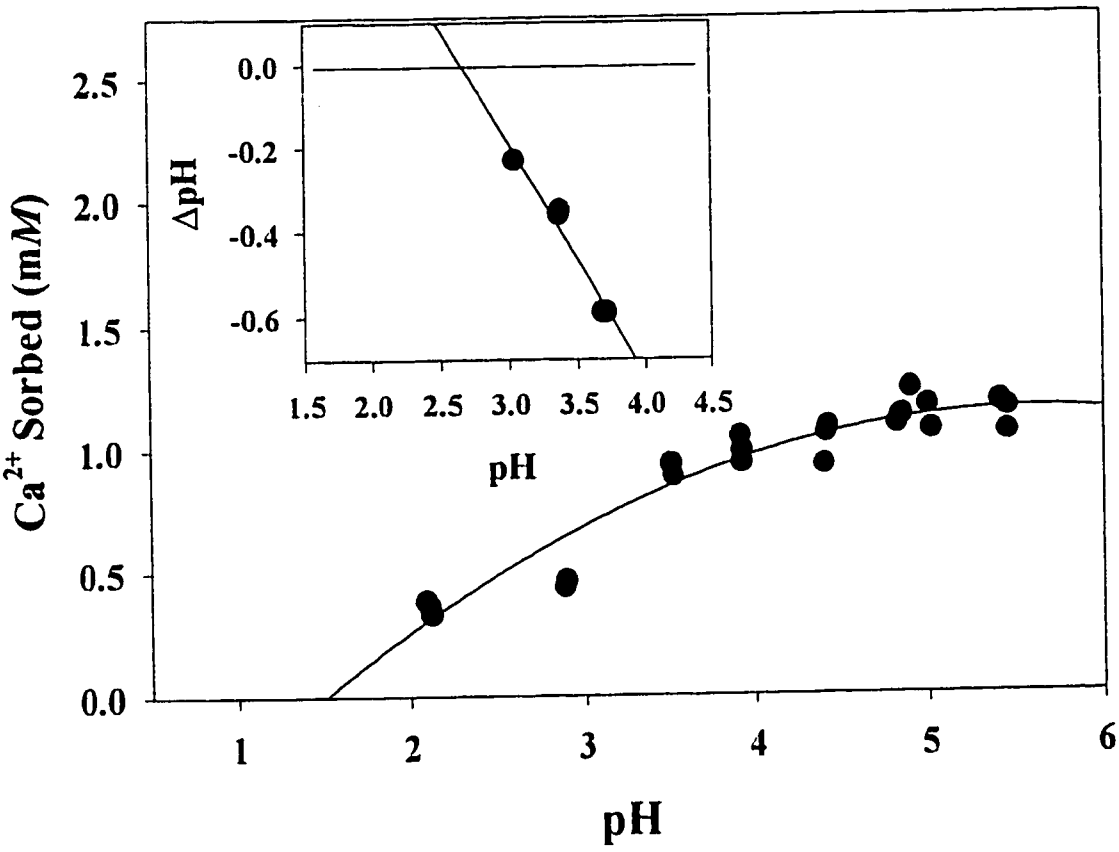

Figure A.2 Calcium sorption on birnessite as a function of pH to estimate the point of zero charge (PZC) as described by Balistrieri and Murray (1982). An extrapolation of the data to the pH where no Ca^{2+} was sorbed resulted in a PZC of 1.5. The inset indicates the extrapolated PZC of 2.6 using the ΔpH method of Kinniburgh et al. (1976).

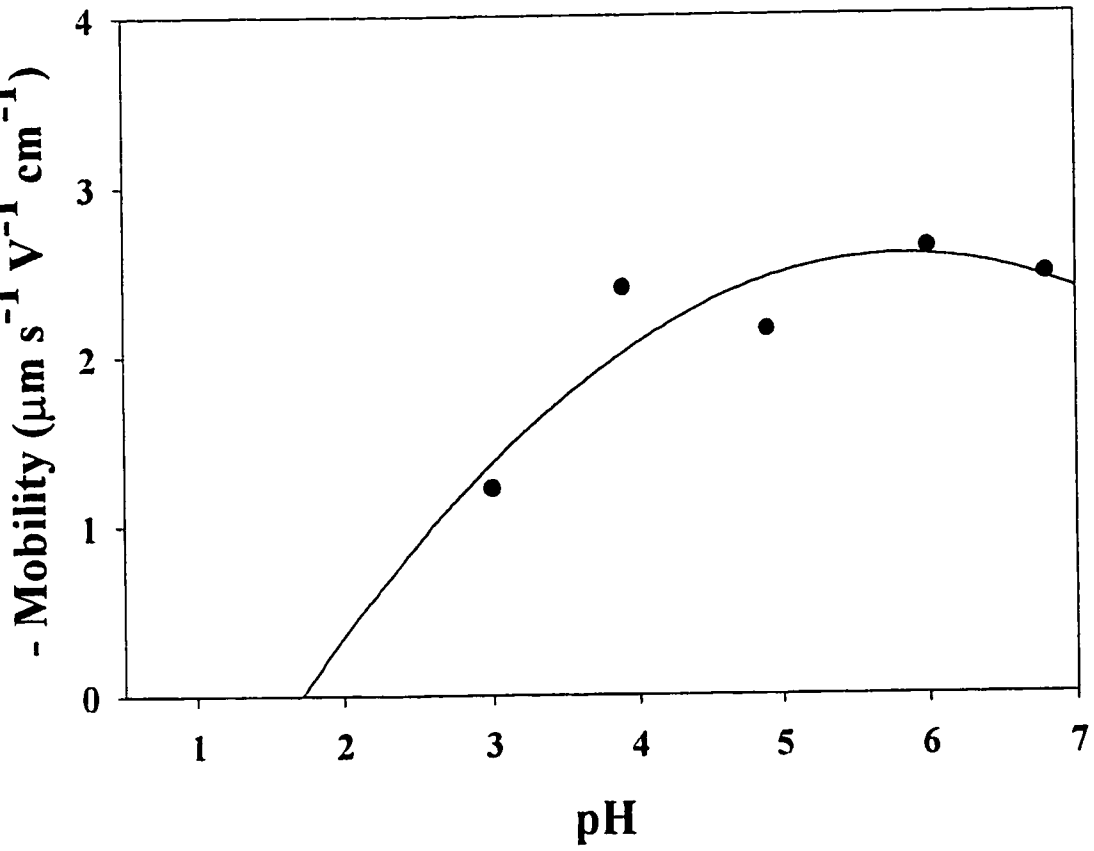

Figure A.3 Representative electrophoretic mobilities for birnessite as a function of pH. Positive mobilities were never observed and extrapolation (with a 2nd order polynomial) to zero yielded a PZC of 1.81 ± 0.04.

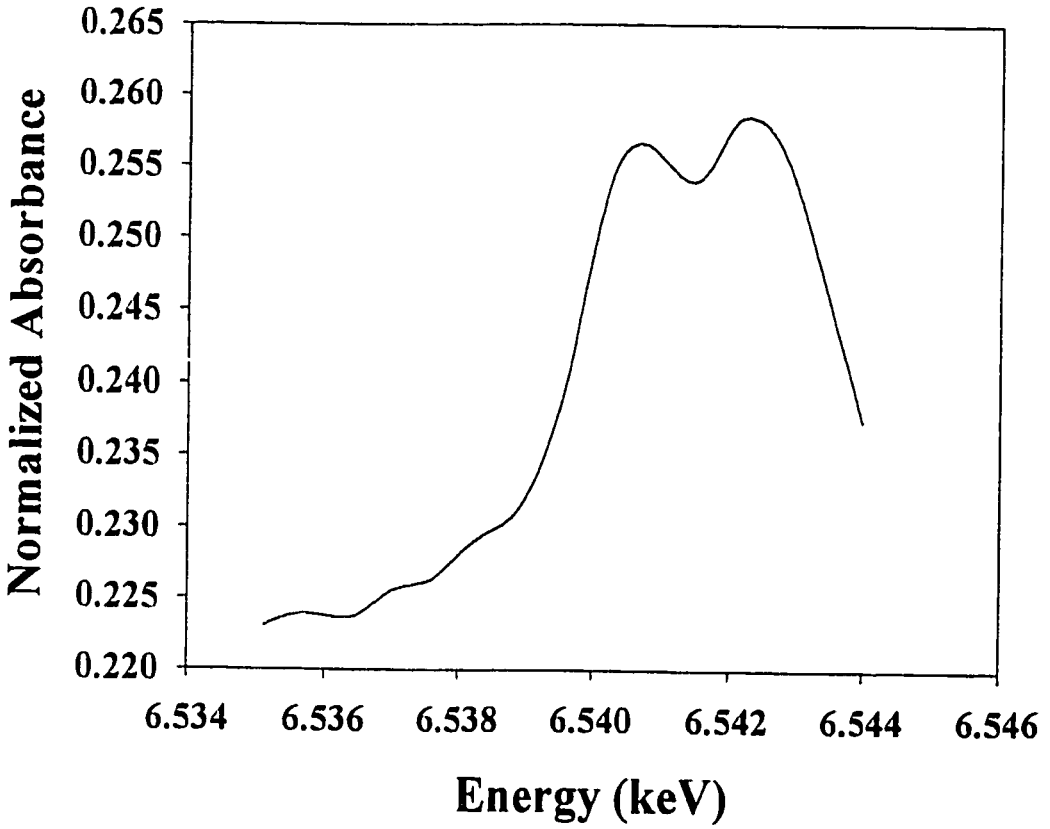

Figure A.4 MnK preedge spectrum of synthesized birnessite. The shoulders below 6.54 keV may represent Mn(II) species.

Appendix B

SUPPLEMENTARY MATERIAL FOR CHAPTER 3

Table B.1 Physical and chemical characteristics of Mn(III,IV) (hydr) oxides.

Mineral	Oxidation State	BET Surface Area	Point of Zero Charge
Birnessite (δ–MnO_2)	3.44	40	2
Manganite (γ-MnOOH)	3.02	32	6.3
Pyrolusite (β-MnO_2)	3.92	8	7.0

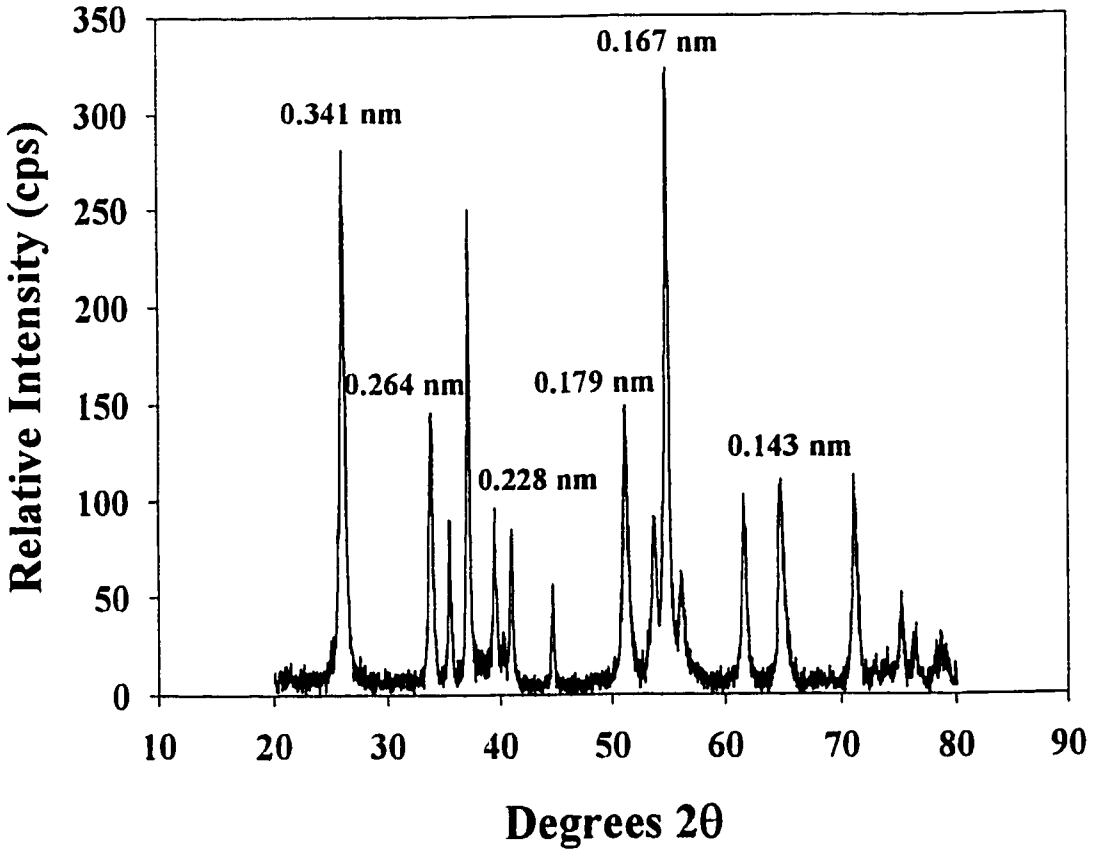

Figure B.1 X-ray diffractogram of untreated manganite. Scans were taken using CuKα radiation with Al sample holders and a step size of 0.03 °2θ at 2 s/step.

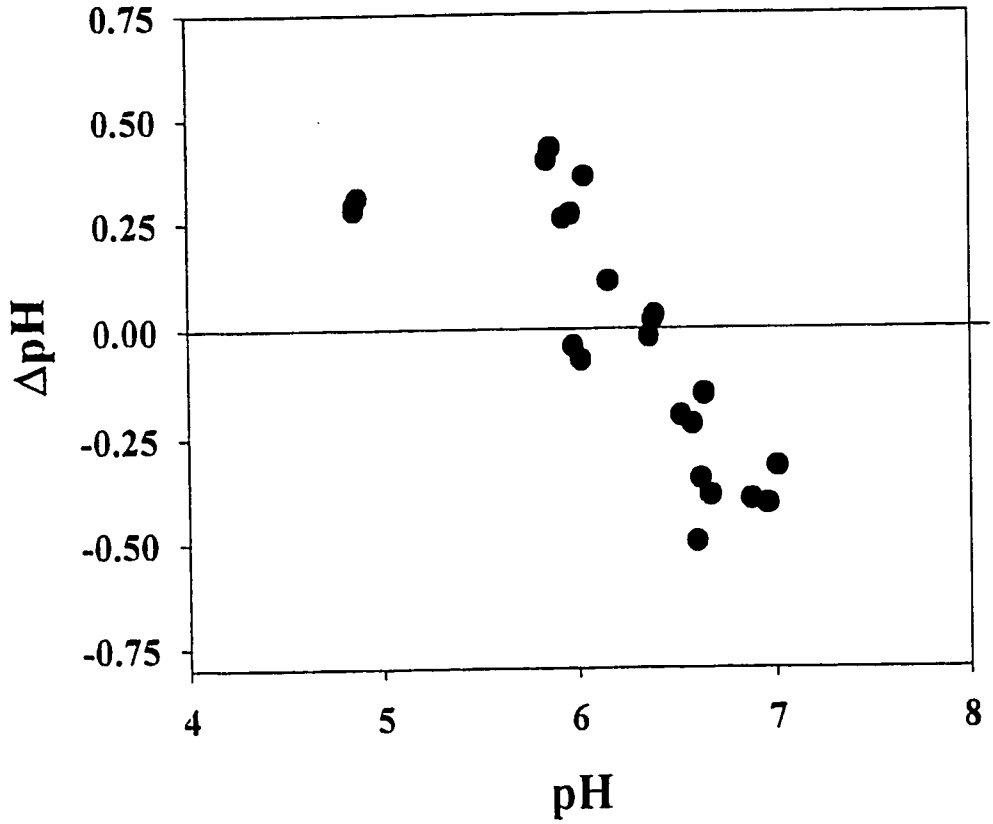

Figure B.2 Estimated PZC of manganite. The ΔpH represents the the change in pH during 1 h after increasing the ionic strength concentration from 1 to 1000 mM using NaCl as the ionic medium (Kinniburgh et al., 1976). The PZC is the point where ΔpH=0. For manganite, PZC=6.3± 0.06, which agreed with previous values for this mineral (Xyla et al., 1992).

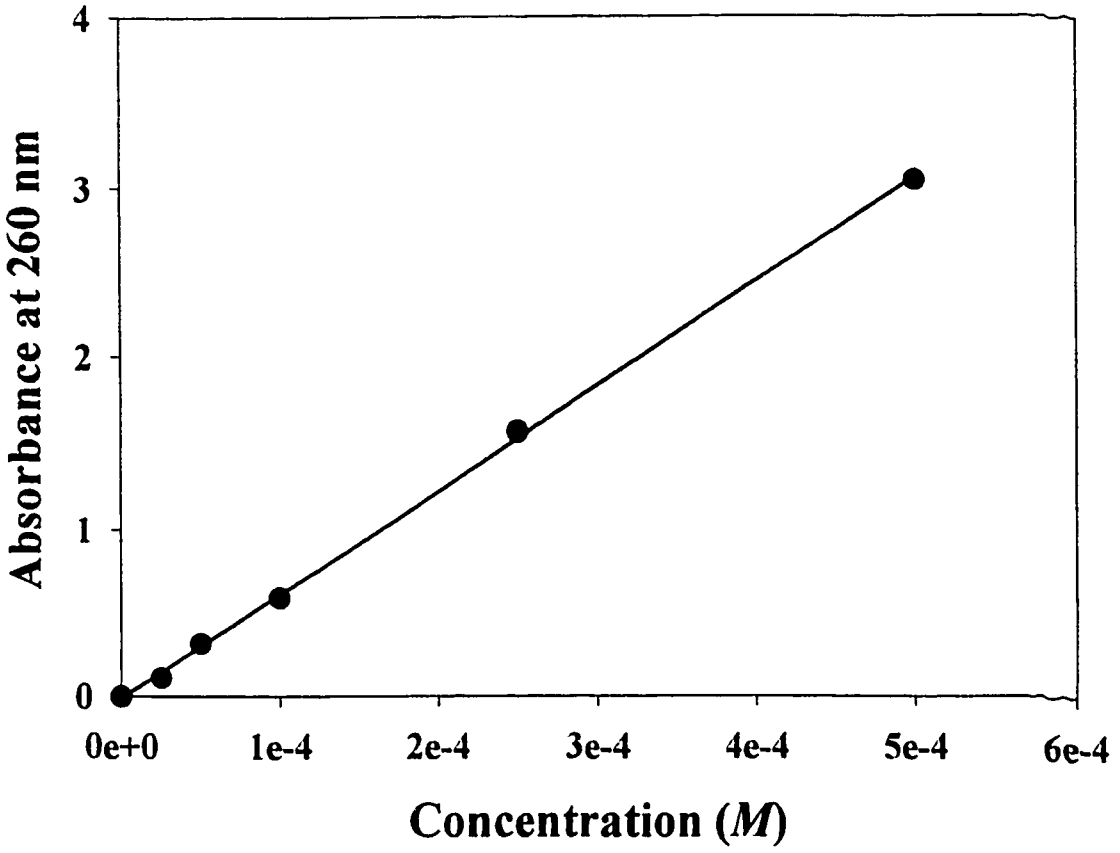

Figure B.3 Typical standard calibration curve relating absorbance at 260 nm to Mn(III) concentration in 50 m*M* pyrophosphate at pH 6.5.

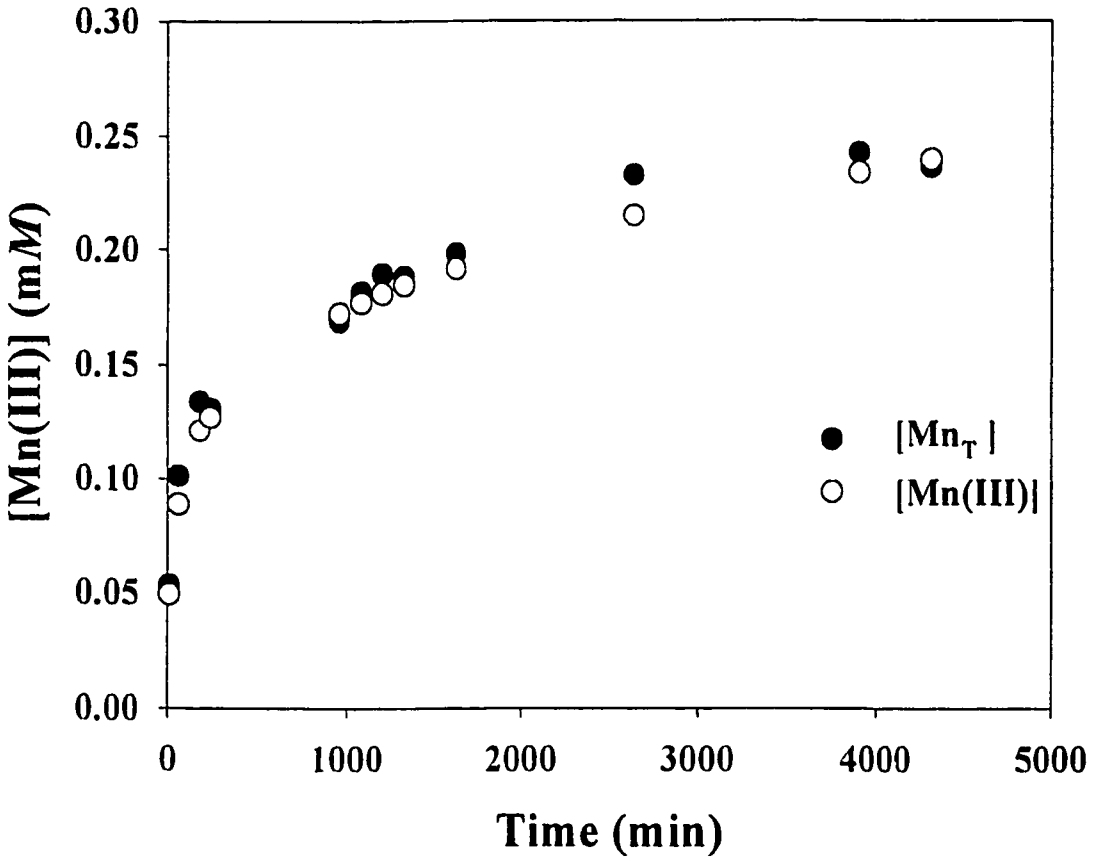

Figure B.4 Extraction of structural Mn(III) from birnessite with 50 m*M* pyrophosphate. The collapse of total Mn determined by flame AAS ([Mn_T]) and [Mn(III)] on the same curve confirms that [Mn(III)] species were measured.